Melanoma displays an evolutionarily conserved resistance to modulation of phagocytic signals

A DISSERTATION
SUBMITTED TO THE FACULTY OF
UNIVERSITY OF MINNESOTA
BY

Katie Lynne Anderson

IN PARTIAL FULFILLMENT OF THE REQUIREMENTS
FOR THE DEGREE OF
DOCTOR OF PHILOSOPHY

Advisors: Dr. Jaime F Modiano, VMD, PhD and Dr. Yoji Shimizu, PhD

August 2017

ACKNOWLEGEMENTS

The work presented in this dissertation would not have been possible without the support of many people, from professors and collaborators to family and friends.

First and foremost, I would like to thank my graduate advisor and mentor, Dr. Jaime Modiano. My success in this program has been a direct result of Dr. Modiano's tireless devotion to educating veterinary scientists. His passion for science is infectious and inspirational. Throughout my education, Dr. Modiano provided a nurturing and challenging environment in which I was free to take risks, learn from my mistakes, and grow as a scientist. I truly appreciate his advice and guidance, and I wouldn't be the veterinarian or scientist that I am today without his mentorship.

I would also like to thank my co-mentors, Dr. Matthew Mescher and Dr. Yoji Shimizu, for their input in the project, for their willingness to share their knowledge, and for instilling me with a passion for immunology and T cell biology. I was also fortunate to have had Drs. Mark Rutherford and Bruce Walcheck as committee members. Their guidance and insightful ideas truly improved the quality of my research, and I appreciate their support throughout this experience.

While my mentoring team certainly influenced my scientific growth, I could not have succeeded without the support of my fellow lab members and collaborators. Thank you to all the members of the Modiano and Mescher labs for your help when I needed it the most. You truly made the lab feel like home, and I will miss our scientific discussions as well as the laughter that kept me going on the hard days. Thank you to the my fellow CMB students as well as Lisa and Kate for all your help and encouragement over the years.

Finally, I would like to thank my incredible family and friends for their love and support. Thank you to my parents, Dale and Lynette, for encouraging my curiosity, for supporting my dreams, and for catching me every time I've stumbled. I cannot put into words how grateful I am for your unconditional love and guidance. Thank you to my brother David for always being able to make me laugh and for your endless pet sitting during scientific conferences. I also need to thank my wonderful friends for celebrating the good times and lending a shoulder to cry on during the bad. Thank you for forgiving my absences and for your patience while I chattered excitedly about immunology. I consider myself beyond lucky to have such wonderful people in my life, and I could not have done this without them.

DEDICATION

To my grandparents, Erwin and Donna Sauve, who truly believe in the power of education and have given me so much love and support throughout this journey

ABSTRACT

Therapeutic activation of macrophage phagocytosis has the ability to restrain tumor growth through phagocytic clearance of tumor cells and activation of the adaptive immune response. The objective of this thesis was to evaluate the effects of modulating pro- and anti-phagocytic pathways in malignant melanoma. We observed that melanoma cells from mice, humans, and dogs displayed an unexpected resistance to phagocytosis that could not be fully mitigated by blockade of the “don’t eat me” signal CD47 or by chemotherapeutic enhancement of known “eat me” signals. In addition, combination doxorubicin chemotherapy and CD47 blockade did not consistently promote an anti-tumor adaptive immune response. Phagocytosis of melanoma cells was not enhanced by inhibition of secretory pathways, and phagocytosis of sensitive lymphoma tumor cells was not impaired in the presence of melanoma culture supernatants, indicating that soluble factors did not mediate phagocytosis resistance. siRNA mediated knockdown of 47 candidate “don’t eat me” signals similarly did not enhance melanoma cell phagocytosis, suggesting that these proteins do not disable macrophage phagocytosis. We conclude melanoma cells possess a mechanism of resistance to phagocytosis. Further investigation will be needed to define this mechanism and to develop strategies to overcome melanoma cell resistance to the innate immune response.

TABLE OF CONTENTS

LIST OF TABLES

LIST OF FIGURES

Chapter 1

Introduction

Section 1: Malignant melanoma

Malignant melanoma is a lethal form of skin cancer that arises from melanocytes, the pigment forming cells of the skin derived from the neural crest [2]. Although genetic factors contribute to the risk of melanoma, environmental factors, particularly prolonged exposure to UV radiation, are thought to greatly influence the development of melanoma in humans. The incidence rate of this cancer has risen rapidly over the past 30 years, and melanoma currently represents the fifth and sixth most common cancer in men and women, respectively [3]. An estimated 87,110 new cases will be diagnosed and 9,730 people will die from malignant melanoma in 2017 [3]. Although most patients are diagnosed with stage I or II disease, one quarter to one third of all patients with melanoma will eventually experience recurrence and development of more advanced stage disease [4]. Due to its aggressive nature and propensity for metastasis, malignant melanoma results in the majority of human skin cancer deaths, despite representing less than five percent of skin cancers overall [2]. The lethality of this cancer emphasizes the need to further our understanding of melanoma cell biology and develop improved treatments for patients with advanced disease.

1.2 Advances in melanoma treatment

Five-year overall survival rates for melanoma diagnosed prior to metastasis and treated with surgery alone exceed 90% [3]. However, the prognosis for patients with metastatic disease remains poor despite recent

therapeutic advances, with five-year overall survival rates around 18% [3]. Historically, metastatic melanoma was treated with resection of the primary tumor, radiation, and chemotherapy. In 1975, the DNA-methylating compound dacarbazine became the first chemotherapeutic drug to receive FDA approval for the treatment of melanoma [5]. Although this compound induces complete responses in only 5% of malignant melanoma patients, it remained the most efficacious treatment for this disease for more than 30 years [4,5].

Recent advances in tumor biology and immunology have led to the development of targeted agents and immunotherapies which have significantly improved the overall survival rate of patients with malignant melanoma [4]. Genome-wide screens of cancer mutations revealed that 66% of malignant melanomas contain a mutation in the *BRAF* gene, a serine/threonine kinase in the MAP kinase pathway [6]. The discovery that 90% of these mutations result in a glutamic acid substitution for valine at amino acid 600 (BRAF V600E) led to the development of small-molecule BRAF inhibitors, such as vemurafenib and dabrafenib [5]. These targeted agents improved overall response rates in advanced melanoma from 5% with dacarbazine alone to nearly 50% with vemurafenib and extended progression-free survival from 1.6 months to 5.3 months [5]. Unfortunately, virtually all of the patients who initially respond to the therapy develop resistance to BRAF inhibition and demonstrate disease progression within 6-8 months [4,5].

The most promising advances in treatment of malignant melanoma have

come from the field of immunotherapy. The immune system's ability to recognize and eliminate tumor cells was postulated more than a century ago [7], but only recent breakthroughs in our understanding of tumor immunology have led to the development of immunotherapeutic strategies capable of producing sustained clinical responses. At the forefront of these therapies are antibodies targeting immune-checkpoints. Signaling via checkpoint molecules, such as CTLA-4 and PD-1, acts to limit the efficacy of the anti-tumor response by inducing anergy or exhaustion in activated T cells [8,9]. Antibodies against CTLA-4, PD-1, and its corresponding ligand PD-L1 aim to reactivate tumor-specific T cells and cause a robust anti-tumor immune response [8,9]. Melanoma is generally regarded as one of the most immunogenic cancers due to a high prevalence of somatic mutations [10]; thus, many immunotherapies have been pioneered for the treatment of this disease. The use of immune checkpoint inhibitors has revolutionized the treatment of advanced melanoma, with overall response rates of 11%, 31%, and 59% for CTLA-4 blockade (Ipilimumab), PD-1 blockade (Nivolumab), and combination CTLA-4 and PD-1 blockade, respectively [11,12]. A subset of malignant melanoma patients experience durable, complete remissions lasting several years. However, the fact that more than 40% of patients with malignant melanoma do not respond to combination checkpoint blockade underscores the need to develop additional therapeutics for the treatment of this disease.

Section 2: Comparative Oncology

Throughout the history of cancer research, animal models have played an invaluable role in understanding tumor biology and developing new cancer therapies. The ideal model system simulates the features of a human primary tumor, such as proliferation, invasion, and metastasis, and the tumor microenvironment as closely as possible. Due to their distinct advantages and disadvantages, each model system can provide unique insights to improve our understanding of cancer biology and drive therapeutic development [13,14].

The majority of cancer research studies to date have relied on inbred mouse models of disease [15]. Mouse models are widely used due to the ability to control experimental variables, the ability to manipulate the mouse genome, and the ability to easily harvest tumors and immune organs for further study. While these models offer valuable insight into the mechanism of action and the efficacy of a therapeutic agent, they hold several challenges for clinical translation. Mouse xenograft models often underestimate the complexity of the heterogeneous tumor microenvironment and, because these model require the use of immunodeficient mice, they fail to account for the complex interplay between human immune cells and cancer cells [15,16]. In addition, specific pathogen free (SPF) housing conditions may affect immune system development and alter the gut microbiota of mice, which has recently been shown to play a role in the efficacy of immunotherapy [17,18]. Finally, the use of young, inbred mouse strains fails to represent the older, obese, and genetically heterogeneous

population of human cancer patients, and therapies that succeed in young, otherwise healthy animals may not be efficacious in older patients with weakened immune systems or comorbidities [15,19]. These inherent challenges may explain why only 11% of oncology drugs that demonstrate success in preclinical mouse models complete the process of approval for use in human patients [15] and emphasize the need to develop better preclinical models of human cancer.

The study of spontaneous cancers in companion dogs and cats represents an attractive translational model for immunotherapy research [15,16]. Comparative oncology has the potential to improve the lives of companion animals with cancer and to simultaneously inform the design of human clinical trials. Client-owned dogs and cats develop spontaneous cancers that harbor comparable genetic abnormalities and develop in the presence of similar environmental exposures as human cancers. Dogs and cats represent a more outbred population than traditional mouse models and are more reflective of the heterogeneity seen in the human population. In addition, these animals are immunocompetent and allow the study of anti-tumor immune responses and the effects of immunotherapy, including long-term efficacy and toxicity, in a realistic clinical setting [15,16]. Although murine and canine models have unique advantages and disadvantages (summarized in Table 1-1), both models have the potential to significantly inform our understanding of multiple human cancers, including melanoma, lymphoma, osteosarcoma, and breast cancer, among others.

Table 1-1: Advantages and disadvantages of animal models of cancer

Disease model	Advantages	Disadvantages
Murine model	-Experimental variables (housing, environment, diet) are easily controlled -Inbred mice are genetically identical (may increase experimental reproducibility) -Genome can be easily manipulated -Tumors and organs can be easily harvested for further study	-Controlled environment and diet do not accurately reflect human life -Young, inbred mice do not accurately reflect the outbred, aging human population -Xenograft models and genetically induced models may be less heterogeneous than human tumors -Xenograft models are immunodeficient
Canine or feline model	-Develop spontaneous tumors that may be more heterogeneous -Immunocompetent -Similar environmental exposures to humans -Outbred compared to mouse models -Disease presents in animals of differing ages and disease status, which is reflective of the human population	-Difficult to control for confounding variables and to standardize treatments -Heterogeneous tumors, immune responses, and genetics may affect reproducibility -Increased ethical regulations and expectation for standard of care treatment -Limited experimental reagents

2.2 Murine models of malignant melanoma

Mouse models of melanoma have been traditionally used to study tumor growth and the interaction of tumor cells with the host immune system. Mouse dermal melanocytes reside deeper within the skin and are better protected from

UV radiation than human melanocytes. Due to this difference in melanocyte localization, mice rarely develop spontaneous, UV-induced melanoma, and if spontaneous tumors do develop, they present with unique histopathological properties that are dissimilar to the human disease [14,20]. However, a number of clinically relevant mouse models of melanoma have been developed using tumor engraftment techniques and genetic modification (reviewed in [14]).

Tumor xenograft models facilitate the study of human tumor growth *in vivo* and have played a significant role in cancer drug discovery. In this model, human melanoma tumors are engrafted into an immunocompromised mouse and allowed to directly interact with the host stroma, including lymphatics and blood vessels [13,14]. Although orthotopic engraftment is thought to better mimic human tumor formation, melanomas are usually engrafted subcutaneously as intradermal injection leads to rapid skin ulceration [14]. By engrafting established human cell lines grown in similar culture conditions, investigators can better control the timing of tumor growth and reduce interexperimental variability. Cell lines are readily available, easily engrafted into mice, and can be genetically manipulated to study varying aspects of tumor biology. However, many of these lines have been grown under non-physiological conditions for years and may no longer accurately reflect human primary tumors [14]. To address these concerns, patient-derived xenografts (PDXs), consisting of a fresh biopsy sample from a patient, may be engrafted. PDXs are thought to maintain more similarities to actual patient tumors than cultured cell lines and could more accurately reflect

clinical responses [14]. However, PDX models are expensive, time-consuming, and technically challenging. One major limitation of all xenograft models is the lack of an intact immune system, which prevents the study of the anti-tumor immune response or immunotherapeutic efficacy. To overcome this limitation, “humanized” mice can be created by implanting human hematopoietic stem cells capable of regenerating elements of the human immune system into irradiated mice; however, these humanized PDX models remain expensive and a number of technical challenges still hinder model development [13,14].

Syngeneic transplantation models, in which mouse melanoma cell lines are engrafted into immunocompetent mice with similar major histocompatibility complex (MHC) haplotypes, retain the advantages of a xenograft system while permitting the study of the anti-melanoma immune response. The most widely used syngeneic model of melanoma is the B16 cell line, which was derived from a chemically induced melanoma in a C57BL/6J mouse [13]. A number of B16 subclones with varying propensities for proliferation and metastasis were established from the primary tumor and permit the study of different aspects of melanoma cell behavior. These clones include B16F1, which retains low metastatic potential, and B16F10, which retains high metastatic potential [14]. Although B16 cells express low levels of MHC Class I, these cells express high levels of melanoma epitopes, including gp100 and TRP2, that can be recognized by the host immune system. In addition, these cells can be genetically manipulated to express specific tumor antigens. The B16 cell line is commonly

used to study immunotherapeutic efficacy, and a great number of reports have documented an anti-melanoma immune response in this model system [14]. It is important to note that murine melanoma cells differ from human melanoma cells in several respects, including differences in adhesion molecule expression, growth factor production, mechanisms of invasion, and genetic mutations [13,14]. For instance, in direct contrast to human tumors, B16 cells do not contain activating mutations in the *BRAF* oncogene and retain wild type *PTEN* expression [14,21]. Despite these differences, B16 cells remain an important tool in the study of anti-melanoma immune responses. These cells proliferate rapidly, engraft readily into syngeneic mice, can be genetically manipulated, and are capable of forming metastases in distant visceral organs [14].

While mice rarely develop spontaneous melanoma, a number of genetically engineered mouse models (GEMMs) of melanoma have been developed. These models utilize transgenic or knockout mice in which a tumor oncogene (such as *BRAF* or *NRAS*) has been activated or a tumor suppressor (such as *CDKN2A* or *PTEN*) has been deleted in order to mimic the genetic alterations that occur in human melanoma [13]. GEMMs develop spontaneous tumors and may predict drug efficacy more accurately than other preclinical models [14]. However, several limitations of GEMMs exist. It can be difficult to control the timing of tumor growth in GEMMs, and many of the genetic alterations used to create GEMMs induce tumor development in several tissues simultaneously, thus limiting the use of the model for studying melanoma [14].

Melanoma in GEMMs may arise in different locations from the human disease (such as the CNS) [14]. In addition, many of the melanomas in GEMMs lack the radial and vertical growth properties seen in human malignant melanoma, and therefore, do not recapitulate human disease progression. Differences in melanoma growth could be due to the use of one or two genetic alterations to induce melanoma development, which may fail to represent the genetic heterogeneity of spontaneous human tumors. Although these tumors develop in the presence of an intact immune system, their low mutational burden may fail to induce an anti-tumor immune response, and these models are not commonly used to study tumor immunology [14,20].

While there are many advantages to using mouse models to study melanoma, no model can fully recapitulate the complexity of human tumor growth or a human tumor microenvironment. Each model system holds unique advantages and disadvantages that permit the study of varying aspects of melanoma biology. Together, the use of these model systems has led to major advances in the diagnosis and treatment of malignant melanoma.

2.3 Canine malignant melanoma as a model for human disease

Canine malignant melanoma occurs spontaneously in companion dogs and represents another relevant clinical model for human melanoma. Similar to the human disease, canine malignant melanoma can present as a highly aggressive, metastatic neoplasm. Melanomas represent 3-9% of canine neoplasms and 14-45% of canine oral tumors [22]. Unlike human malignant

melanoma, canine malignant melanoma typically arises from pigment cells in the oral cavity, although it can also be found on the skin, lips, digits, and other organs. The pathogenesis of canine melanoma is not fully understood; however, the disease distribution suggests that, unlike human melanoma, ultraviolet radiation is not a risk factor for disease development [23]. Oral malignant melanoma is highly aggressive, with localized invasion present in 57% of tumors, and between 70-90% of tumors undergoing metastasis [22,24]. The median overall survival for all dogs with malignant melanoma of the oral cavity is estimated at less than 150 days [22]. Although oral tumors located at the mucocutaneous junction typically display malignant, aggressive behavior, it is important to note that oral tumors located on the lips or gums are often benign. While less common than oral malignant melanoma, canine acral melanoma (found on the foot pads and nail bed) displays a similarly aggressive nature, with an estimated 30-40% of cases having metastasized at the time of diagnosis [22]. The oral and acral forms of canine malignant melanoma are thought to closely mimic the clinical progression of human mucosal and acral melanoma, respectively [23]. In contrast to the human forms of the disease, canine cutaneous and ocular melanomas are most commonly benign. Most dogs with dermal melanoma of haired skin are cured with surgical excision of the tumor, with an expectation of almost 90% one-year survival following surgical intervention [22].

Despite differences in the disease distribution and etiology, canine

malignant melanoma has been established as a relevant translational model for human melanoma and represents a unique opportunity to study the disease in a large, immunocompetent animal model [23]. Human and canine malignant melanoma share similar clinical presentation, histopathology, and propensity for invasion and metastasis (See Table 1-2) [22,25]. At the subcellular level, human and canine malignant melanoma share multiple molecular similarities and signaling pathways, including activation of the AKT/mTOR pathway, changes in KIT signaling, upregulation of COX-2 and CSPG4, and dysregulation of Wnt/β catenin signaling [26]. Loss of the tumor suppressor PTEN occurs in approximately 20% of human primary tumors and approximately 50% of canine tumors [23,27]. In addition, germline mutations in *CDKN2*, which encodes the tumor suppressor p16, are associated with the development of heritable melanoma in human families [28,29], and loss of p16 occurs frequently in canine melanomas as well [30]. Despite these similarities, some important molecular differences exist between human and canine melanoma; in particular, activating mutations in *BRAF* have not been identified in canine melanoma. Although these mutations are common in the cutaneous form of human melanoma, *BRAF* mutations are also rare in human mucosal melanoma, emphasizing the similarities between the human and canine mucosal forms of the disease [26].

Similar to human disease, loco-regional control of early stage canine oral melanoma can be achieved using radiation or surgery, but few efficacious treatments exist for advanced, metastatic disease. Multiple chemotherapy

protocols have been described, but response rates following chemotherapy are only 8-28%, and there is little evidence that treatment improves overall survival in patients with advanced disease [26,31]. Immunotherapies to stimulate the innate and adaptive immune system, including cytokine therapy and vaccination, have met with varying clinical success [16,26], emphasizing the need to develop new therapeutic modalities for the treatment of advanced canine melanoma.

Table 1-2: Comparison of human malignant melanoma (HMM) and canine malignant melanoma (CMM)

Characteristic	Similarities	Differences
Clinical presentation [3,22]	-Both HMM and CMM can found on the skin, mucosa, ocular cavity, and digits -Middle age to older patients -Similar appearance: raised, usually dark tumors. Amelanotic lesions occur infrequently	-HMM is most commonly cutaneous -CMM is most commonly found on the oral mucosa
Etiology [3,22,26]	-Heritable risk and inflammation are thought to contribute to both HMM and CMM	-UV exposure is a risk factor for HMM, but not CMM
Molecular signaling pathways [6,26,32]	-Both HMM and CMM display: activation of the AKT/mTOR pathway, changes in KIT signaling, upregulation of COX-2 and CSPG4, dysregulation of Wnt/β catenin signaling, and loss of PTEN -Familiar forms of HMM display loss of CDKN2, encoding for p16; loss of p16 is common in CMM -Similar chromosomal	-BRAF mutations occur in 66% of cutaneous HMM, but are absent in mucosal HMM and CMM

	abnormalities exist between mucosal HMM and oral CMM, including a recurrent pattern of copy number gains and losses on canine chromosome 30 and its corresponding region on human chromosome 15	
Histopathology [23]	-Similar appearance: 3 major subtypes, epitheloid, spindloid, or mixed exist for both HMM and CMM -Similar structural features are utilized for diagnosis and staging -Several immunohistochemical markers can be used in the evaluation of both human and canine melanoma cells (melan-A, PNL2, TRP2)	
Biological behavior [22]	-HMM and oral CMM located at the mucocutaneous junction display biologically aggressive behavior with invasion and metastasis	-Cutaneous canine melanoma and oral melanoma located on the lips or gums are often benign
Treatment [5,9,15]	-Stage I/II CMM and HMM are both controlled by radiation and surgery -Chemotherapy has done little to extend survival in both CMM and HMM -Immunotherapies have met with varying success in both CMM and HMM; evidence of an anti-tumor immune response exists in both diseases	-HMM is often treated with BRAF inhibitors and checkpoint inhibitors -Due to the lack of BRAF mutations in CMM, BRAF inhibitors cannot be modeled in dogs and are not used therapeutically for CMM -Reagents for immune checkpoint inhibition have been developed for dogs, but have not undergone clinical trials for CMM

2.4 Other comparative models of human melanoma

In addition to the murine and canine models of malignant melanoma, several other animal species can be used to model this disease. Transgenic fish models of malignant melanoma have been developed in both zebrafish and medaka. Due to the transparency of their embryos, fish models are useful for visualizing melanoma development [13]. In addition to mice, nude rats are popular xenograft models of human melanoma. Another lab animal used in the study of malignant melanoma is the Syrian hamster, which is susceptible to spontaneous and chemically induced melanomas. The South American possum is highly susceptible to UV radiation-induced melanoma and has been used to study the genetics underlying melanoma susceptibility [33]. Miniature Sinclair swine develop spontaneous tumors ranging from benign nevi to malignant melanomas. Many of these tumors naturally regress subsequent to immune activation [34]. Finally, melanocytic tumors commonly occur in horses, representing up to 19% of cutaneous equine tumors. UV radiation is not thought to be a causative agent in the development of equine melanoma; instead, an autosomal dominant mutation resulting in constitutive activation of the ERK pathway is thought to contribute to melanoma formation. In contrast to human melanoma, many equine melanomas display a prolonged period of benign growth, which may or may not progress to malignant transformation and metastasis [20]. The study of melanoma in multiple species has led to a greater understanding of melanoma genetics, disease progression, and response to drug

therapies. However, mouse and canine melanoma remain the most extensively utilized models for the study of melanoma-immune system interactions and immunotherapeutic efficacy.

Section 3: The role of macrophages in the tumor microenvironment

Although the majority of immunotherapies focus on activating the adaptive immune system, the innate immune system also has the potential to mediate tumor rejection [35,36]. Macrophages are universally found in the tumor microenvironment [35] and represent up to 50% of tumor infiltrating leukocytes [37]. These cells have the potential to mediate anti-tumor immune responses and represent an important immunotherapeutic target [38].

Two macrophage phenotypes have been described, termed M1 and M2 [39,40]. Classically activated, or M1, macrophages are thought to act as pro-inflammatory mediators [37,39]. M1 macrophages have the potential to mediate robust anti-tumor immunity through phagocytic clearance of tumor cells, pro-inflammatory cytokine production, antagonism of myeloid-derived suppressor cells (MDSCs) and T regulatory cells, and antigen presentation to the adaptive immune system [37,39]. In particular, $CD169^+$ macrophages in the tumor microenvironment have been shown to phagocytose and cross-present antigens from apoptotic tumor cells. Cross-presentation, in which exogenous antigens are presented on MHC class I molecules, leads to the activation of cytotoxic $CD8^+$ T cells and promotes an anti-tumor adaptive immune response [41,42]. A number

of cancer therapies rely on the activity of M1 macrophages. For example, preclinical models of tumor specific antibodies suggest that cellular Fcγ receptors, particularly activating receptors on monocytes and macrophages (FcγRI, III, and IV in mice and FcγRIa, IIa, and IIIa in humans), are the central mediators of antibody activity and tumor depletion *in vivo* [43]. Antibodies against CD47 specifically aim to activate macrophage-mediated phagocytosis of tumor cells and will be discussed in detail later in this introduction (Section 3.4) [44].

In contrast, alternatively activated, or M2 macrophages are thought to produce anti-inflammatory cytokines, have poor antigen-presenting capability, and inhibit T cell responses. M2 polarized macrophages have been shown to promote tumor progression, angiogenesis, and metastasis in a number of cancer types, including breast, kidney, and bladder cancer [37].

Tumor associated macrophages (TAMs) are often thought to possess a cancer-promoting, “M2-like” phenotype. However, the tumor microenvironment is extremely heterogeneous, and recent studies have demonstrated that both M1 and M2 phenotypes are differentially distributed within solid tumor tissues [37]. In addition, TAMs may possess mixed phenotypes that display both M1 and M2 characteristics [40,45]. In these cells, the balance of immunosuppressive and inflammatory characteristics can be altered by environmental signals, which creates an opportunity to therapeutically bias these cells towards an anti-tumor phenotype [45,46].

There is some evidence that macrophages have the potential to mediate

anti-tumor immunity in malignant melanoma. In a preclinical mouse model of melanoma, antibody-mediated tumor-cell killing was found to be critically dependent on macrophage activity. In this model, $CD68^+$ macrophages containing ingested tumor material could be visualized within the tumor microenvironment [47]. This study suggests that macrophage-activating therapies may be efficacious in the treatment of malignant melanoma.

3.2 Regulation of phagocytosis: pro-phagocytic signals

One mechanism by which macrophages mediate anti-tumor immunity is through the phagocytosis and direct elimination of tumor cells. Phagocytosis relies on a balance of pro-phagocytic ("eat me") and anti-phagocytic ("don't eat me") signals expressed on the surface of target cells [48]. Several pro-phagocytic and anti-phagocytic signals have been identified and will be briefly reviewed here.

Pro-phagocytic signals, such as phosphatidylserine and calreticulin, are expressed on the surface of cells undergoing immunogenic cell death. In live cells, the phospholipid phosphatidylserine (PS) is asymmetrically distributed to the inner leaflet of the plasma membrane [49]. PS exposure on the outer leaflet of the membrane is one of the earliest events in apoptosis and occurs prior to the loss of membrane integrity [50]. Multiple receptors on the surface of macrophages are capable of recognizing PS (such as TIM family receptors and BAI1) and facilitating apoptotic cell engulfment. Although PS exposure is known

to provide a pro-phagocytic signal, whether this signal alone is sufficient to stimulate phagocytic uptake remains a matter of debate [50].

Calreticulin (CRT) is an endoplasmic reticulum (ER) chaperone protein exposed on the surface of cells during the ER stress response and is often expressed on pre-apoptotic cells prior to PS exposure [51]. Many cancer cells constitutively express cell surface CRT, which may be a consequence of cellular stress in the tumor microenvironment [51,52]. CRT promotes phagocytosis by binding to CD91 on the surface of phagocytic cells, including macrophages and dendritic cells. In addition, CRT exposure is thought to determine the immunogenicity of cancer cell death by promoting the phagocytosis of dying cancer cells by $CD11c^+$ dendritic cells, which subsequently present tumor-associated antigens to anti-tumor T cells and stimulate an anti-tumor immune response [51,53]. CRT exposure and immunogenic cell death can be induced by treatment with chemotherapy drugs in the anthracycline class, such as doxorubicin [53].

3.3 Regulation of phagocytosis: anti-phagocytic signals

Anti-phagocytic, or “don’t eat me,” signals play an important physiologically role by inhibiting the phagocytosis of normal somatic cells. The best-characterized “don’t eat me” signal is CD47, a cell surface molecule that inhibits phagocytosis by binding to SIRPα on the surface of phagocytes [48]. CD47 is a member of the immunoglobulin superfamily of membrane proteins and contains five membrane spanning segments with a single extracellular

immunoglobulin variable domain [54]. CD47's corresponding receptor, signal-regulatory protein alpha (SIRPα) [55], is a receptor tyrosine kinase that is highly expressed on the surface of myeloid cells, including macrophages, granulocytes, monocytes, and myeloid-derived dendritic cells [56]. Ligation of SIRPα's extracellular domain by CD47 results in phosphorylation of an intracellular immunoreceptor tyrosine-based inhibitory motif (ITIM) and activation of the inhibitory phosphatases SHP-1 and SHP-2 [57]. The resulting signaling cascade inhibits the accumulation of myosin within the phagocytic synapse and prevents the contractile engulfment of target cells [58].

The first evidence that CD47 acts as a "don't eat me" signal came from experiments demonstrating that loss of CD47 leads to the removal of aged or damaged red blood cells by splenic macrophages [59]. CD47 has a similar role in platelet removal [60], and it has been shown that circulating hematopoietic stem cells upregulate CD47 expression to avoid macrophage-mediated clearance [61]. Further studies demonstrated that CD47 is ubiquitously expressed on normal tissues and acts as a marker of self to prevent cell phagocytosis [48,62].

Although CD47 was first identified as a tumor antigen on ovarian cancer cells [63], it has since been identified on all cancer cells tested, including hematopoietic and solid tumors [1,44]. Multiple tumor types display increased expression of CD47 compared to their normal cell counterparts, and increased expression of CD47 is associated with poor clinical prognosis in acute myeloid leukemia (AML), acute lymphoblastic leukemia (ALL), Non-Hodgkin's lymphoma

(NHL), ovarian cancer, and glioblastoma [61,64-66]. Therefore, it is thought that CD47 acts as a mechanism of immunoevasion by inhibiting cancer cell phagocytosis [1].

3.4 Therapeutic targeting of the CD47/SIRPα axis

The identification of CD47 on the surface of human cancer cells and its proposed role in immunoevasion led to the development of therapies to inhibit the CD47-SIRPα pathway. These therapies include anti-CD47 monoclonal antibodies [67], recombinant SIRPα proteins [44], SIRPα mimotopes [68], and bispecific molecules targeting CD47 along with a tumor-specific antigen [69,70]. The efficacy of CD47 blocking therapies was first examined in a preclinical model of AML [64]. Treatment with anti-CD47 antibodies led to macrophage phagocytosis of AML cells *in vitro* and demonstrated anti-tumor effects in xenograft models of human AML as well as immunocompetent models of mouse AML [64]. Additional studies demonstrated the efficacy of CD47 blockade in a number of hematopoietic tumors, including ALL [71], NHL [65], and multiple myeloma [72]. Recently, CD47 blockade has been shown to stimulate phagocytosis and suppress tumor growth in preclinical models of a number of solid tumors, including ovarian [66], breast [66,73], bladder [66], leiomyosarcoma [74], colon [75], pancreatic [76], and lung [77] cancers. Based on these promising preclinical results, a number of phase I and II clinical trials investigating the use of anti-CD47 monoclonal antibodies and recombinant SIRPα polypeptides in the treatment of both hematopoietic and solid tumors are currently underway [44].

In addition to being a potential therapeutic target for human malignant melanoma, CD47 blockade has the potential to stimulate anti-tumor immune responses for the treatment of canine malignant melanoma. The CD47-SIRPα axis is conserved both biologically and functionally in canine tumor cells, and high affinity SIRPα variants have demonstrated efficacy in a mouse xenograft model of canine lymphoma [78].

3.5 CD47 blockade: mechanisms of action

CD47 blockade mediates anti-tumor immunity through a variety of effector mechanisms (Figure 1-1). The majority of preclinical studies to date have investigated the effects of CD47 blockade on macrophage activation. These studies used fluorescent microscopy and flow cytometry to demonstrate an increase in macrophage-mediated phagocytosis of tumor cells *in vitro* following CD47 blockade [64-66,68]. The role of macrophages as the primary mediators of anti-tumor immunity following CD47 blockade has been supported by *in vivo* studies in which clodronate-mediated macrophage depletion abrogated the anti-tumor effects of an anti-CD47 antibody [64,65]. CD47 blockade is also capable of promoting tumor regression in immunocompromised, B and T cell deficient mice, in which macrophages are the most likely effectors of an anti-tumor immune response [64-66]. In addition, CD47 blockade was shown to alter the activation state of tumor associated macrophages by converting these cells from an M2 phenotype to a pro-inflammatory, anti-tumor (M1) phenotype [79]. There is also some evidence that CD47-blocking therapies promote additional recruitment of

macrophages. One study demonstrated that phagocytosis in response to CD47 blockade stimulated the production of cytokines and chemokines, including monocyte-chemotactic protein 3 (MCP-3), that have the potential to recruit additional phagocytes to the tumor microenvironment [77]. Based on these studies, macrophages likely play a major role in the immune response following CD47 blockade.

While enhanced macrophage-mediated phagocytosis is generally thought to be responsible for the anti-tumor effects of CD47 blockade, a number of other immune cells express SIRPα and are capable of responding to CD47-targeted therapies. One study demonstrated an increase in neutrophil antibody-dependent cellular cytotoxicity (ADCC) in a preclinical model of breast cancer following CD47 blockade [80]; however, this effect may be reliant on the specific anti-CD47 antibody isotype used in the study [1]. Natural killer (NK) cells also express CD47, but the effects of CD47 blockade on NK cell activation are currently unclear: one study demonstrated NK cell-mediated ADCC of head and neck cancer cells following CD47 blockade [80] while another study found no direct effect of CD47 blockade on NK cell activity [65]. Further studies are needed to elucidate the effects of CD47-targeting therapies on NK cell activation. Finally, myeloid-derived dendritic cells (DCs) express SIRPα [81,82] and are capable of phagocytosing tumor cells in response to CD47 blockade [75,82,83]. In addition to regulating phagocytosis, ligation of SIRPα by CD47 suppresses DC maturation

and cytokine production [84], thus inhibiting DC activation and functional responses.

In addition to activating the innate immune response, CD47 blockade promotes an anti-tumor adaptive immune response in immunocompetent mouse models. Treatment with anti-CD47 antibodies promotes antigen presentation by both macrophages and DCs *in vitro* [75,83]. *In vivo,* adoptive transfer of macrophages following CD47-mediated phagocytosis of colon cancer cells was able to protect immunocompetent mice from subsequent tumor challenge [75]. Another study using preclinical models of lung cancer and lymphoma demonstrated that the anti-tumor effects of CD47 blockade were reliant on cross-presentation of antigens by $CD11c^+$ DCs to $CD8^+$ T cells. In this study, the therapeutic effects of CD47 blockade were abrogated in T cell-deficient mice, which indicates that T cells also play a key role in the anti-tumor response following CD47 blockade [83]. The effects of CD47-targeted therapies on the adaptive immune response suggest that these therapies may synergize with existing immunotherapies to promote anti-tumor immune responses. Although further exploration of immunotherapeutic combinations is needed, one study suggests CD47 blockade may synergize with anti-PD-1 therapy to mediate an anti-tumor immune response [85].

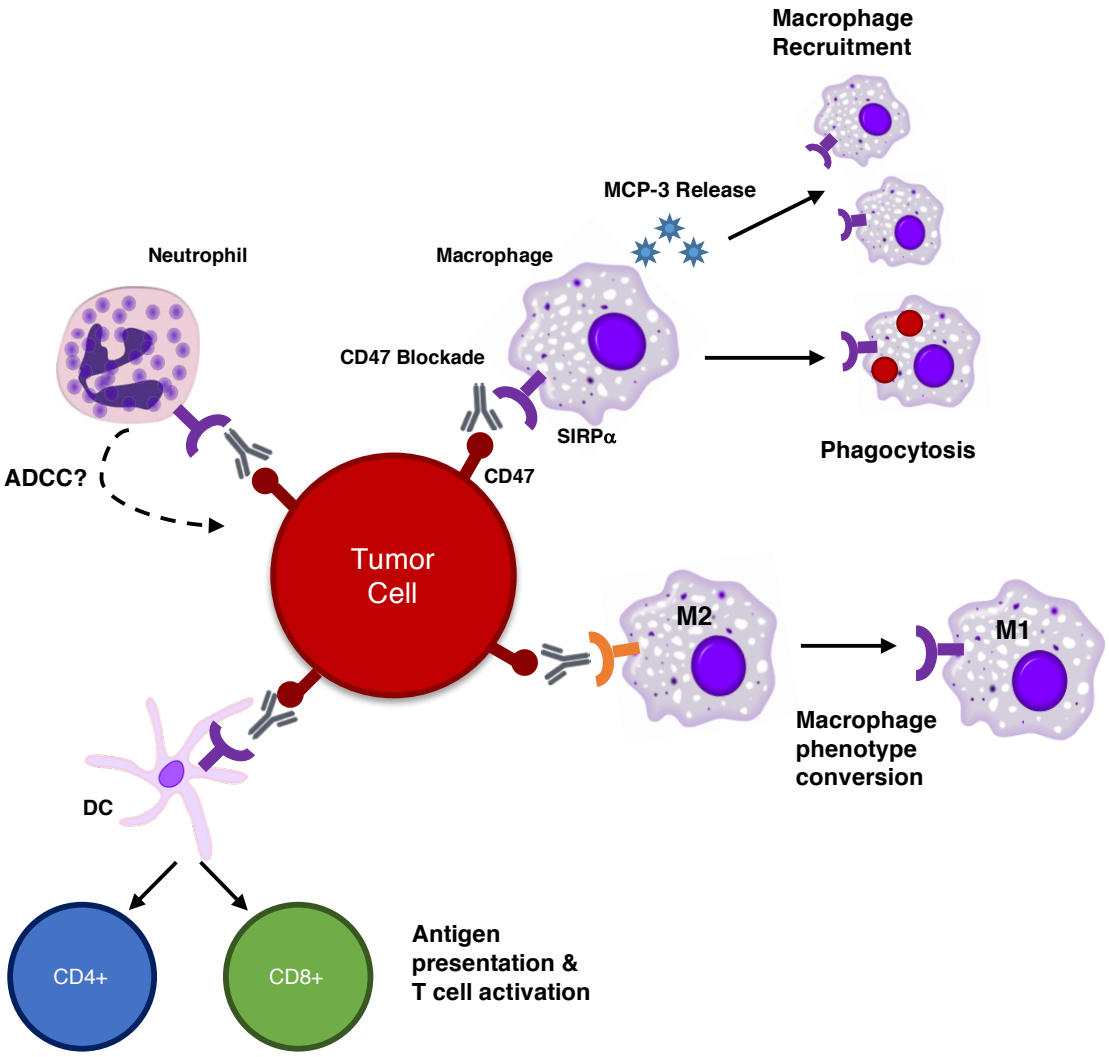

Figure 1-1: Mechanisms of action for CD47 targeting therapies. CD47 blockade has the ability to mediate anti-tumor immunity through several mechanisms. Macrophage-mediated phagocytosis can eliminate tumor cells directly and lead to the production of cytokines, such as MCP-3, which recruit additional macrophages to the tumor microenvironment. CD47 blockade may also convert pro-tumor, M2 macrophages to a more anti-tumor, M1 phenotype. Depending on the isotype of the anti-CD47 antibody used, neutrophil ADCC may be induced through Fc dependent mechanisms. Finally, CD47 blockade can enable phagocytosis and antigen presentation to activate anti-tumor $CD4^+$ and $CD8^+$ T cells. (Figure based on ref [1]).

3.5 Combination strategies to enhance macrophage-mediated phagocytosis

Therapeutic strategies that provide a pro-phagocytic stimulus have the potential to synergize with CD47 blockade to mediate tumor rejection. Indeed, there is some evidence that pro-phagocytic signals are required for phagocytosis following CD47 blockade. Although CD47 is expressed on both tumor cells and their normal cell counterparts, CD47 blockade leads to the selective elimination of tumor cells while the majority of normal cells fail to undergo phagocytosis [52,64,65]. To explain this contradictory result, one study examined cell surface expression of the pro-phagocytic signal calreticulin (CRT) and found that some tumor cells express CRT on their cell surface while normal cells do not (Figure 1-2) [52]. shRNA knockdown of CRT abrogated the effects of CD47 blockade on phagocytosis, demonstrating that, in addition to blocking a “don’t eat me signal,” an “eat me” signal must be present for phagocytosis to occur [52]. Thus, treatment strategies which promote additional CRT expression, such as anthracycline chemotherapy, have the potential to synergize with CD47 blockade. While promising, these combination strategies have yet to be examined in preclinical models.

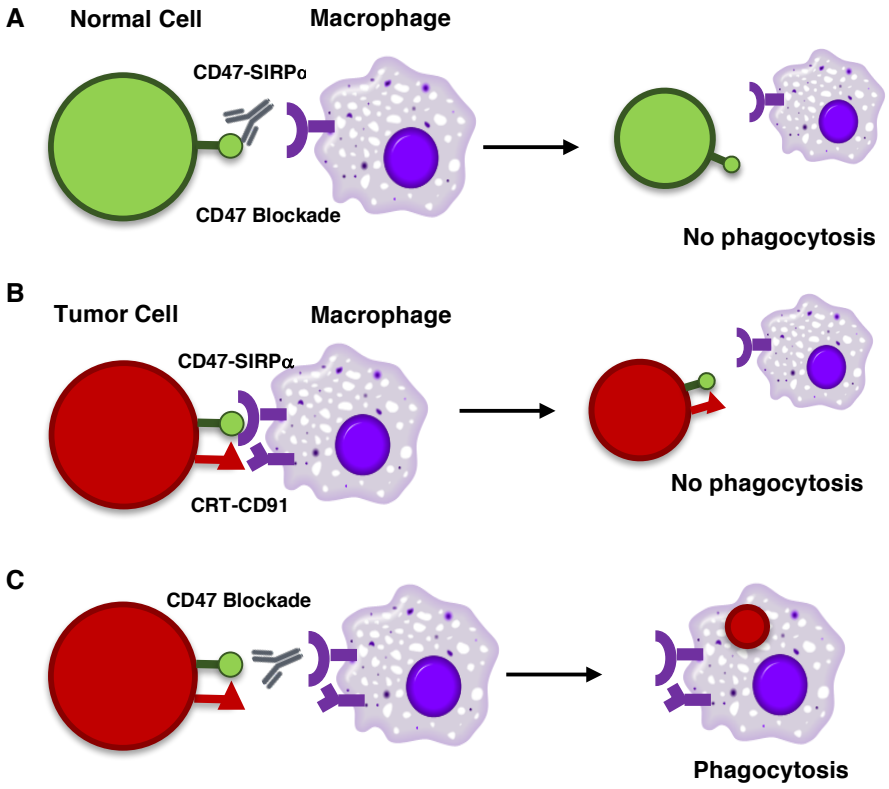

Figure 1-2: Pro-phagocytic signals are necessary to enable phagocytosis following CD47 blockade. A. In the presence of CD47 blockade, normal, non-apoptotic cells are not phagocytosed due to the lack of "eat me" signal expression. B. Some tumor cells express the "eat me" signal calreticulin (CRT) on their surface, but expression of CD47 inhibits the phagocytosis of these cells. C. In the presence of CD47 blockade, CRT provides a pro-phagocytic stimulus to macrophages, which results in tumor cell phagocytosis.

Antibody Fc chains provide a robust stimulus for macrophage activation and phagocytosis [86], and a number of studies have examined the effects of combining anti-CD47 antibodies with tumor-specific antibodies capable of stimulating Fc-mediated functions. Combination CD47 blockade and rituximab or trastuzumab led to synergistic tumor elimination in preclinical models of NHL and breast cancer, respectively [65,80]. In addition, SIRPα monomers, which block CD47 but do not provide a Fc stimulus, synergized with rituximab, trastuzumab,

and cetuximab to promote tumor cell phagocytosis *in vitro* [68]. A number of these antibody combinations are currently under investigation in phase I clinical trials [44]. Again, these studies demonstrate that combining blockade of a “don’t eat me” signal with strategies to provide a “eat me” signal have the potential to synergistically result in an anti-tumor immune response.

3.6 Modulation of phagocytic signals for the treatment of malignant melanoma

Although therapies targeting the CD47-SIRPα axis have demonstrated efficacy in a variety of hematopoietic and solid tumor types [64-66], the effect of blocking CD47 for the treatment of malignant melanoma is unclear. The first paper to evaluate the effects of CD47 blockade on melanoma growth treated a syngeneic mouse model of melanoma (B16 melanoma) using intravenous delivery of a CD47-targeting siRNA [87]. This paper showed a small increase in melanoma cell phagocytosis (from 2 to 14%) following siRNA knockdown of CD47 *in vitro* as well as a reduction in tumor volume following CD47 siRNA administration *in vivo.* Although effective, siRNA-mediated knockdown of CD47 is unlikely to be therapeutically relevant in clinical trials. A second paper examining the effects of CD47 blockade in a B16 mouse model of melanoma demonstrated no increase in tumor cell phagocytosis and no inhibition of tumor growth following treatment with a more therapeutically relevant anti-mouse CD47 nanobody [85]. This paper suggested CD47 blockade alone is insufficient to overcome immune resistance in melanoma. Finally, a recent article utilized an anti-CD47 antibody

for the treatment of primary human melanoma xenografts. This article demonstrated an increase in melanoma cell phagocytosis *in vitro* as well as a decrease in tumor metastasis *in vivo* following CD47 blockade [88]. The contradictory results of these studies indicate that a systematic evaluation of melanoma cell sensitivity to phagocytosis and to CD47 blockade is needed. In addition, the effects of modulating pro-phagocytic signals in combination with CD47 blockade has yet to be examined for the treatment of malignant melanoma. My objective in this dissertation was to characterize the anti-tumor immune response following modulation of pro-phagocytic and anti-phagocytic signals in malignant melanoma.

In this study, we utilized a multi-species approach and compared the responses of human, mouse, and canine melanoma cells to phagocytosis. In order to provide a framework for preclinical testing, it is important to understand the similarities and differences in melanoma cell biology between species. Identifying similarities in tumors from multiple species could reveal evolutionarily conserved mechanisms of immunoevasion that are likely to be important for tumor cell survival. However, it is equally important to understand the differences in human melanoma cell biology as compared to mouse or canine cells in order to avoid over interpretation of data gained from animal models. Using a multi-species approach to advance our understanding of how melanoma cells avoid elimination by the innate immune system may lead to the development of new

therapeutic strategies to improve patient responses and overcome resistance in the subset of patients who currently fail to respond to immunotherapies.

Chapter 2

Materials and Methods

MATERIALS AND METHODS

Cell lines and culture: Lymphoma cell lines: The CLBL-1 canine diffuse large B-cell lymphoma cell line [89] was obtained from Dr. Barbara Rütgen (University of Vienna, Austria) and grown in Iscove's Modified Dulbecco's Medium (IMDM) (Invitrogen, Carlsbad, California, USA) supplemented with 20% fetal bovine serum (Peak Serum, Fort Collins, Colorado, USA), 1% L-glutamine (Sigma-Aldrich, St. Louis, Missouri, USA), and 100 μg/mL Primocin (Invitrogen, Carlsbad, California, USA). A20 mouse B cell lymphoma cells (ATCC, Manassas, Virginia, USA) and Raji human B cell lymphoma cells (ATCC, Manassas, Virginia, USA) were cultured in RPMI 1640 supplemented with 10% fetal bovine serum (Peak Serum, Fort Collins, Colorado, USA), 1% L-glutamine (Sigma-Aldrich, St. Louis, Missouri, USA), 2 mM sodium pyruvate (Gibco, Gaithersburg, Maryland, USA), 10 mM HEPES buffer (HyClone, Logan, Utah, USA), 1% non-essential amino acids (Gibco, Gaithersburg, Maryland, USA), and 100 μg/mL Primocin (Invitrogen, Carlsbad, California, USA). Melanoma cell lines: The M21 and M21-GFP human melanoma cell lines were obtained from Dr. David Cheresh (University of California San Diego, USA). B16-OVA mouse melanoma cells were obtained from Dr. Ross Kedl (University of Colorado Denver, USA). Canine melanoma cell lines TLM1, CMGD2, and CMGD5 were obtained and cultured as described [90,91]. Breast cancer cell lines: The canine breast cancer cell line CMT12 was obtained from Dr. Curtis Bird (Auburn University, USA), and the feline breast cancer cell line K12 was obtained from Dr. Bill Hardy (Rockefeller

University, USA [92]). The mouse breast cancer cell line 4T1 was obtained from Dr. Kaylee Schwertfeger (University of Minnesota, USA) and was cultured in RPMI 1640 (Gibco, Gaithersburg, Maryland, USA) supplemented with 10% fetal bovine serum, 1% L-glutamine (Sigma-Aldrich, St. Louis, Missouri, USA), 2 mM sodium pyruvate (Gibco, Gaithersburg, Maryland, USA), 10 mM HEPES buffer (HyClone, Logan, Utah, USA), and 100 μg/mL Primocin (Invitrogen, Carlsbad, California, USA). Osteosarcoma cell lines: The canine osteosarcoma cell lines OSCA-40 and OSCA-78 were obtained and cultured as described [93]. The human osteosarcoma cell line SAOS2 was obtained from ATCC (Manassas, Virginia, USA), and the mouse osteosarcoma cell line K12 was obtained from the National Cancer Institute. Note: Both the feline breast cancer and mouse osteosarcoma cell lines were originally named K12. Throughout this manuscript, the feline cell line will be referred to as K12, and the mouse line as K12 mOS. All melanoma, osteosarcoma, and breast cancer lines as well as J774 macrophages (ATCC, Manassas, Virginia, USA) were cultured in Dulbecco's Modified Eagle Medium (Thermo Fisher Scientific, Waltham, Massachusetts, USA) with 10% fetal bovine serum (Peak Serum, Fort Collins, Colorado, USA) and 100 μg/mL Primocin (Invitrogen, Carlsbad, California, USA) unless otherwise noted.

Therapeutic agents: The high-affinity SIRPα protein CV1-hIgG4 [68] and the anti-CD47 monoclonal antibody Hu5F9-G4 [67] were produced as previously described and provided by Dr. Irving Weissman (Stanford University, USA). The corresponding isotype control antibody, huIgG4, the mouse anti-CD47 antibody

MIAP301, and its corresponding isotype control antibody, mIgG2a, were obtained from eBioscience (San Diego, California, USA). CD271 monoclonal antibody (clone ME20.4) was obtained from eBioscience (San Diego, California, USA).

Detection of CD47 expression and blocking of the CD47/SIRPα axis: CD47 expression was analyzed using Alexa Fluor 488 Hu5F9-G4, BV786 mouse anti-human CD47 (Clone B6H12, BD Biosciences, San Jose, California, USA), or PE anti-mouse CD47 (Clone MIAP301, Biolegend, San Diego, California, USA). Briefly, $1x10^6$ cells of each cell line were incubated with normal mouse immunoglobulin for 10 minutes on ice. Cells were subsequently labeled using Alexa Fluor 488 Hu5F9-G4, BV786 mouse anti-human CD47, PE anti-mouse CD47, or an isotype control antibody (Biolegend, San Diego, California, USA) and incubated on ice for 30 minutes. Analysis was performed using a LSRII flow cytometer (BD Biosciences, San Jose, California, USA), and geometric mean fluorescence intensity was determined using FlowJo (Tree Star, Ashland, Oregon, USA). To analyze the blocking ability of CV1-hIgG4, $1x10^6$ cells of each line were incubated with varying concentrations of CV1-hIgG4 for 15 minutes on ice. Cells were subsequently labeled using Alexa Fluor 488 Hu5F9-G4 and incubated on ice for 30 minutes. Analysis was performed as described above, and data were fit to sigmoidal dose-response curves using Prism 6 (GraphPad, La Jolla, California, USA).

Macrophage phagocytosis assays: J774 mouse macrophages were activated 24 hours prior to phagocytosis assays using 100 ng/mL recombinant mouse IFNγ

(eBioscience, San Diego, California, USA). Cancer cells used in the assay were either GFP+ or labeled with CFSE according to the manufacturer's protocol (Thermo Fisher Scientific, Waltham, Massachusetts, USA). Cancer cells were incubated with CD47 blocking reagents or isotype controls (10 μg/mL) for 30 minutes prior to the assay. 50,000 J774 mouse macrophages were then co-cultured in 96 well non-adherent plates with 50,000 cancer cells (1:1 ratio). Phagocytosis in response to therapeutic treatments was evaluated after two hours of co-culture and analyzed by flow cytometry (Figure 2-1). Macrophages were identified by staining with PE/Cy7 or APC-anti-mouse F4/80 as described above (Biolegend, San Diego, California, USA). Phagocytosis was evaluated using a LSRII flow cytometer (BD Biosciences, San Jose, California, USA) and analyzed using FlowJo (Tree Star, Ashland, Oregon, USA) as the percentage of F4/80+ J774 cells that engulfed CFSE+/GFP+ tumor cells per total F4/80+ population (Figures 2-2, 2-3). Dead cells were excluded using propidium iodide (PI, Biolegend, San Diego, California, USA) to eliminate non-specific staining. If excessive macrophage or tumor cell death occurred (macrophages represented <40% or >60% of the total cell population), the assay was not included in the final analysis as the assay is designed to test a 1:1 macrophage: tumor cell ratio. This occurred in approximately 2% of phagocytosis assays performed. For soluble factor assays, Raji cells and J774 macrophages were suspended in supernatant harvested from cultured M21 melanoma cells titrated with new IMDM medium for the duration of the phagocytosis assay. Alternatively, M21 cells and J774

macrophages were suspended in supernatant harvested from cultured Raji melanoma cells titrated with new IMDM medium for the duration of the phagocytosis assay.

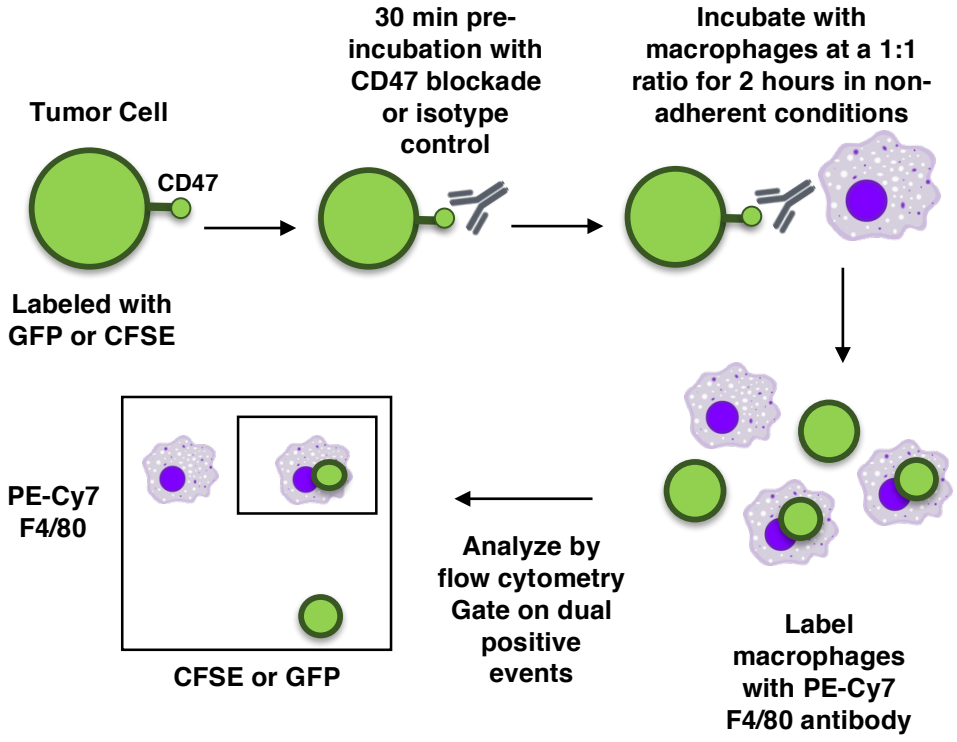

Figure 2-1: Schematic of phagocytosis assays

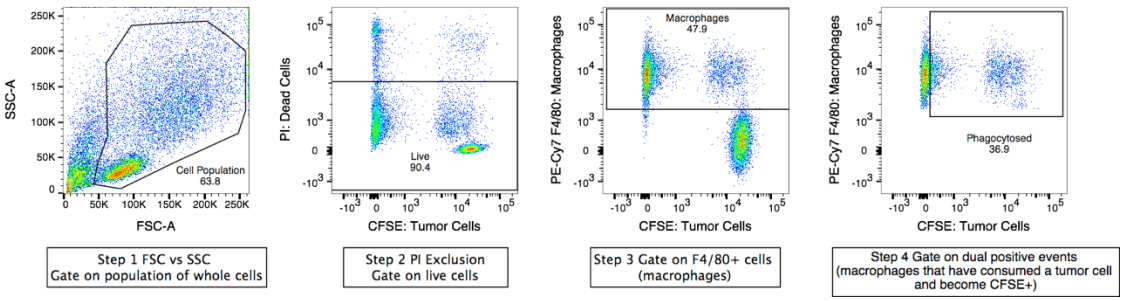

Figure 2-2: Schematic of the gating scheme for phagocytosis assays. Analysis was performed in FlowJo v10.2. Gates are set based on unstained cells or macrophages stained with PE-Cy7 F4/80 alone.

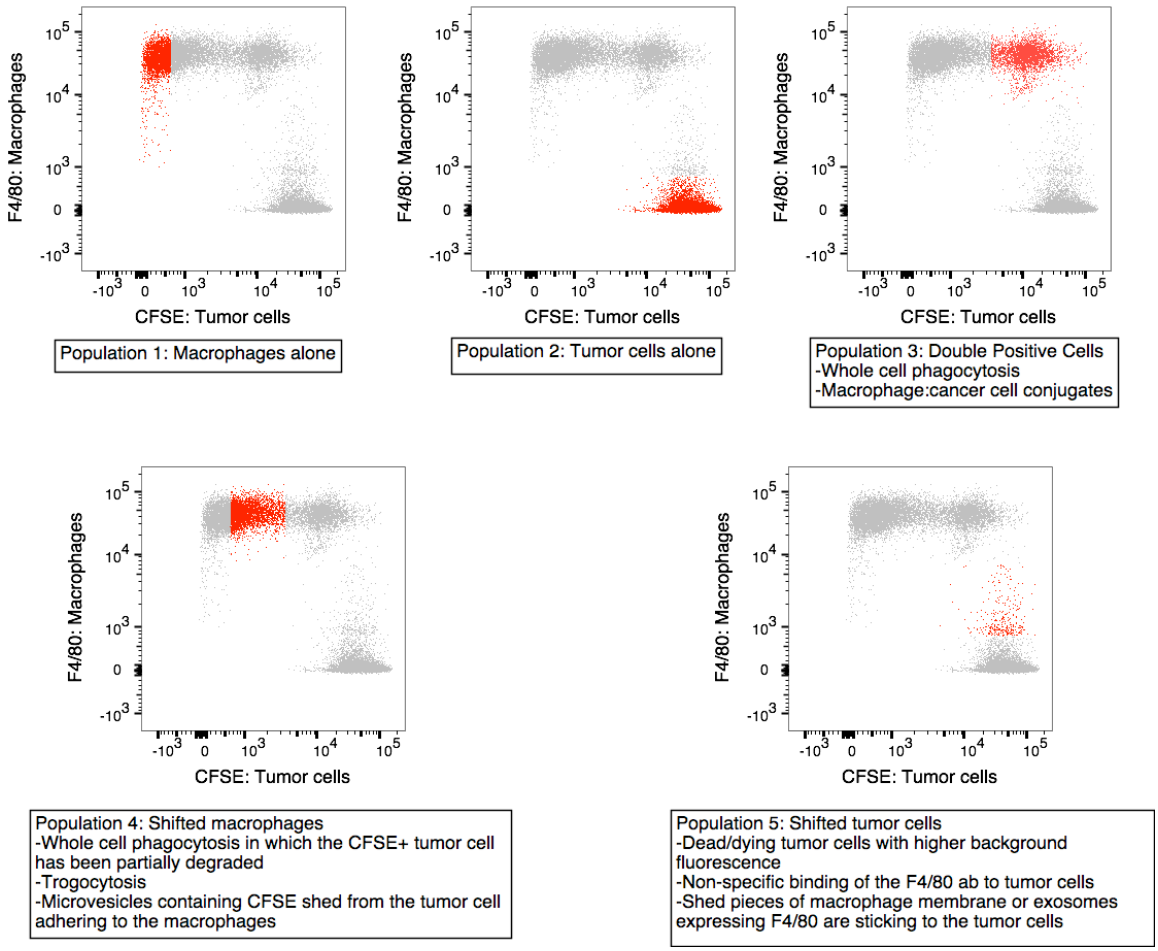

Figure 2-3: Rationale for the phagocytosis assay gating scheme. Populations 3 and 4 have the potential to contain whole cell phagocytosis; therefore, the phagocytosis gating scheme includes these two populations.

Chemotherapeutic Treatment: B16-OVA cells were treated with 0.03 μM doxorubicin chemotherapy (Teva Parenteral Medicines, Inc, Israel) for 24 hours prior to analysis or to placement in a phagocytosis assay (as described above). To analyze pro-phagocytic signal expression, cells were harvested and stained with propidium iodide and APC Annexin V according to the manufacturer's protocol (Biolegend, San Diego, California, USA). Display of membrane phosphatidylserine exposure was evaluated by flow cytometry and is represented

by the %Annexin V+PI- cells. Alternatively, cells were labeled with an Alexa Fluor 647 anti-mouse calreticulin antibody (clone ERP3924, Abcam, Cambridge, United Kingdon) and incubated on ice for 30 minutes prior to flow cytometry analysis on a LSRII flow cytometer (BD Bioscience, San Jose, California, USA) and data analysis using FlowJo (Tree Star, Ashland, Oregon, USA).

Brefeldin A Treatment: M21-GFP or Raji cells labeled with CFSE were incubated with 5.0 μg/mL Brefeldin A solution (Biolegend, San Diego, California, USA) for two hours prior to placement in a phagocytosis assay (as described above). 5.0 μg/mL Brefeldin A solution was added to the phagocytosis assay medium to ensure continued secretory inhibition.

Clustering of TCGA expression data for extracellularly expressed proteins: The results published here are in whole or part based upon data generated by the TCGA Research Network: http://cancergenome.nih.gov/. Uniformly processed TCGA expression data in transcripts per million (TPM) was obtained from GEO accession GSE62944 [94]. Extracellular genes were identified using the COMPARTMENTS database [95] and GOType labels plasma membrane, cell surface, extracellular region, extracellular matrix and a score > 4. Expression data for these extracellular genes (n = 5,082) in the cancer types of interest (DLBC, COAD, BRCA, LUAD, LUSC and SKCM) was isolated and used in further analysis. Variance of expression was calculated for each gene across all tumor samples and the top 500 most variable genes were clustered based on gene expression values using Euclidean distance.

siRNA literature-based selection: 48 genes were included in the siRNA panel (Table 2-1). All of these genes (except Bcl-2) are expressed on the surface of melanoma cells based on a literature search (PubMed) and using the COMPARTMENTS online subcellular localization database [95]. Bcl-2 was chosen as a control on the basis that siRNA knockdown of this gene should increase cell apoptosis. The other genes were chosen based on 1 of 4 criteria: (1) the gene has been identified as a "don't eat me" signal in the literature, (2) gene expression is restricted almost exclusively to melanoma cells, (3) the gene has been shown to contribute to melanoma cell growth and metastasis or (4) the gene has been associated with immune suppression in the tumor microenvironment. Some of the genes selected are also expressed on phagocytosis-sensitive cells; however, we did not exclude these genes as melanoma cells may post-translationally modify these proteins in a way that causes them to act as an anti-phagocytic signal.

Table 2-1: Rationale for siRNA gene selection

Gene Symbol	Gene Name	Rationale	References
BCL2	Bcl-2	Anti-apoptotic protein; siRNA KD should increase cell death (control)	[96]
CD200	CD200	"Don't eat me" signal expressed on myeloid cells and the CNS; binds to CD200R on macrophages to inhibit macrophage activation (role in phagocytosis unclear)	[48]
PECAM1	Pecam-1 or CD31	"CD31 prevents phagocyte engulfment of leukocytes in a homophilic manner by transmitting detachment signals from the phagocyte...Thus, CD31 functions as a don't eat me signal by regulating tethering between the phagocyte and the target cell." Also interacts with $\alpha v\beta 3$ integrin (see the αv or $\beta 3$ integrin sections)	[48,97]

CD151	CD151	Tetraspanin. Promotes B16F10 metastasis and melanoma cell invasion. Expressed on the plasma membrane of human melanoma cells	[98,99]
CD81	CD81	Tetraspanin. Enhances melanoma cell motility and invasion. Expressed on the surface of melanoma cells. Shown to have an immunosuppressive role in the TME (promotes Treg and MDSC function)	[100,101]
SERPINE1	PAI-1	Expressed on neutrophils and endothelial cells. Acts as a “don’t eat me” signal; however, the receptor on macrophages is unknown (may inhibit CRT)	[48]
ANXA1	Annexin 1	Anti-inflammatory mediator. Inhibits macrophage PG and NO production. Inhibits phagocytic activity of peritoneal macrophages	[102]
MIF	Macrophage migration inhibitory factor (MIF)	Necessary for MDSC activation and immune suppression. Inhibits macrophage migration. Promotes melanoma cell proliferation, cell survival, and anchorage-independent growth. Poor prognostic indicator in melanoma	[103,104]
SELPLG	PSLG-1	Augments the growth and metastasis of B16 melanoma. However, absent on other tested melanoma cell lines. Has been shown to act as a T cell checkpoint molecule	[105,106]
ECM1	Extracellular matrix protein 1	Overexpressed in melanoma; important for melanoma cell attachment	[107]
CDH1	Cadherin-1 (E-cadherin)	Expressed in melanoma cells; associated with benign/low grade tumors. Loss of CDH1 correlates with metastasis. Increases growth through beta-catenin signaling; plays a role in the early metastatic cascade	[97,108,109]
CDH2	Cadherin-2 (N-cadherin)	Expressed in melanoma cells; associated with high grade/metastatic tumors. Loss of CDH1 and gain of CDH2 correlated with metastasis. Increases melanoma cell survival, metastasis, and invasion. Mediates communication between melanoma cells and fibroblasts	[97,109]
CDH3	Cadherin-3 (P-cadherin)	Expressed in melanoma cells; associated with benign/low grade tumors	[110,111]
CLDN1	Claudin 1	Overexpressed in melanoma; contributes to melanoma cell motility, invasion, and MMP expression	[112]
CLDN12	Claudin 12	Expressed in melanoma cells	[113]
ALCAM	Activated leukocyte cell adhesion molecule or CD166	Mediates cell-cell adhesion in invading melanoma. Regulates adherens junctions and may increase invasiveness	[114,115]

MCAM	Melanoma cell adhesion molecule or CD146 or MUC18	Mediates cell-cell adhesion in melanoma; overexpression activates the AKT pathway in melanoma. Increases MMP-2 expression to promote invasion. Upregulates FAK to protect cells from anoikis. Contributes to melanoma metastasis and tumorigenicity. Binds to galectin-1 on immune cells and endothelial cells to dampen anti-tumor immunity and promote angiogenesis	[114,116,117]
NCAM1	Neural cell adhesion molecule 1	Potentiates melanoma cell growth, invasion, and metastasis. Regulates Wnt signaling in B16 cells	[118]
CEACAM1	Carcinoembryonic antigen-related cell adhesion molecules 1	Expressed in melanoma; correlates with metastatic spread, invasion, tumor growth. Linked to inflammation and angiogenesis	[119]
BCAM	Basal cell adhesion molecule	BCAM has an amino acid sequence with structural homology to MUC18; may have related effects on phagocytosis (could see multiple hits by targeting similar genes)	[120]
L1CAM	L1 cell adhesion molecule	Overexpressed in melanoma; associated with poor prognosis and advanced disease. Induces a motile and invasive phenotype and supports aggressive tumor growth, metastasis, and chemoresistance. Can interact with several integrins to promote cell adhesion and motility. Can activate NFkB in tumor cells to promote growth	[121]
MADCAM1	Mucosal vascular addressin cell adhesion molecule-1	Expressed on B16 cells; may play a role in melanoma cell aggregation/homotypic interactions	[122]
EPCAM	Epithelial cell adhesion molecule	Not expressed in most melanomas; is involved in macrophage-tumor cell fusions isolated from the blood of melanoma patients.	[123]
F11R	Junctional adhesion molecule A (JAM-A)	Involved in melanoma cell transmigration	[124]
JAM3	Junctional adhesion molecule C (JAM-C) or 3	Involved in melanoma cell transmigration and metastasis	[124,125]
ITGAV	Integrin alpha v subunit	In most melanomas, the αv subunit forms complexes with the β1, β3, β5, or β6 subunits. Expressed regardless of disease stage. $\alpha v\beta 3$ integrin expression correlates with poor prognosis and metastasis. *In vitro* blockade assays suggest a role in growth and invasion. However, effects may depend on stage; it has been suggested that $\alpha v\beta 3$ plays a critical role in the transition from	[97]

		radial to vertical growth phases. Plays a role in localizing MMP-2 to the cell surface and in transendothelial migration through PECAM/L1 interactions.	
ITGA2	Integrin alpha 2 subunit	Expression on advanced tumors/metastasis. Involved in melanoma progression and motility, correlates with metastasis.	[126]
ITGA3	Integrin alpha 3 subunit	Overexpressed in 85% of human metastatic melanoma; expressed in all canine lines tested. Associated with increased cell motility, invasiveness, and metastasis in mouse models	[127]
ITGA4	Integrin alpha 4 subunit	Expressed on melanoma cells; may mediate adhesion to activated endothelial cells during metastasis	[128]
ITGA5	Integrin alpha 5 subunit	Expressed on melanoma; may be involved in invasion of the basement membrane and metastasis	[128]
ITGA6	Integrin alpha 6 subunit	Expressed on melanoma in low levels; pairs with β1 as a laminin receptor	[128]
ITGA7	Integrin alpha 7 subunit	Expressed on melanoma cells (complexed with β1). Rarely expressed on other cancer types	[128]
ITGB1	Integrin beta 1 subunit	Pairs with αv to mediate melanoma cell attachment to the basement membrane	[128]
ITGB3	Integrin beta 3 subunit	In most melanomas, the β3 subunit predominantly pairs with the αv subunit. Primarily expressed in the vertical growth phase; correlates with poor prognosis. αvβ3 integrin expression correlates with poor prognosis and metastasis. *In vitro* blockade assays suggest a role in growth and invasion. However, the effects may depend on stage; it has been suggested that αvβ3 plays a critical role in the transition from radial to vertical growth phases. Plays a role in localizing MMP-2 to the cell surface and in transendothelial migration through PECAM/L1 interactions.	[97]
ITGB4	Integrin beta 4 subunit	Expressed by B16 cells. Involved in metastasis: binds to ligands on endothelial cells during transmigration to the lung. Associated with FAK complexing, activation, and signaling.	[129]
ITGB5	Integrin beta 5 subunit	Expressed in M21 melanoma cells; involved in adhesion to vitronectin	[130]
ICAM1	Intercellular adhesion molecule 1	Expressed on melanoma cells	[131]
AGER	Advanced glycosylation end-	Upregulated in melanoma; levels are highest in stage 4 melanoma. Involved in melanoma cell metastasis	[132,133]

	product specific receptor or RAGE		
LGALS1	Galectin-1	Expressed by immune cells, endothelial cells, and some cancer cells. Proangiogenic effects, protects melanoma cells from the action of anti-tumor cytolytic T-cells, confers chemoresistance.	[134]
LGALS3	Galectin-3	Involved in melanoma metastasis and invasion; increases MMP activity. Leads to T cell apoptosis in the tumor microenvironment. Stimulates angiogenesis.	[134]
DSC3	Desmocollin 3	Expression is associated with a lack of a Th1 immune signature in melanoma	[135]
CAV1	Caveolin 1	Expressed in melanoma; mediates beta-catenin signaling to promote melanomagenesis and metastasis	[136]
ST8SIA1	Ganglioside GD3 synthase	Type II membrane protein that catalyzes the transfer of sialic acid from CMP-sialic acid to GM3 to produce gangliosides GD3 and GT3. GD3 enhances melanoma cell adhesion and recruits integrins to lipid rafts	[137,138]
MLANA	Melan-A, MART-1, melanoma antigen recognized by T-Cells 1	Melanoma antigen often used for IHC diagnosis of melanoma. Expression very restricted to melanoma; often used as an antigen to activate anti-tumor CD8+ cells	[139,140]
PMEL	Melanocytes lineage-specific antigen GP100 premelanosome protein	Melanocyte-specific type I transmembrane glycoprotein. Expression very restricted to melanoma; often used as an antigen to activate anti-tumor CD8+ cells	[141]
TRPC1	TRP-1	Commonly used melanoma antigen in anti-tumor immune studies; melanosomal protein used as a differentiation marker. Expression restricted to melanoma.	[142]
MFGE8	Milk fat globule-EGF factor 8 protein	Expressed at high levels during the vertical growth phase of melanoma. Coordinates $\alpha v\beta 3$ integrin signaling; enhances tumorigenicity and metastasis through Akt and Twist pathways. Bridging molecule: binds exposed PS on apoptotic cells and $\alpha v\beta 5$ integrin on macrophages to promote efferocytosis. Efferocytosis leads to an anti-inflammatory response (decreased antigen cross-presentation by DCs, increased Treg production, M2 polarization, and decreased TIL activation).	[143,144]
PXN	Paxillin	Role in melanoma growth, adhesion, and metastasis	[138]

siRNA Mediated Knockdown: ON-TARGETplus siRNA pools targeting 48 melanoma proteins, siRNAs targeting CD47, the non-targeting control siRNA pool, and the siGLO Red Transfection Indicator were validated by and purchased from Dharmacon (Lafayette, Colorado, USA). Utilizing a random number generator, we combined the 48 siRNAs into pools of three siRNAs plus a siRNA targeting CD47 (Figure 2-4). Each siRNA was used in four different pools. siRNA pools were tested in seven groups, each with its own set of controls (untransfected M21 cells, M21 cells transfected with non-targeting siRNA, and Raji lymphoma cells as a positive control for phagocytosis). 230,000 M21-GFP cells were plated 24 hours prior to transfection in antibiotic-free DMEM medium. Cells were transfected using TransIT-TKO reagent (Mirus Bio LLC, Madison, Wisconsin, USA) according to the manufacturer's protocol with either 100 μM of each siRNA in the pool or 400 μM non-targeting control siRNA. Cells were cultured for 48 hours prior to analysis or placement in a phagocytosis assay (as previously described).

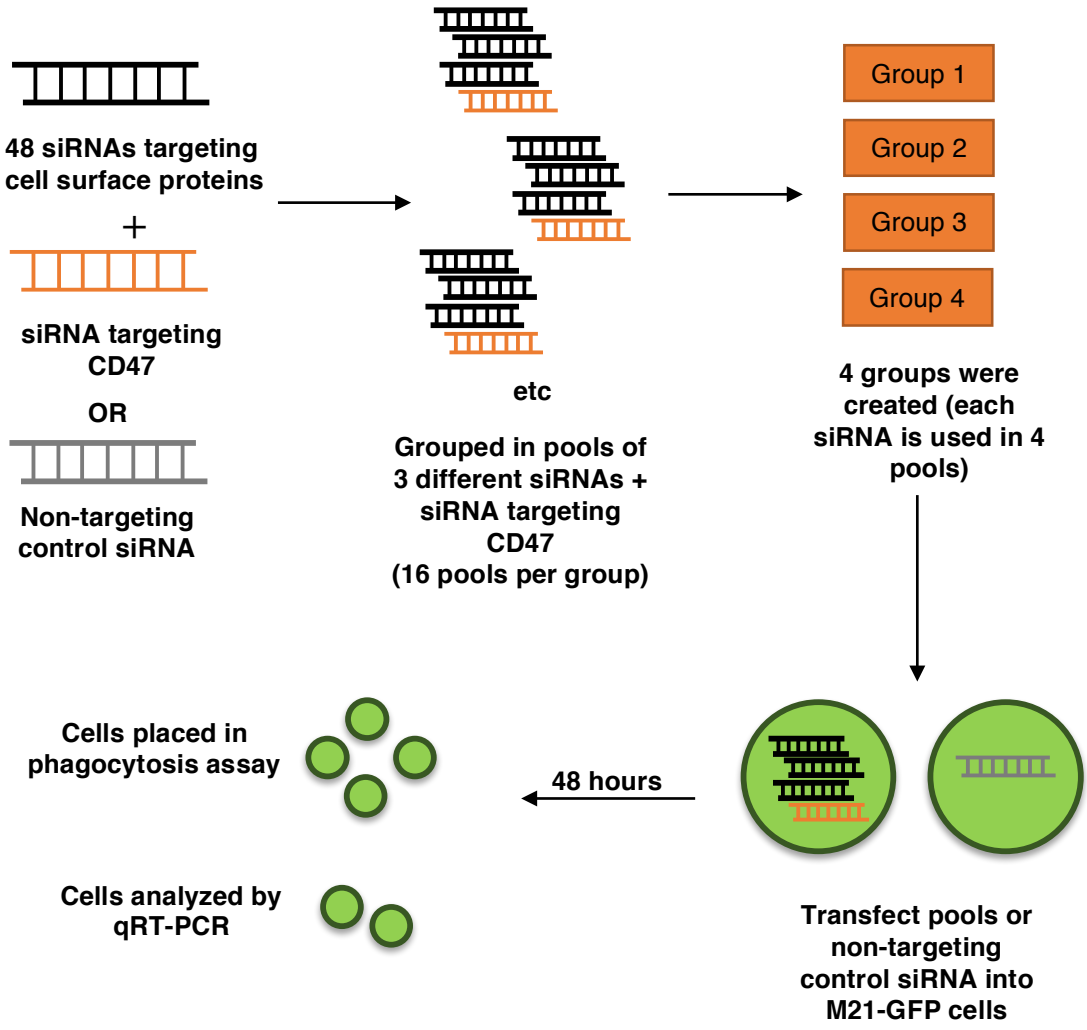

Figure 2-4: Schematic of siRNA knockdown assays

RNA preparation and quantitative reverse-transcriptase PCR (qRT-PCR):

RNA was isolated and purified from cells using a RNeasy Mini Kit (Qiagen, Hilden, Germany) and concentrations were measured using a NanoDrop ND-1000 UV–vis spectrophotometer (Thermo Fisher Scientific, Waltham, Massachusetts, USA). cDNA was synthesized using a QuantiTect Reverse Transcription Kit (Qiagen, Hilden, Germany) according to the manufacturer's

protocol. Eight genes targeted in the siRNA pool were chosen by a random number generator and checked to ensure that multiple protein families were represented by these genes. Primers were designed using NCBI's Primer Blast tool (see Table 2.2 for primer sequences). qRT-PCR was performed using a LightCycler® 96 (Roche Applied Science, Basel, Switzerland) with FastStart SYBR Green Master Mix (Roche Applied Science, Basel, Switzerland). Samples in which the template was omitted were used as negative controls. Relative mRNA values were expressed as delta-Ct values normalized to GAPDH.

Table 2-2: Primer Sequences for qRT-PCR

Gene ID	Forward Primer (5'-3')	Reverse Primer (5'-3')
CD47	CAACCTCCTAGGAATAACTGAAGTG	GGGTCTCATAGGTGACAACCAG
CD81	AATTTCGTCTTCTGGCTGGCT	CCAACGAACATCATGACAGCG
MCAM	TGGGCGCTGTCCTCTATTTC	GTTCGCTCTTACGAGACGGG
JAM3	GACAAGTGACCCCAGGATCG	ACCTCACAGCGATAAAGGGC
ICAM1	TGACCGTGAATGTGCTCTCC	TCCCTTTTTGGGCCTGTTGT
LGALS1	CCTGACGCTAAGAGCTTCGT	GGAAGGGAAAGACAGCCTCC
MLANA	TGTGCCCTGACCCTACAAGA	AATACCAACAGCCGATGAGCA

Harvest of bone-marrow derived macrophages: C57BL/6J mice were euthanized according to IACUC guidelines (IACUC Protocol 1406-31578A). Bone marrow was harvested by flushing the excised femur and tibia with sterile PBS. Macrophages were cultured in IMDM medium with 10 ng/mL GM-CSF and enriched by adherence in cell culture for one week prior to use.

Harvest of OT-I and OT-II T cells: OT-I.PL mice (generated by crossing $OVA_{257–264}$/H-$2K^b$ specific, TCR transgenic OT-I mice with Thy1-congenic B6.PL-Thy1a/Cy (Thy1.1) mice and breeding to homozygosity) were generously provided by Dr. Matthew Mescher (University of Minnesota). OT-II.PL mice (generated by crossing $OVA_{323–339}$/I-A^b specific, TCR transgenic OT-II mice with Thy1-congenic B6.PL-Thy1a/Cy (Thy1.1) mice and breeding to homozygosity) were generously provided by Dr. Marc Jenkins (University of Minnesota). Experiments were conducted under specific pathogen-free conditions and performed in compliance with relevant laws and guidelines, and with approval of the Institutional Animal Care and Use Committee at the University of Minnesota (breeding and harvest of OT-I/II mice: IACUC Protocol 1210A22387; tumor experiments: IACUC Protocol 140631578A). OT-I and OT-II T cells were harvested as previously described [145]. Briefly, "inguinal, axillary, brachial, cervical, and mesenteric lymph nodes (LN) were harvested from OT-I/PL mice, pooled, and disrupted to obtain a single cell suspension. OT-I/PL LN cells were enriched for $CD8^+CD44^{low}$ cells by negative selection using MACS magnetic cells sorting (Miltenyi Biotec, Bergisch Gladbach, Germany). Cells were coated with FITC-labeled antibodies specific for CD4, B220, I-A^b, CD11c, and CD44. Anti-FITC magnetic MicroBeads (Miltenyi Biotec, Bergisch Gladbach, Germany) were added to the cells, which were passed over separation columns attached to the MACS magnet. The cells that did not bind to the column were collected and were 95% $CD8^+$ and 0.5% $CD44^{high}$" [145]. OT-II T cells were purified in a similar

fashion, selecting for $CD4^{+}CD44^{low}$ cells to 80% purity. For assays in which T cells were activated *in vitro,* OT-I and OT-II cells were stimulated in flat-bottom microtiter wells coated with DimerX H-$2K^{b}$-Ig fusion protein (BD Biosciences, San Jose, California, USA) loaded with $OVA_{257-264}$ peptide (New England Peptide, Gardner, Massachusetts, USA) and recombinant B7-1/Fc chimeric protein (R&D Systems, Minneapolis, Minnesota, USA). OT-I cells were cultured in RPMI 1640 (Gibco, Gaithersburg, Maryland, USA) supplemented with 2% L-glutamine (Gibco, Gaithersburg, Maryland, USA), 1% penicillin-streptomycin (LifeTechnologies, Carlsbad, California, USA), 1% HEPES (Gibco, Gaithersburg, Maryland, USA), 1% NEAA (Sigma-Aldrich, St. Louis, Missouri, USA), 1% sodium pyruvate (Gibco, Gaithersburg, Maryland, USA), 0.05% 2-ME (Gibco, Gaithersburg, Maryland, USA), and 10% fetal bovine serum (Atlas Biologicals, Fort Collins, Colorado, USA). $0.5x10^{6}$ OT-I cells were added to each well along with 2.5ng/mL recombinant mouse IL-12 (R&D Systems, Minneapolis, Minnesota, USA) and cultured for 3 days prior to analysis.

***In vitro* T cell activation assays:** B16-OVA cells were treated with 0.03 μM doxorubicin chemotherapy or an equivalent amount of PBS for 24 hours (Figure 2-5). Cells were placed in a phagocytosis assay with primary bone-marrow derived macrophages in the presence or absence of CD47 blockade (as described above). Following the phagocytosis assay, macrophages were isolated using magnetic cell sorting with CD11b magnetic beads (Miltenyi Biotec, Bergisch Gladbach, Germany) according to the manufacturer's protocol. To

assess macrophage purity, populations obtained by cell sorting were labeled with an anti-mouse F4/80 antibody (PE-Cy7, Biolegend, San Diego, California, USA) and incubated on ice for 30 minutes prior to flow cytometry analysis on a LSRII flow cytometer (BD Bioscience, San Jose, California, USA) and data analysis using FlowJo (Tree Star, Ashland, Oregon, USA). Macrophage purity was consistent between the treatment groups (60-80%). Purified macrophages were incubated with OT-I and OT-II T cells at a 0.1:1, 0.25:1, 0.5:1, or 1:1 macrophage: T cell ratio to allow antigen presentation to occur. Supernatant was harvested from the cultures at 24, 48, 72, and 96 hours of incubation and analyzed for IFNγ and IL-2 production by ELISA according to the manufacturer's protocols (Biolegend LegendMax ELISA kits, San Diego, California, USA). Cells were harvested at the assay endpoint and labeled with an anti-mouse CD11b antibody (PE-Cy7), anti-mouse CD69 antibody (PE), anti-mouse CD44 antibody (FITC), anti-mouse CD8 antibody (Pacific Blue), and anti-mouse CD4 antibody (APC) (eBioscience, San Diego, California, USA). Cells were incubated on ice for 30 minutes prior to flow cytometry analysis on a LSRII flow cytometer (BD Bioscience, San Jose, California, USA) and data analysis using FlowJo (Tree Star, Ashland, Oregon, USA).

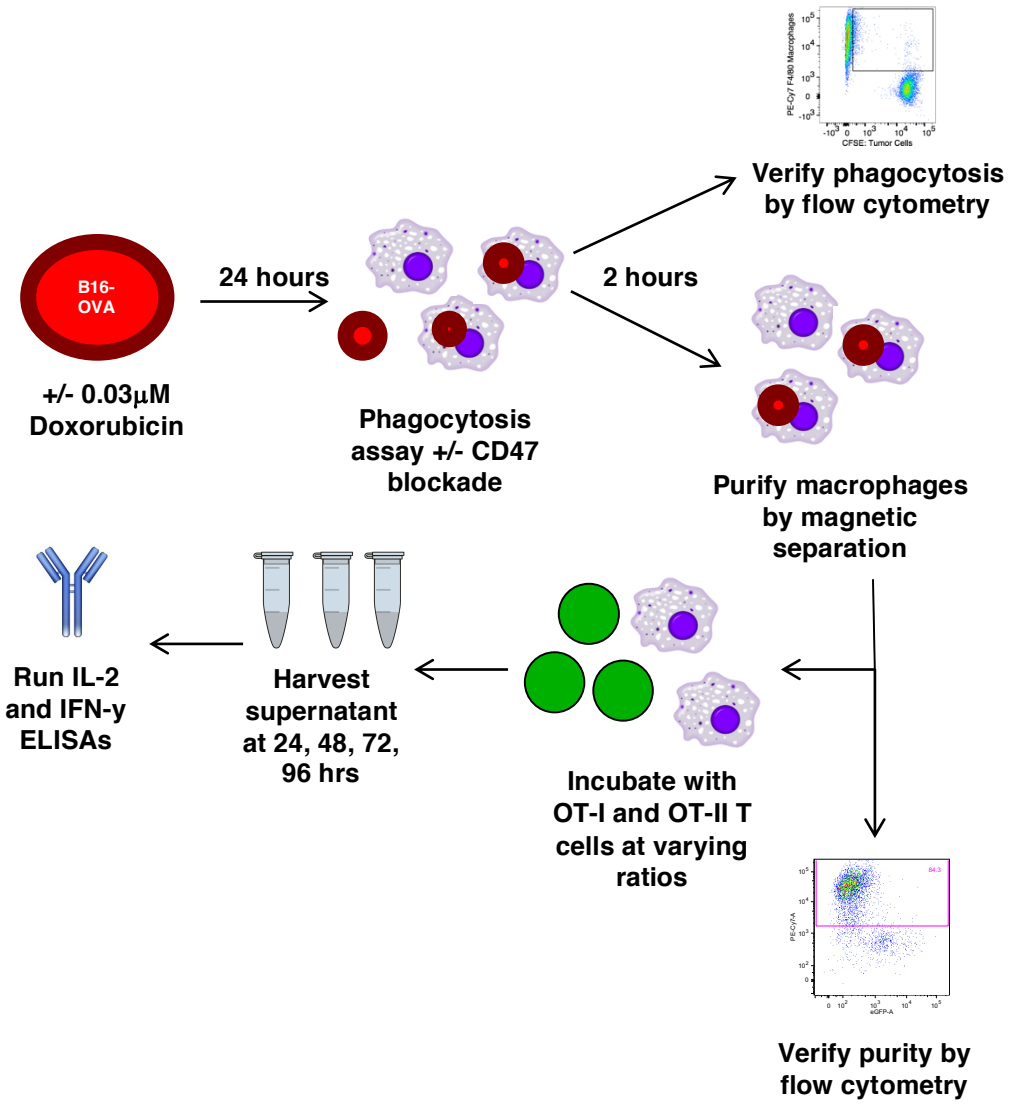

Figure 2-5: Schematic of experimental design to assess the effects of doxorubicin chemotherapy and CD47 blockade on *in vitro* T cell activation

***In vivo* T cell activation assay:** Experiments were conducted under specific pathogen-free conditions and performed in compliance with relevant laws and guidelines, and with approval of the Institutional Animal Care and Use Committee at the University of Minnesota (IACUC Protocol 1406-31578A). Syngeneic CD45.2 C57BL/6 recipient mice were injected subcutaneously (SC) with $2x10^5$

B16-OVA cells (Figure 2-6). Once tumors were visibly established (9 days after implantation), mice received intraperitoneal (IP) injections of the anti-mouse CD47 antibody, MIAP301, or control mouse IgG2a (200 µg i.p.) on days 9 and 11. On day 13, OT-I and OT-II T cells were harvested and purified as described above and labeled with CellTrace Violet (CTV) according to the manufacturer's instructions (Thermo Fisher, Waltham, Massachusetts, USA). Prior to transfer, the cells were analyzed by flow cytometry (LSRII BD Biosciences, San Jose, California, USA) to assess $CD8^+$ and $CD4^+$ cell purity. The activation markers CD25, CD69, and CD44 were also assessed to ensure the cells were not activated prior to adoptive transfer. Transferred OT-I cells were >90% $CD8^+$ and OT-II cells were >75% $CD4^+$. $1x10^6$ of each OT-I and OT-II cells were transferred via the tail vein into recipient mice. As negative controls, one non-tumor bearing mouse received OT-I and OT-II cells, and one tumor-bearing mouse did not receive OT-I or OT-II cells. As a positive control, one tumor-bearing mouse received OT-I and OT-II cells along with 50 µg $OVA_{257–264}$ peptide and 50 µg $OVA_{323–339}$ peptide resuspended in PBS. Three days following adoptive transfer, the tumor draining lymph node, non-draining (contralateral) lymph node, and tumor were harvested from each mouse and homogenized into a single cell suspension. Cells were labeled with antibodies against CD8, CD4, CD69, CD44, Thy1.1, and CD45.1. Adoptively transferred cells were identified by congenic markers and CTV labeling. T cell activation and percent division was assessed

by CTV dilution. Analysis was performed in FlowJo (Tree Star, Ashland, Oregon, USA).

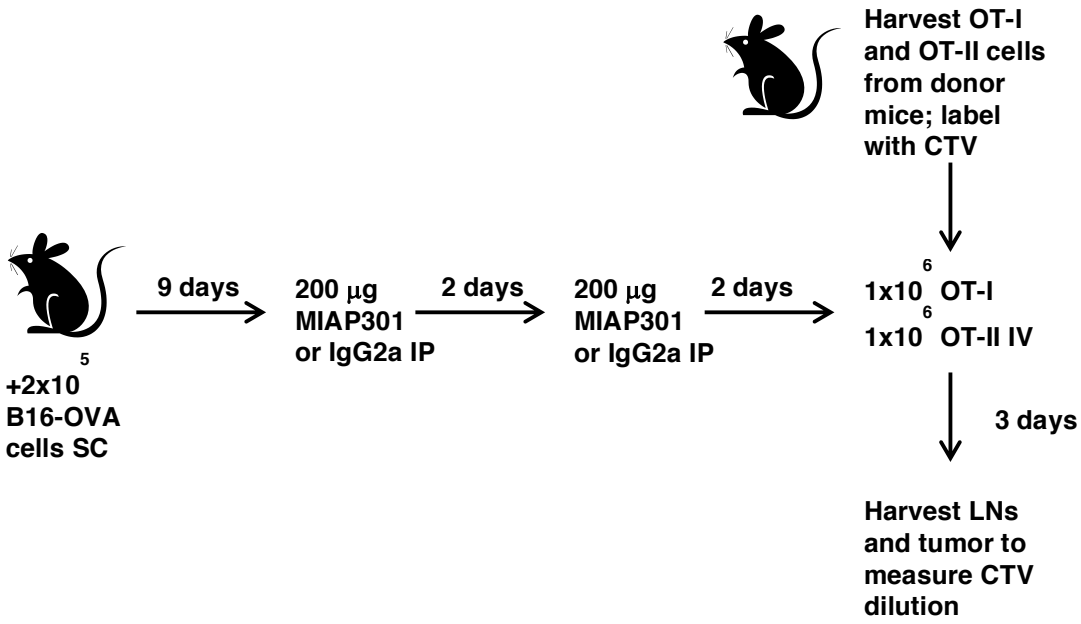

Figure 2-6: Schematic of the experimental design to assess the effects of CD47 blockade on antigen-specific T cell activation *in vivo*

***In vivo* T cell activation assay with doxorubicin:** T cell activation assay was performed as described above. In this experiment, mice received 5 mg/kg doxorubicin chemotherapy on day 10, and OT-I and OT-II T cells were transferred 4-6 hours after the second antibody injection (Figure 2-7). Controls were utilized as described above. Analysis was performed as described above.

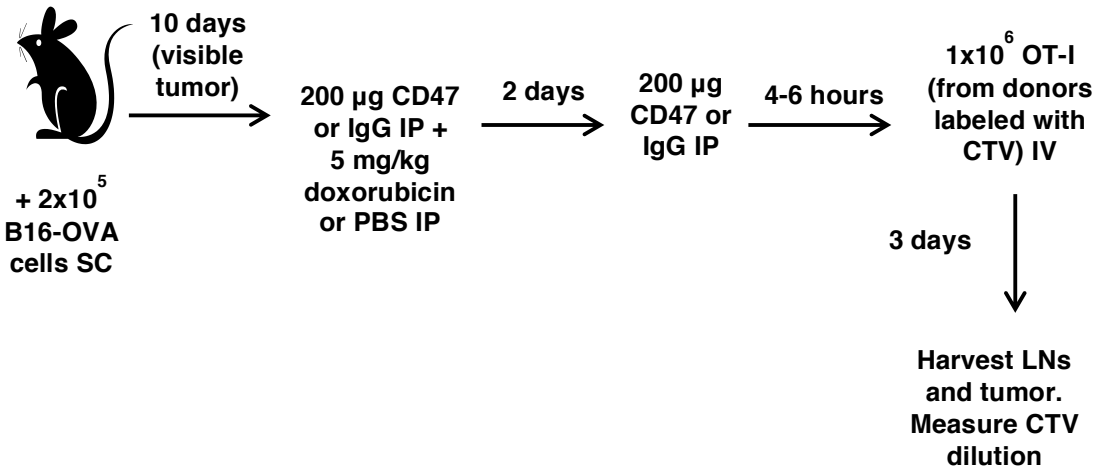

Figure 2-7: Schematic of the experimental design to assess the effects of CD47 blockade and doxorubicin chemotherapy on antigen-specific T cell activation *in vivo*

Chapter 3

Melanoma displays a unique resistance to phagocytosis that cannot be mitigated by CD47 blockade

Rationale and Objectives: Therapies which inhibit the CD47/SIRPα axis have been shown to increase tumor cell phagocytosis *in vitro* and anti-tumor immune responses *in vivo* in a number of preclinical models, including both hematopoietic and solid tumors [64-66,83], but the effect of modulating pro- and anti-phagocytic signals for the treatment of malignant melanoma remains unknown. In this chapter, our objective was to characterize the anti-tumor immune response to melanoma following CD47 blockade.

Results

Mouse melanoma cells display resistance to phagocytosis that is not fully mitigated by CD47 blockade

To determine whether the anti-phagocytic signal CD47 protects melanoma cells from macrophage-mediated phagocytosis, we utilized the mouse B16F10 cell line, which is a well-characterized, preclinical model of melanoma [146]. In addition, we utilized mouse A20 lymphoma cells, which have demonstrated sensitivity to CD47 blockade [65,83], as a positive control. We first evaluated CD47 protein expression on B16 melanoma and A20 lymphoma cells by flow cytometry. We confirmed surface expression of CD47 in both cell types (Figure 3-1A). The expression of CD47 on B16 cells suggests that this innate immune checkpoint could be a therapeutic target in melanoma.

To block the CD47/SIRPα axis in this model system, we utilized two different reagents: a high-affinity SIRPα-Fc fusion protein, CV1-hIgG4 [68], and

an anti-mouse CD47 monoclonal antibody, MIAP301 [83]. To assess the ability of CV1-hIgG4 to block CD47 on the surface of mouse cells, we incubated B16 and A20 cells with increasing concentrations of unlabeled CV1-hIgG4, followed by staining with a fluorescently-conjugated anti-CD47 antibody (PE MIAP301). CV1-hIgG4 competitively blocked interactions between the anti-CD47 antibody and mouse CD47 expressed on the surface of both cell types (Figure 3-1B and 3-1C). The ability of MIAP301 to block CD47 on A20 cells has been previously established in the literature [83], but this reagent's use in B16 cells has not been reported. Therefore, we performed similar blocking assays using increasing concentrations of unlabeled MIAP301 followed by staining with a fluorescently-conjugated mouse recombinant SIRPα to assess the effect of MIAP301 on B16 cells. Higher concentrations of MIAP301 were needed to block the interactions between rSIRPα and mouse CD47 compared to CV1-G4 (Figure 3-1D); however, the concentration needed to effectively block CD47 was well below the concentration we used in subsequent phagocytosis assays. Therefore, both CV1-G4 and MIAP301 are efficacious CD47 blocking reagents in the mouse model.

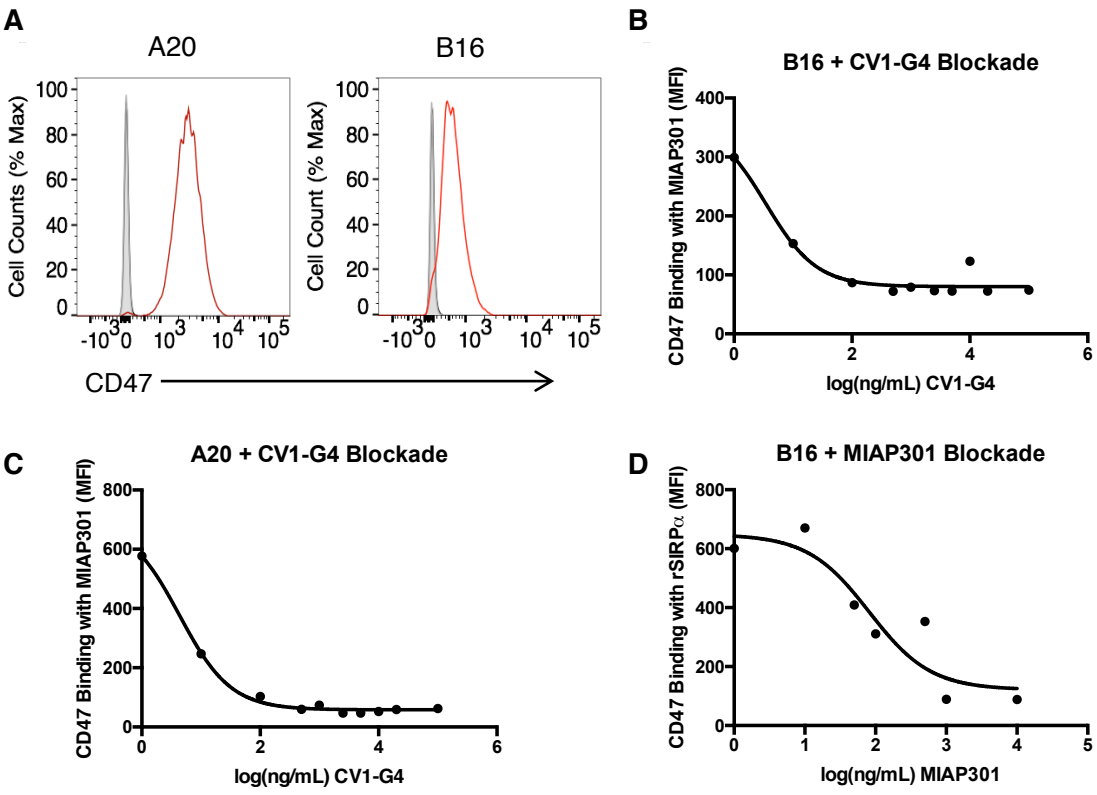

Figure 3-1: CD47 expression and blockade on mouse tumor cell lines. A. CD47 expression on target cells. Labeling of mouse melanoma (B16-OVA) and lymphoma (A20) cell lines with the anti-CD47 mAb MIAP301 conjugated to PE was detected by flow cytometry. B and C. Efficacy of CD47 blockade with CV1-G4 on (B) B16 melanoma cells and (C) A20 lymphoma cells. Cells were incubated with unlabeled CV1-G4 at the indicated concentrations for 15 minutes, followed by subsequent labeling with PE-MIAP301 to detect unoccupied CD47 binding sites. D. Efficacy of CD47 blockade with MIAP301 on B16 melanoma cells. Cells were incubated with unlabeled MIAP301 at the indicated concentrations for 15 minutes, followed by subsequent labeling with PE-rSIRPα to detect unoccupied CD47 binding sites.

To evaluate the ability of CD47 blockade to enhance phagocytosis of mouse melanoma cells *in vitro*, we incubated CFSE-labeled B16 cells with activated mouse J774 macrophages in the presence or absence of CV1-hIgG4. Phagocytosis was evaluated by flow cytometry and measured as the percent of F4/80+ J774 macrophages that engulfed CFSE+ tumor cells per total F4/80+ population. Phagocytosis of A20 lymphoma cells was evaluated as a positive

control. A20 lymphoma cells displayed a high level of phagocytosis in the absence of antibodies (average of 43.1 ± 5.2%), which was further increased upon the addition of CV1-G4 (to 60.3 ± 7.5%, Figures 3-2A and 3-2B) and upon the addition of MIAP301 (to 51.0% ± 6.8%, Figures 3-2C and 3-2D). In contrast, B16 cells were poorly phagocytosed by J774 macrophages in the absence of antibodies (average of 6.4 ± 1.2%, Figures 3-2A-D). Treatment with CV1-hIgG4 or MIAP301 lead to a modest increase in melanoma cell phagocytosis (to 10.6 ± 3.9% and 12.8 ± 3.2%, respectively). However, the overall level of melanoma cell phagocytosis remained low compared to sensitive lymphoma cells (Figures 3-2A-D). We observed similar results using primary mouse bone-derived macrophages, demonstrating that the defect in phagocytosis is not macrophage dependent (data not shown). These findings show that mouse melanoma cells display a resistance to phagocytosis that cannot be fully mitigated by CD47 blockade alone.

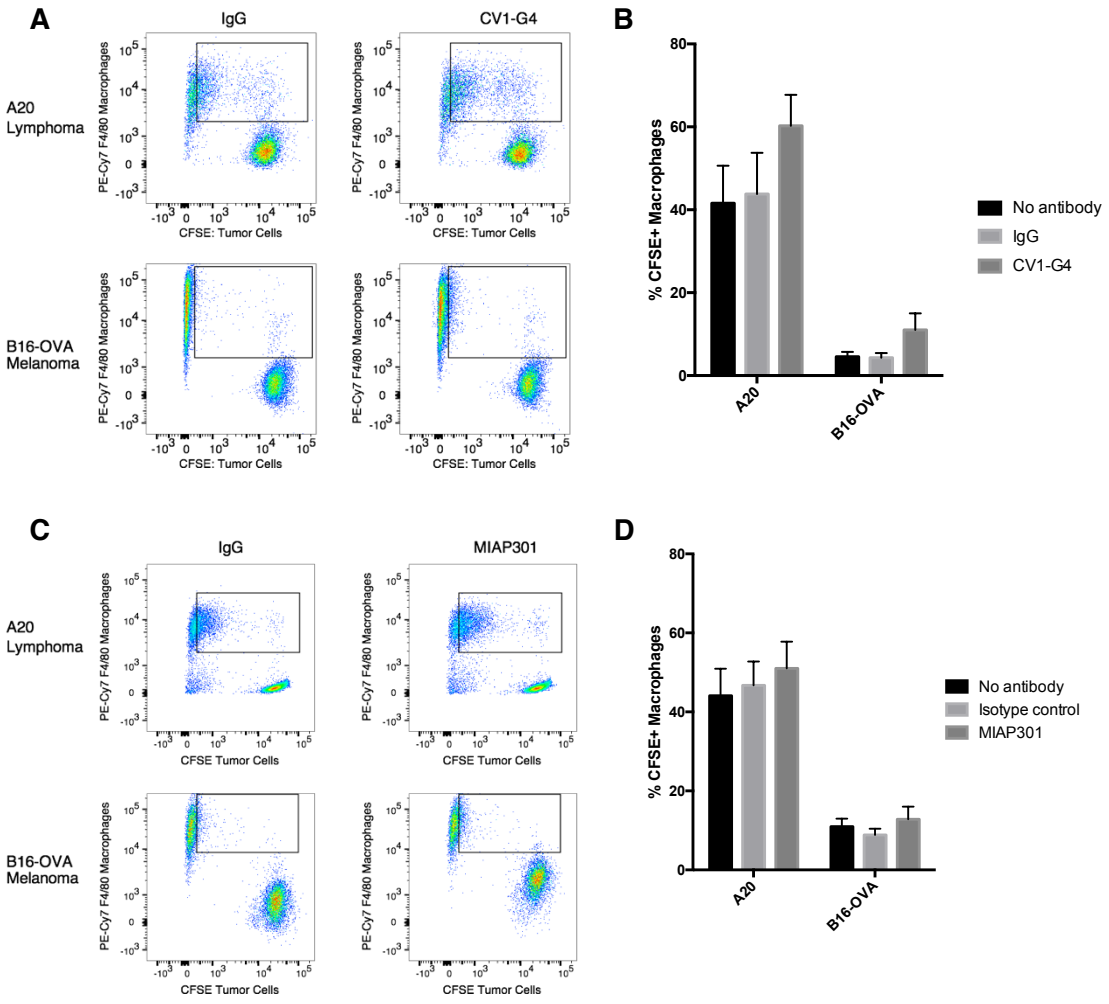

Figure 3-2: Mouse melanoma cells display resistance to phagocytosis that is not fully mitigated by CD47 blockade. Phagocytosis of mouse tumor cells. CFSE-labeled tumor cells were incubated with J774 macrophages in the presence of (A) control IgG4 or CV1-G4 (C) IgG2a or MIAP301. Phagocytosis was quantified as the percent of $F4/80^+$ J774 cells that engulfed $CFSE^+$ tumor cells per total $F4/80^+$ population. Flow cytometry plots representing the mean percent phagocytosis are shown. B. Quantification of phagocytosis assays from Figure A. For B16-OVA cells, bars represent 6 experiments repeated in triplicate (mean± SEM); p=0.7850, Kruskal-Wallis test. For A20 cells, bars represent 3 experiments (mean± SEM); p=0.3259, Kruskal-Wallis test. D. Quantification of phagocytosis assays from Figure C. For B16-OVA cells, bars represent 5 experiments (mean± SEM); p=0.5375, Kruskal-Wallis test. For A20 cells, bars represent 4 experiments repeated in triplicate (mean± SEM); p=0.2480, Kruskal-Wallis test.

CD47 blockade fails to initiate an anti-tumor adaptive immune response or mediate B16 melanoma tumor rejection

In preclinical models, including a syngeneic model using A20 lymphoma cells, phagocytosis in response to CD47 blockade has been shown to elicit an anti-tumor adaptive immune response through antigen cross-presentation and priming of cytotoxic $CD8^+$ T cells [75,83]. Therefore, despite observing only a small increase in B16 melanoma cell phagocytosis in response to CD47 blockade (Figure 3-2), we sought to characterize whether this increase could similarly improve anti-tumor T cell responses *in vivo*.

To assess T cell activation, we utilized the transplantable B16F10 mouse melanoma cell line (haplotype $H2^b$) stably transfected with chicken ovalbumin (B16-OVA). This system allows the quantification of antigen-specific T cell responses using T cells with transgenic receptors that recognize OVA peptides presented in the context of class I (OT-I) and class II (OT-II) MHC [147,148]. B16-OVA is a syngeneic tumor capable of growing in an immunocompetent C57BL/6 mouse, which allows us to study *in vivo* anti-tumor immune responses.

Prior to assessing the anti-tumor T cell response following CD47 blockade, we performed a series of assays evaluating the direct effects of our anti-CD47 antibody on T cell activation. Previous reports have shown that CD47 is highly expressed on the surface of T cells [55,84], and our data examining CD47 expression on the surface of naïve and activated OT-I T cells confirms these previous reports (Figure 3-3A). Anti-CD47 monoclonal antibodies have

been reported to have inhibitory or costimulatory effects on T cell activation depending on the antibody clone and the concentrations used [149]. Therefore, to ensure that T cell activation in our model system would result from macrophage antigen presentation and not from exposure to our anti-CD47 monoclonal antibody (MIAP301), we performed a series of activation assays. We harvested OT-I T cells from transgenic mice and activated the cells *in vitro* in the presence or absence of MIAP301. We observed no change in the expression of T cell activation markers (CD69, CD44) in OT-I cells treated with MIAP301 (Figures 3-3B and 3-3C), demonstrating that treatment with MIAP301 alone does not alter T cell activation. According to the blocking assays previously performed, the concentrations of MIAP301 used in this experiment were saturating and thus should have the greatest possible impact on T cell activation. This experiment was performed *in vitro* under ideal T cell activation conditions, and T cells activated *in vivo* will likely be exposed to lower levels of MIAP301. Therefore, any changes in we observed in T cell activation *in vivo* likely resulted from antigen presentation and not from direct antibody stimulation.

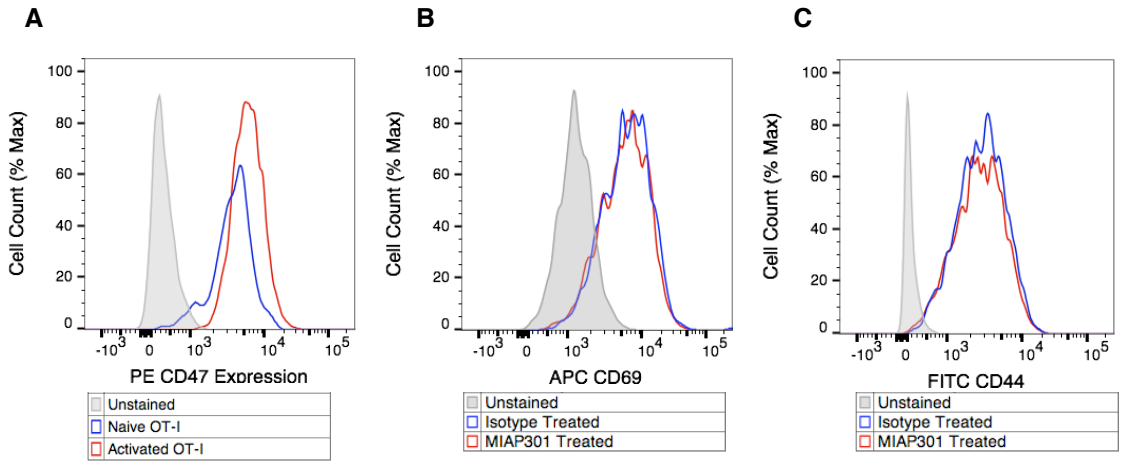

Figure 3-3: CD47 blockade does not alter T cell activation *in vitro.* A. CD47 expression on OT-I T cells. OT-I T cells were harvested and purified by magnetic enrichment. Cells were activated *in vitro* using Kb/B7, SIINFEKL peptide, and IL-12. Labeling of OT-I cells with the anti-CD47 mAb MIAP301 conjugated to PE was detected by flow cytometry. B. OT-I T cells were activated *in vitro* as described above in the presence of 10 μg/mL IgG2a or MIAP301. Three days following activation, cells were labeled with anti-mouse CD69 (APC) and anti-mouse CD44 (FITC) and expression was evaluated by flow cytometry.

Next, we performed a series of assays to evaluate whether CD47 blockade could enhance antigen presentation and priming of antigen-specific T cells *in vivo*. We injected syngeneic Thy1.2 C57BL/6 mice subcutaneously with B16-OVA tumor cells. Once tumors were visibly established (9 days post tumor cell injection), the mice received two injections of PBS, the anti-CD47 antibody MIAP301, or an isotype control antibody (Figure 3-4). Two days after the second injection, we harvested OT-I and OT-II T cells from transgenic recipients, labeled the cells with the vital dye CellTrace™ Violet (CTV), and adoptively transferred the cells into tumor bearing mice. As a negative control, we adoptively transferred OT-I and OT-II T cells into a non-tumor bearing mouse to assess the basal level of T cell activation *in vivo*. As a positive control, we adoptively transferred OT-I and OT-II T cells into a tumor-bearing mouse along with an

injection of SIINFEKL peptide (recognized by OT-I cells) and $OVA_{323-339}$ peptide (recognized by OT-II cells) to stimulate the cells. Three days after the adoptive transfer, we harvested T cells from the tumor, tumor-draining lymph node, and non-draining (contralateral) lymph node. Using flow cytometry, we identified OT-I and OT-II T cells by the congenic marker Thy1.1 and CTV labeling and assessed T cell activation by measuring CTV dye dilution, which marks the number of cell division cycles OT-I and OT-II cells underwent *in vivo*. Instances in which fewer than 100 OT-I or OT-II cells were collected from the lymph node or tumor were not included in the final analysis as it was not possible to assess CTV dye dilution accurately with low cell numbers.

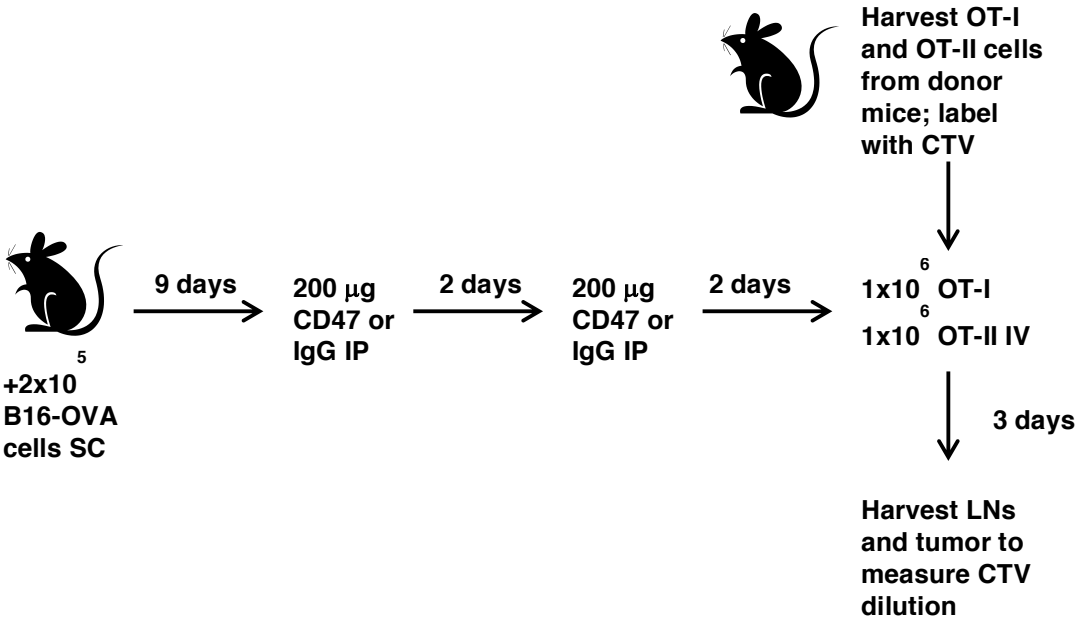

Figure 3-4: Schematic of the experimental design to assess the effects of CD47 blockade on antigen-specific T cell activation *in vivo*

In the tumor draining lymph node (DLN), treatment with MIAP301 slightly increased the number of mice in which OT-I cells were activated and dividing, and the average percent division of the OT-I T cells increased from 24.5 ± 4.4%

in the isotype control treated mice to 41.7 ± 10.2% in the MIAP301 treated mice (Figure 3-5A). We observed no change in the division of OT-I cells harvested from the non-draining (contralateral) lymph node (NDLN), which indicates that a tumor-specific response had occurred (Figure 3-5B). We observed a slight increase in the number of mice with activated OT-II T cells following treatment with MIAP301, and the percent division in the DLN increased slightly from 14.4 ± 3.6% in the isotype control treated mice to 23.3 ± 7.7% in the MIAP301 treated mice (Figure 3-5C). However, we also observed an increase in the percent division of OT-II cells isolated from the NDLN, which may indicate that a systemic response, not a tumor-specific response, occurred (Figure 3-5D). It is also possible that the OT-II cells were activated during isolation and processing prior to being adoptively transferred. It is important to note that, for the NDLN, we recovered sufficient numbers of OT-II cells for analysis from only two mice per group; therefore, we may lack sufficient power to accurately gauge the OT-II response in this model system. We did not recover enough OT-I or OT-II T cells from the tumor to assess T cell responses in the tumor microenvironment, which may indicate that MIAP301 did not increase T cell trafficking to the tumor. It is unlikely that we did not adoptively transfer sufficient numbers of OT cells to detect their presence in the tumor, as the adoptive transfer protocol we used in this experiment has been successfully implemented for the study of intratumoral T cells [147]. Overall, these results suggest that treatment with MIAP301 leads to a slight increase in antigen-specific $CD8^+$ T cell activation in the tumor DLN.

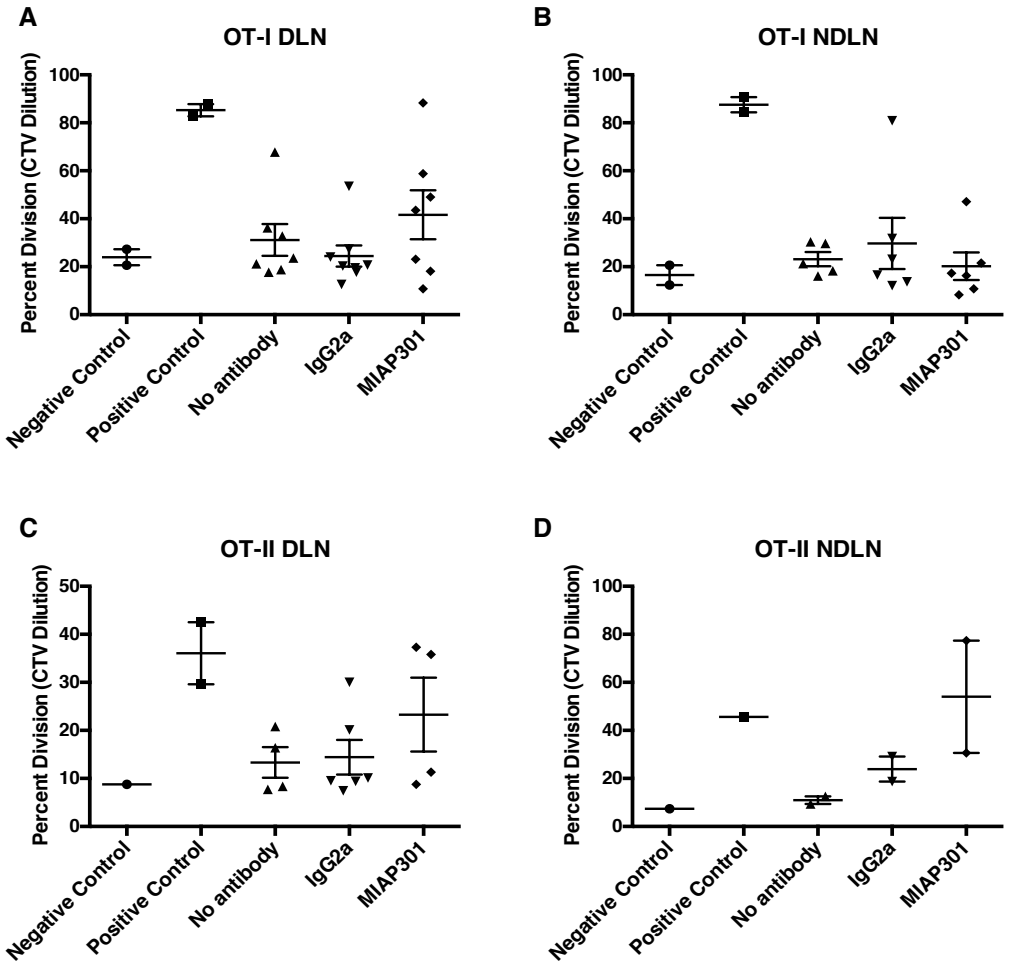

Figure 3-5: Activation of antigen-specific class I (OT-I) and class II (OT-II) T cells is enhanced by CD47 blockade. B16-OVA tumor bearing mice received injections of either PBS (no antibody), IgG2a isotype control antibody, or anti-CD47 monoclonal antibody (MIAP301) on days 10 and 12 following tumor cell inoculation (200μg IP/injection or equivalent volume of PBS). $1x10^6$ OT-I and OT-II T cells were purified, labeled with Cell-Trace Violet (CTV), and injected IV on day 14. Negative control: OT-I and OT-II T cells were injected into a non-tumor bearing mouse. Positive control: OT-I and OT-II T cells were injected into a tumor bearing mouse along with SIINFEKL peptide and $OVA_{323-339}$ peptide. On day 17, the tumor draining lymph node (DLN) and the contralateral, non-draining lymph node (NDLN) of each mouse were harvested, and cells were analyzed by flow cytometry. Gating of OT-I and OT-II cells was performed using congenic markers and percent division was determined by CTV dye dilution. T cell activation was assessed if more than 100 OT cells were recovered. Each symbol represents a different mouse; assay was performed 3 times with 3 mice per experimental group and 1-2 mice per control group. A. Division of OT-I cells in the DLN. p=0.4975, Kruskal-Wallis test. B. Division of OT-I cells in the NDLN. p=0.6173, Kruskal-Wallis test. C. Division of OT-II cells in the DLN. p=0.4675, Kruskal-Wallis test. D. Division of OT-II cells in the NDLN. p=0.0667, Kruskal-Wallis test.

To determine if the slight increase observed in antigen-specific $CD8^+$ T cell activation in response to CD47 blockade was capable of mediating tumor rejection, we monitored B16-OVA tumor growth over the course of three weeks. Tumor-bearing C57BL/6 mice received three injections of the anti-CD47 antibody MIAP301 or an isotype control antibody (Figure 3-6). We adoptively transferred OT-I and OT-II T cells following antibody treatment as previously described. In addition, two groups received transfers of $5x10^6$ OT-I and OT-II cells as a positive control, as it is known that this number of OT cells is capable of suppressing tumor growth (M. Mescher, unpublished data).

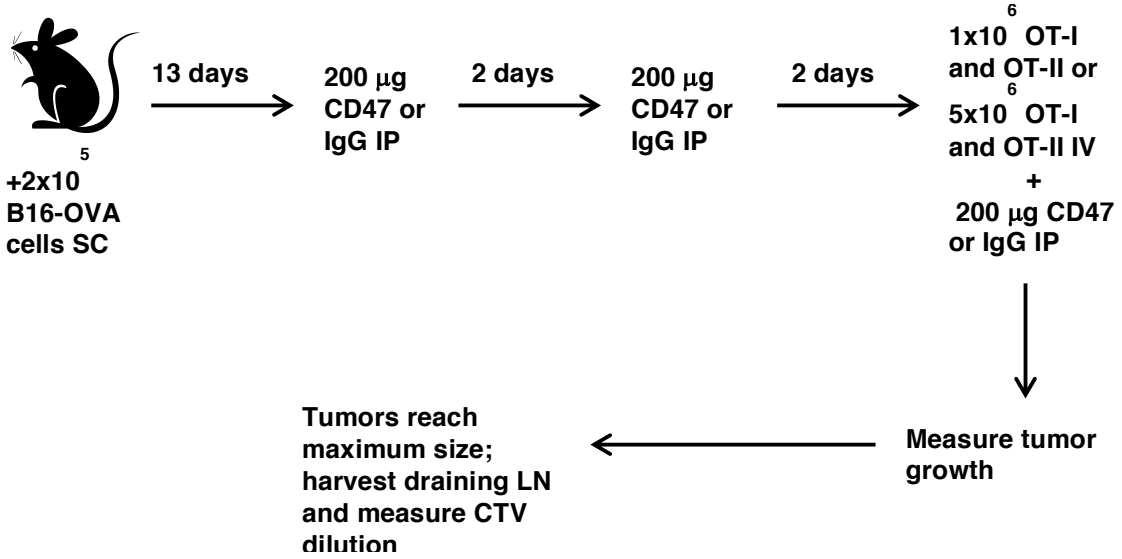

Figure 3-6: Schematic of the experimental design to assess the effects of CD47 blockade on B16-OVA tumor growth

In agreement with previous observations, increased numbers of OT-I and OT-II T cells ($5x10^6$ versus $1x10^6$ cells) provided greater tumor control (Figure 3-7), demonstrating that antigen-specific T cells are capable of controlling tumor growth in this model system. However, we observed no differences in tumor

growth between the isotype control and MIAP301 treated animals (Figure 3-7). This result demonstrates that although CD47 blockade leads to a small increase in phagocytosis as well as OT-I and OT-II T cell activation, this increase is not therapeutically significant in the B16 melanoma model. Therefore, unlike previously studied model systems in which CD47 blockade induced tumor regression [64,66,75,83], B16 mouse melanoma appeared to be resistant to CD47 blockade therapy.

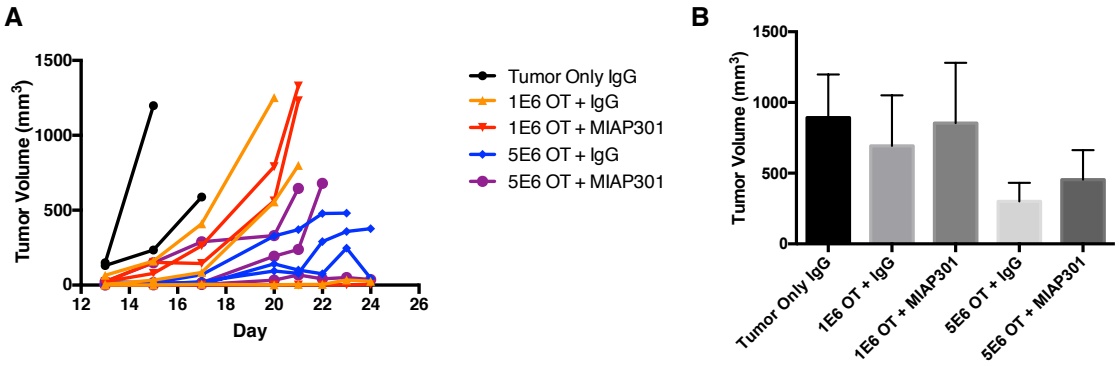

Figure 3-7: CD47 blockade does not enhance antigen-specific rejection of B16-OVA melanoma tumors *in vivo*. B16-OVA tumor-bearing mice received IP injections of either IgG2a isotype control antibody or MIAP301 on days 13, 15, and 17 following tumor cell inoculation (200µg IP/injection). On day 17, OT-I and OT-II T cells were purified, labeled with cell trace violet (CTV), and injected intravenously. Groups received either $1.0x10^6$ or $5.0x10^6$ of each OT-I and OT-II cells. Tumor growth was measured with calipers, and volume was calculated as length x $width^2$ x 0.52. A. Graph represents a spider plot of tumor growth in individual mice. B. Bar graph (mean ± SEM) representing tumor burden at the experimental endpoint (day 24 or maximum tumor volume). P=0.79 Kruskal-Wallis test.

Melanoma cell resistance to phagocytosis is evolutionarily conserved

To evaluate if melanoma cell resistance to phagocytosis was unique to mouse B16 cells, we examined the sensitivity of human and canine melanoma and lymphoma cells to macrophage-mediated phagocytosis. This multi-species approach allowed us to identify evolutionarily conserved mechanisms of immunoevasion that are necessary for melanoma cell survival. We first confirmed that human (M21) and canine (TLM1) melanoma cell lines express CD47 at levels comparable to human (Raji) and canine (CLBL1) lymphoma cells (Figure 3-8A). The CD47 blocking reagent CV1-G4 has previously demonstrated efficacy in both the Raji [65] and CLBL1 [78] models, but it has not yet been tested in human or canine melanoma. Therefore, we performed competition assays to validate the ability of this reagent to block CD47 on melanoma cells. In these assays, CV1-hIgG4 efficiently blocked interactions between anti-CD47 antibodies and CD47 expressed on the surface of human (Figure 3-8B) and canine (Figure 3-8C) melanoma cells.

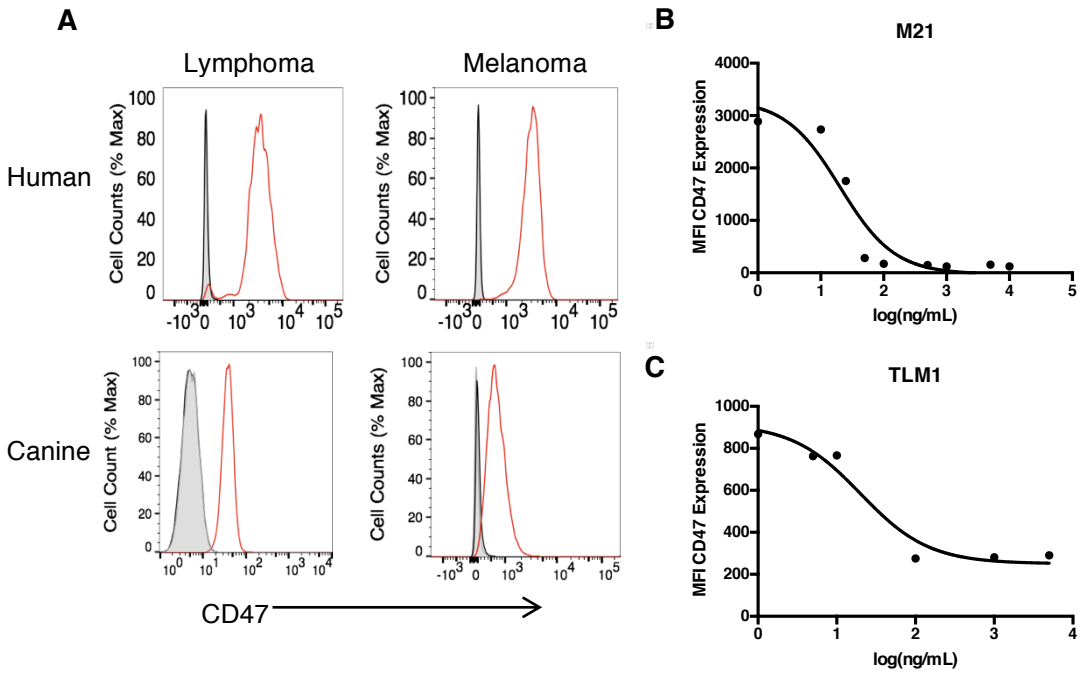

Figure 3-8: CD47 Expression and blockade on human and canine tumor cell lines. A. CD47 expression on target cells. Labeling of human melanoma (M21) and lymphoma (Raji) cell lines and canine melanoma (TLM1) and lymphoma (CLBL1) cell lines with the anti-CD47 mAb 5F9 conjugated to Alexa 488 was detected by flow cytometry. B and C. Blockade of CD47 using CV1-G4. Human M21 melanoma cells (B) or canine TLM1 melanoma cells (C) were incubated with unlabeled CV1-G4 at the indicated concentrations for 15 minutes, followed by subsequent labeling with Alexa-488 hu5F9 mAb. The ability of the labeled antibody to bind CD47 on the cell surface was evaluated by flow cytometry (MFI).

To compare the sensitivity of human and canine melanoma and lymphoma cells to phagocytosis, we performed a series of *in vitro* phagocytosis assays. As our group and others have previous shown [65,78], Raji and CLBL1 lymphoma cells demonstrated sensitivity to phagocytosis (31.6 ± 2.9% and 50.3 ± 0.9% phagocytosis, respectively) that was further enhanced by the addition of CV1-hIgG4 (to 55.6 ± 3.3% and 80.0 ± 2.0%, respectively, Figure 3-9A-C). While we observed small increases in M21 and TLM1 melanoma cell phagocytosis in

response to CD47 blockade, the overall percent phagocytosis of these cells (3.7 ± 1.0% and 12.4 ± 2.0%, respectively) remained very low compared to lymphoma cells (Figure 3-9A-C). Based on the *in vivo* data we obtained with the B16 mouse melanoma model (Figures 3-5 and 3-7), it is likely that this increase in phagocytosis, while statistically significant, is not therapeutically significant. Thus, the resistance to phagocytosis that we observed in mouse melanoma cells seems to be conserved in melanoma cells across species.

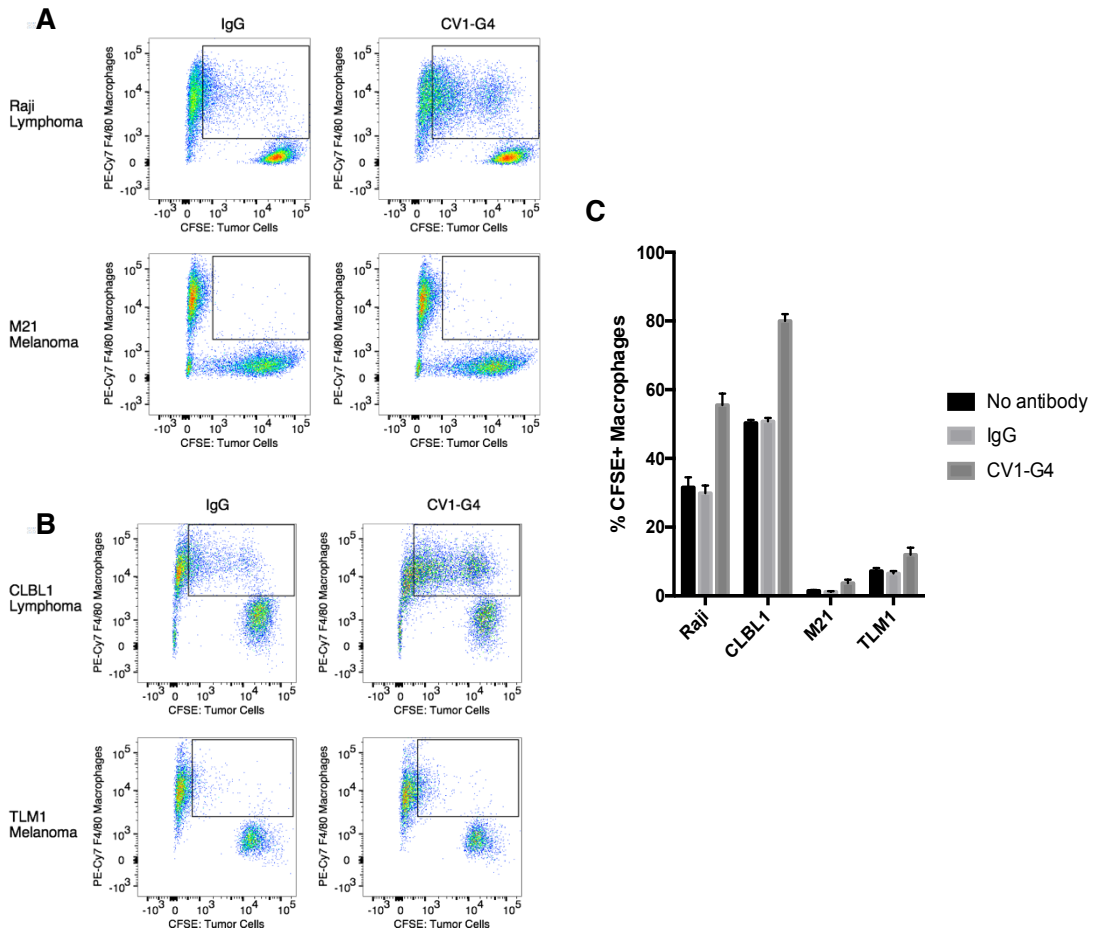

Figure 3-9: Melanoma cell resistance to phagocytosis is conserved across species. A. Phagocytosis of human tumor cells. CFSE-labeled tumor cells were incubated with J774 macrophages in the presence of control IgG4 or CV1-G4. Phagocytosis was quantified as the percent of F4/80^{+} J774 cells that engulfed CFSE^{+} tumor cells per total F4/80^{+} population. Flow cytometry plots representing the mean percent phagocytosis are shown B. Phagocytosis of canine tumor cells as described in A. C. Quantification of phagocytosis assays. Bars represent 3 experiments (CLBL1 p=0.0078, TLM1 p=0.0985), 12 experiments (M21, p=0.0076), or 16 experiments (Raji, p<0.0001) repeated in triplicate (mean± SEM). P values were determined by Kruskal-Wallis test or one-way ANOVA.

Previous reports have demonstrated the therapeutic efficacy of CD47 blockade against a number of solid tumor types [66,75]. To compare the phagocytosis of other solid tumors to melanoma cell phagocytosis, we performed additional *in vitro* phagocytosis assays using human, canine, feline, and mouse breast/mammary cancer cells as well as human, mouse, and canine

osteosarcoma cells. Breast cancer and osteosarcoma cells displayed lower basal levels of phagocytosis (10.5 $\pm$ 1.0% and 15.6 $\pm$ 1.3%, respectively) than lymphoma cells but remained more sensitive to phagocytosis than melanoma cells (Figure 3-10A-B). In contrast to melanoma cells, both cell types exhibited a substantial increase in phagocytosis (to 31.2 $\pm$ 2.6% and 25.8 $\pm$ 2.1%, respectively) in response to CD47 blockade (Figure 3-10A-B). We observed similar results while performing phagocytosis assays with a human colon adenocarcinoma and a mouse lung adenocarcinoma cell line (data not shown). Therefore, melanoma resistance to phagocytosis appears to be unique, at least as compared to lymphoma and the other solid tumors tested (Figure 3-10C).

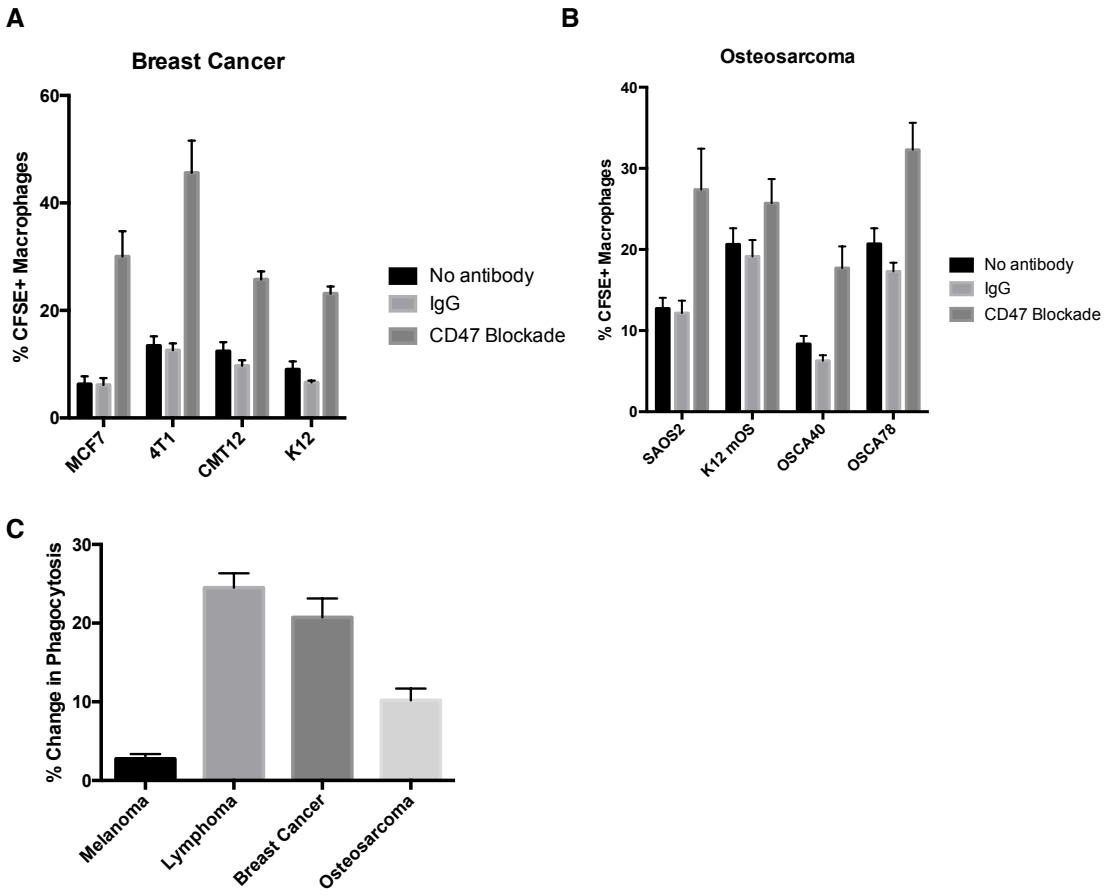

Figure 3-10: Melanoma resistance to phagocytosis is unique compared to other solid tumors. CFSE-labeled tumor cells were incubated with J774 macrophages in the presence of control IgG4 or CV1-G4. Phagocytosis was quantified as the percent of $F4/80^+$ J774 cells that engulfed $CFSE^+$ tumor cells per total $F4/80^+$ population. Bars represent two experiments were performed in triplicate (mean ± SEM). A. Phagocytosis of human (MCF7), mouse (4T1), canine (CMT12), and feline (K12) breast cancer cells. $p<0.005$ for all cell lines by Kruskal-Wallis test B. Phagocytosis of human (SAOS2), mouse (K12 mOS), and canine (OSCA40 and OSCA78) osteosarcoma cells. $p<0.05$ for SAOS2, OSCA40, OSCA78. $p=0.1393$ for K12 mOS by Kruskal-Wallis test. C. Summary of phagocytosis assays for all species tested. $p<0.0001$ by one-way ANOVA.

Conclusions: In this chapter, we evaluated the susceptibility of mouse, human, and canine melanoma cells to phagocytosis mediated by CD47 blockade. We confirmed the expression of CD47 on the surface of melanoma cell lines and validated the ability of a SIRPα mimotope, CV1-G4, and an anti-CD47

monoclonal antibody, MIAP301, to block the CD47-SIRPα axis on these cells. Our data demonstrate that melanoma cells display a resistance to phagocytosis that is not seen in lymphoma, breast cancer, or osteosarcoma cells and cannot be fully mitigated by CD47 blockade. In addition, CD47 blockade failed to prime an anti-tumor adaptive immune response or mediate tumor regression in an antigen-specific model of mouse melanoma. The conservation of this resistance in melanoma cells from three species suggests that this mechanism may be necessary for tumor cell immunoevasion and survival. In the next chapter, we will investigate whether modulation of pro-phagocytic signals in addition to CD47 blockade can overcome melanoma resistance to phagocytosis.

Chapter 4

Modulation of known phagocytic signals cannot overcome melanoma resistance to phagocytosis

Rationale and Objective: Phagocytosis relies on a balance of pro-phagocytic ("eat me") and anti-phagocytic ("don't eat me") signals expressed on the surface of target cells [48]. Pro-phagocytic signals, such as phosphatidylserine (PS) and calreticulin (CRT), are expressed on the surface of cells undergoing immunogenic cell death and can be induced by treatment with chemotherapy drugs in the anthracycline class, such as doxorubicin [48,53]. Previous reports have indicated that CRT expression is necessary for tumor cell phagocytosis and for a form of immunogenic cell death that leads to an anti-tumor immune response [52,53]. Our objective in this chapter was to evaluate whether increasing pro-phagocytic signals in combination with CD47 blockade could enhance melanoma cell phagocytosis and activation of a tumor-specific T cell response.

Results

Modulation of pro-phagocytic signals fails to enhance the phagocytosis of melanoma cells

Previous reports have demonstrated that anthracycline chemotherapies, including the drug doxorubicin, induce rapid translocation of the "eat me" signal calreticulin (CRT) to the surface of colon cancer cells, but the effects of chemotherapy on pro-phagocytic signal expression in melanoma cells is currently unknown. Melanoma cells are notoriously resistance to chemotherapy-induced apoptosis both *in vitro* and *in vivo* [150]. Therefore, we investigated whether low-

dose doxorubicin chemotherapy could induce “eat me” signal expression and enhance the anti-tumor immune response in the absence of cell death. To optimize the dose of doxorubicin chemotherapy used, we treated B16-OVA melanoma cells with increasing concentrations of doxorubicin and quantified cell viability at 24, 48, and 72 hours using the colorimetric MTS assay. We determined that treatment with 0.03μM doxorubicin for 24 hours did not alter cell viability compared to untreated cells (Figure 4-1A). We then demonstrated that this dose of doxorubicin chemotherapy was capable of inducing PS exposure and CRT expression in the treated cells without loss of membrane integrity (Figures 4-1B-C).

To investigate whether the induction of pro-phagocytic signals would synergize with CD47 blockade to enhance melanoma cell phagocytosis *in vitro*, we placed doxorubicin-treated B16 cells in a phagocytosis assay with mouse macrophages in the presence or absence of CV1-hIgG4. We observed no difference in phagocytosis following doxorubicin treatment alone or in combination with CD47 blockade (Figure 4-1D).

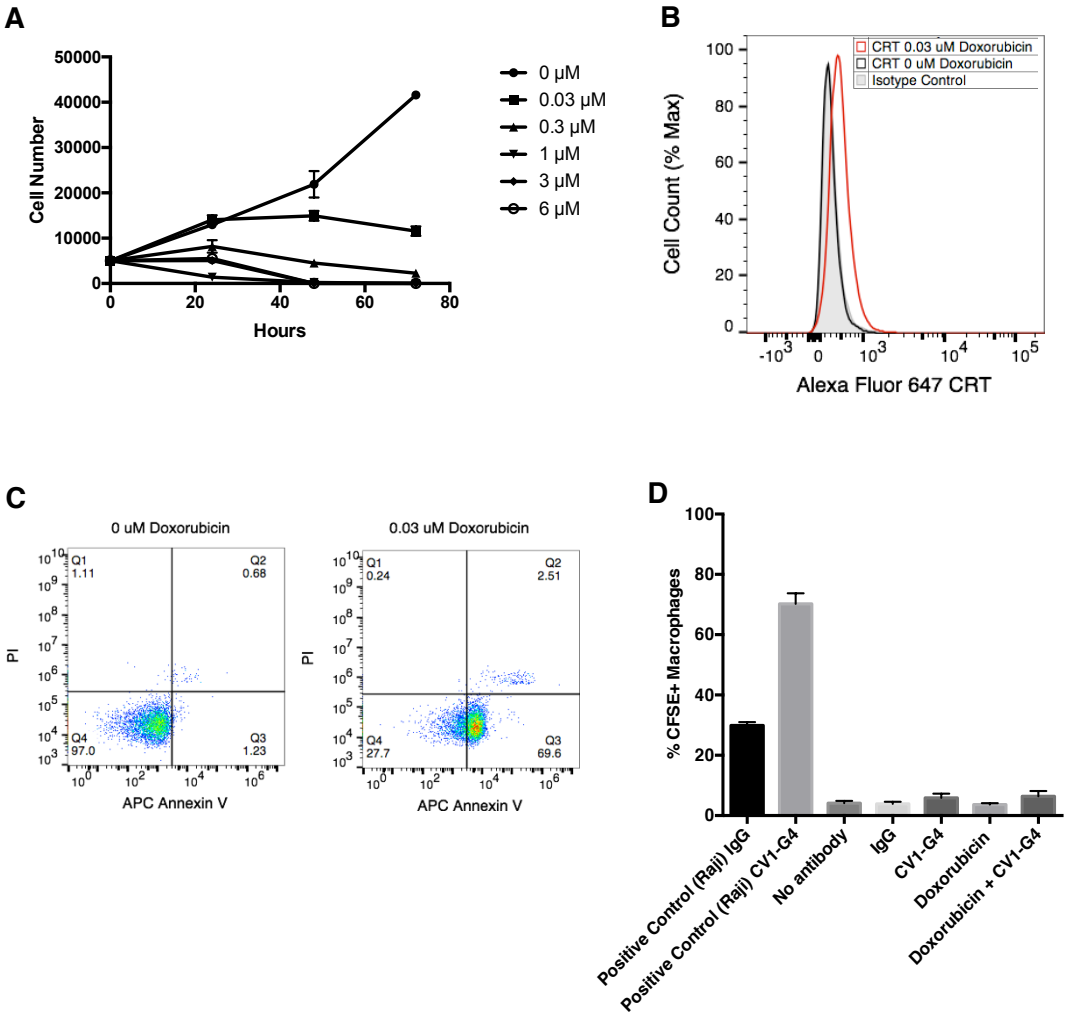

Figure 4-1: Upregulation of "eat me" signals following chemotherapeutic treatment fails to enhances the phagocytosis of B16-OVA cells. A. B16-OVA cells were cultured in 96 well plates with the indicated doses of doxorubicin chemotherapy. Cell viability was assessed at 24, 48, and 72 hours using the MTS assay. B-D. B16-OVA tumor cells were treated for 24 hours with 0.03µM doxorubicin chemotherapy or PBS. B. Phosphatidylserine (PS) exposure following doxorubicin treatment. Display of membrane PS was evaluated by flow cytometry and is represented by the %Annexin V+Propidium Iodide- cells. B. Calreticulin (CRT) exposure following doxorubicin treatment. Cells were labeled with an anti-mouse CRT antibody (Alexa Fluor 647) and analyzed by flow cytometry. C. Phagocytosis of doxorubicin treated cells. Treated cells were incubated with J774 macrophages in the presence of control IgG4 or CV1-G4. Phagocytosis was quantified as the percent of $F4/80^+$ J774 cells that engulfed GFP^+ tumor cells per total $F4/80^+$ population. Bars represent 3 experiments were performed in triplicate (mean ± SEM) p=0.3089, one-way ANOVA. Positive control p=0.0082, 2-tailed t-test.

Combining a tumor cell-specific monoclonal antibody with CD47 blockade has also been shown to enhance phagocytosis by providing a pro-phagocytic stimulus through the Fc receptor [68,78]. To investigate whether this pro-phagocytic stimulus could promote the phagocytosis of melanoma cells, we utilized a monoclonal antibody targeting the neural stem cell marker CD271 [88]. We confirmed CD271 expression on the surface of human M21 melanoma cells (Figure 4-2A). However, we found that combining CD47 blockade with an anti-CD271 antibody failed to enhance the phagocytosis of M21 melanoma cells (Figure 4-2B). Overall, these results demonstrate that modulation of pro-

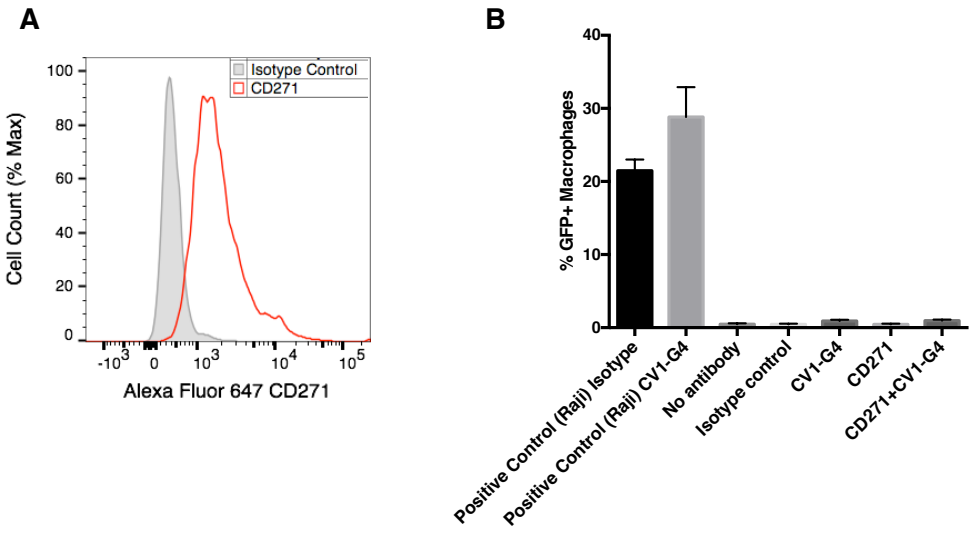

Figure 4-2: Addition of a tumor-specific antibody fails to enhance CD47 mediated phagocytosis of melanoma cells. A. CD271 expression on human melanoma cells. Labeling of human melanoma (M21-GFP) cells with an anti-CD271 antibody conjugated to Alexa Fluor 647 was detected by flow cytometry. B. M21-GFP tumor cells were incubated with J774 macrophages in the presence of control huIgG4, CV1-G4, anti-CD271, or a combination of antibodies. Phagocytosis was quantified as the percent of $F4/80^+$ J774 cells that engulfed $CFSE^+$ tumor cells per total $F4/80^+$ population. Experiments were performed in triplicate and repeated twice. Bars represent mean ± SEM. $p>0.05$ for all M21 conditions, Mann-Whitney test.

phagocytic signals in combination with CD47 blockade cannot overcome melanoma cell resistance to phagocytosis.

Combination doxorubicin chemotherapy and CD47 blockade fail to enhance tumor-specific T cell activation

Although traditionally thought to be immunosuppressive, accumulating evidence indicates that several types of chemotherapy, including doxorubicin, are capable of promoting anti-tumor immune responses. Doxorubicin has been shown to promote type I interferon signaling, the influx of myeloid and lymphoid cells into mouse tumors, and dendritic cell maturation [151]. Therefore, doxorubicin affects multiple immune cells in the tumor microenvironment, and, although we did not observe an increase in phagocytosis *in vitro* following combination doxorubicin and CD47 blockade therapy, it was possible that these agents would synergize to activate an adaptive anti-tumor immune response.

To test whether combination chemo-immunotherapy is capable of activating T cells *in vitro*, we again utilized B16-OVA melanoma cells and OT-I/OT-II antigen specific T cells (see Chapter 3 for a description of this model antigen system). B16-OVA cells were treated with PBS or doxorubicin chemotherapy at the dose optimized previously (Figure 4-1). We then performed a phagocytosis assay in which B16-OVA cells were cultured with primary bone marrow-derived mouse macrophages in the presence or absence of CD47 blockade (Figure 4-3). Following the assay, we verified that phagocytosis had

occurred and isolated the macrophage population by magnetic separation. Macrophage purity was consistent between the treatment groups (60-80%). We then incubated the purified macrophages with OT-I and OT-II T cells at a 0.1:1, 0.25:1, 0.5:1, or 1:1 macrophage: T cell ratio to allow antigen presentation to occur. At 24, 48, 72, and 96 hours of incubation, supernatant was collected from each well and analyzed for IFNγ and IL-2 production by ELISA. At 72 hours, we analyzed expression of the T cell activation markers CD44 and CD69 by flow cytometry. Negative controls included macrophages alone, naïve OT-I and OT-II T cells cultured alone, and naïve T cells cultured with macrophages that had not been placed in a phagocytosis assay. T cells activated *in vitro* using Kb/B7, SIINFEKL and OVA 323-339 peptides, and IL-12 served as a positive control.

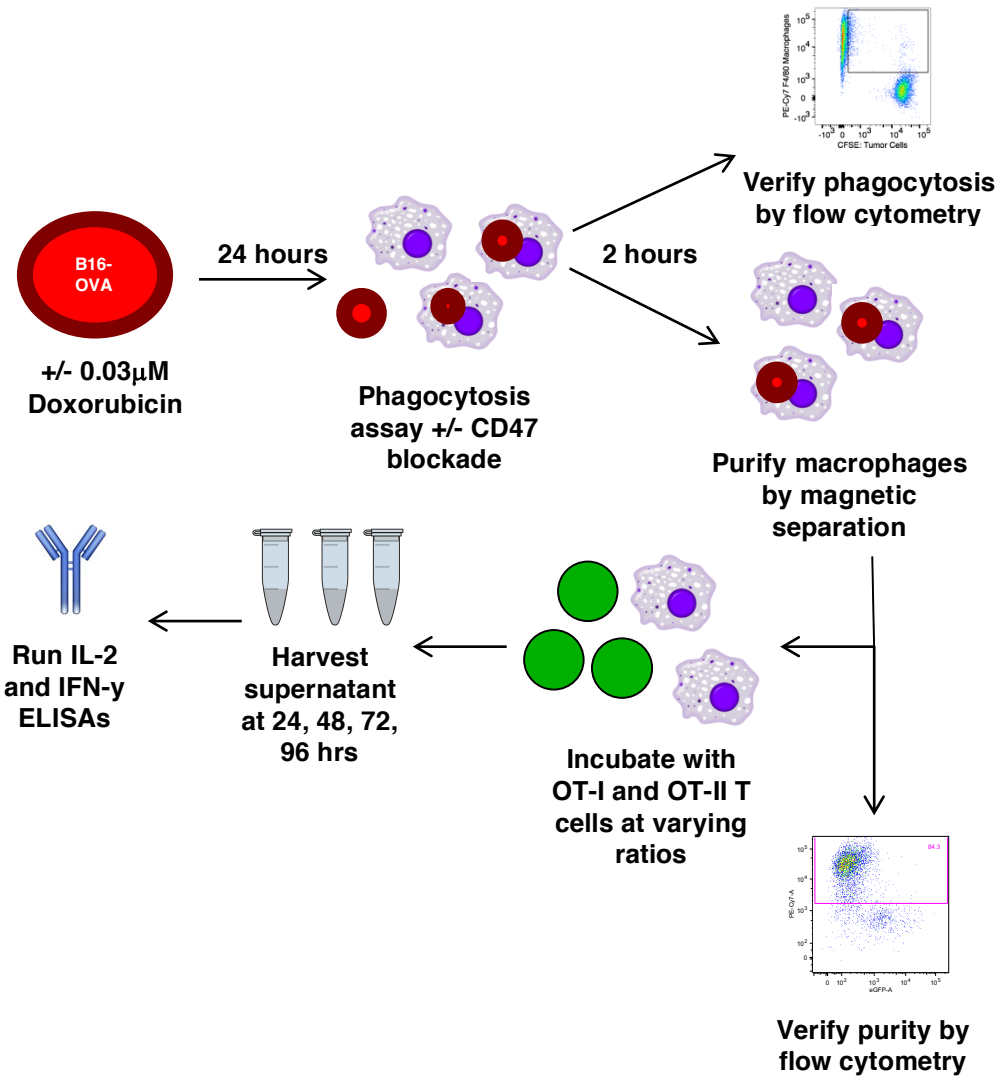

Figure 4-3: Schematic of experimental design to assess the effects of doxorubicin chemotherapy and CD47 blockade on *in vitro* T cell activation.

In general, higher macrophage to T cell ratios induced greater T cell activation as measured by expression of the activation markers CD69 and CD44. However, we saw no consistent differences in CD69 or CD44 expression between the treatment groups (Figure 4-4A-B). Overall, cytokine production as detected by ELISA was very low for all the treatment groups tested. We detected

no IL-2 production by ELISA at 24 hours, and we observed no differences in IL-2 production between the treatment groups at 48, 72, or 96 hours (Figure 4-4C). IFNγ production was only detected at 72 hours in wells cultured with a 0.5:1 macrophage to T cell ratio; again, we observed no differences in IFNγ production between the groups (Figure 4-4D). Based on the low cytokine production, it appears that the OT-I and OT-II T cells were poorly activated by the macrophages in this assay. B16-OVA cells are poorly phagocytosed by macrophages (Figure 3-2), which may lead to suboptimal levels of macrophage antigen presentation or cytokine production and therefore reduced T cell activation in this assay. Low levels of T cell activation could also be a result of the *in vitro* activation conditions; however, previous reports have demonstrated successful *in vitro* activation of OT T cells in a similar assay [152]. Overall, combination doxorubicin chemotherapy and CD47 blockade were unable to increase antigen specific T cell activation *in vitro*.

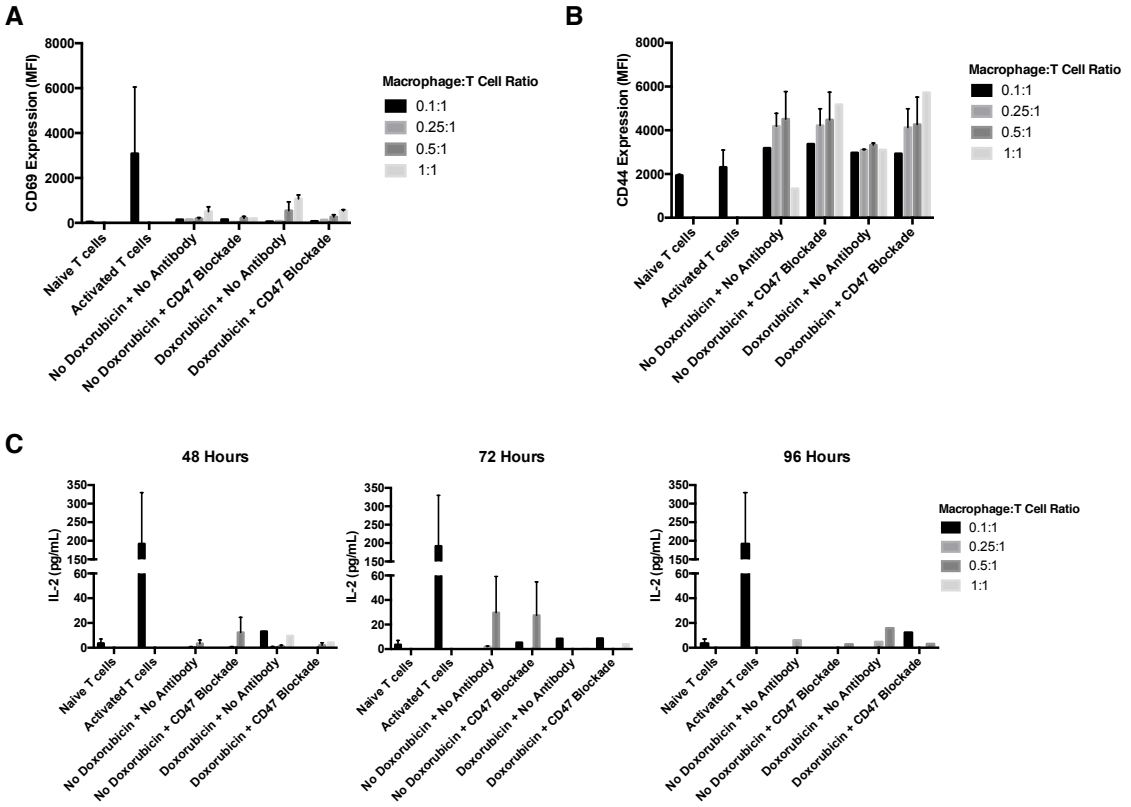

Figure 4-4: Combination doxorubicin chemotherapy and CD47 blockade does not enhance T cell activation *in vitro*. B16-OVA cells were treated with 0.03μM doxorubicin for 24 hours prior to being cultured with primary mouse macrophages with or without CD47 blockade. After a 2 hour incubation, macrophages were purified by magnetic selection and cultured with OT-I and OT-II T cells at varying ratios. Negative control: naïve, unstimulated T cells. Positive control: T cells activated with Kb/B7 and SIINFEKL peptide. T cells were evaluated at 72 hours. A. CD69 Expression on OT T cells. Labeling of T cells with an anti-CD69 antibody (PE) was detected by flow cytometry (MFI). p=0.599, Two-way ANOVA B. CD44 Expression on OT T cells. Labeling of T cells with an anti-CD44 (FITC) was detected by flow cytometry (MFI). p=0.6818, Two-way ANOVA C. Production of IL-2 by cultured OT-I/OT-II cells. Supernatant from cultures of macrophages and T cells was harvested at 48, 72, and 96 hours of culture. IL-2 concentration was evaluated by ELISA. Note: production of IL-2 by naïve T cells and activated T cells alone was performed only at 48 hours of culture (reproduced on each graph for reference). p=0.3904 (48 hours), p=0.8362 (72 hours), p>0.999 (96 hours), Two-way ANOVA D. Production of IFNγ by cultured OT-I/OT-II cells. Supernatant of cells cultured at a 0.5:1 macrophage:tumor cell ratio was harvested at 72 hours. IFNγ concentration was evaluated by ELISA. p=0.6147, One-way ANOVA.

One limitation of *in vitro* assays is the lack of a normal tumor microenvironment and immune system components. In addition to stimulating macrophage phagocytosis, CD47 blockade has been shown to increase dendritic cell phagocytosis and antigen presentation [83] and may enhance neutrophil-mediated antibody dependent cellular cytotoxicity [80]. Doxorubicin, as previously mentioned, has also been shown to stimulate activation of other immune components, including dendritic cells [151]. Therefore, despite the fact that combination doxorubicin chemotherapy and CD47 blockade did not enhance antigen-specific T cell activation *in vitro*, we tested whether this combination chemo-immunotherapy would have an effect on melanoma tumor growth *in vivo.* We injected syngeneic Thy1.2 C57BL/6 mice subcutaneously with B16-OVA tumor cells. Once tumors were visibly established (10 days post tumor cell injection), the mice received two injections of the anti-CD47 antibody MIAP301 or an isotype control antibody (Figure 4-5). In addition, mice received one injection of 5 mg/kg doxorubicin or an equivalent amount of PBS. Four to six hours after the second antibody injection, we harvested OT-I T cells from transgenic recipients, labeled the cells with the vital dye CellTrace^{TM} Violet (CTV), and adoptively transferred the cells into tumor bearing mice. As a negative control, we adoptively transferred OT-I cells into a non-tumor bearing mouse to assess the basal level of T cell activation *in vivo*. As a positive control, we adoptively transferred OT-I cells into a tumor-bearing mouse along with an injection of SIINFEKL peptide to stimulate the cells. Three days after the adoptive transfer,

we harvested T cells from the tumor, tumor-draining lymph node (DLN), and non-draining (contralateral) lymph node (NDLN). Using flow cytometry, we identified OT-I cells (CD45.1+CTV+CD8+Thy1.1+) and assessed T cell activation by measuring CTV dye dilution, which marks the number of cell division cycles OT-I cells underwent *in vivo*.

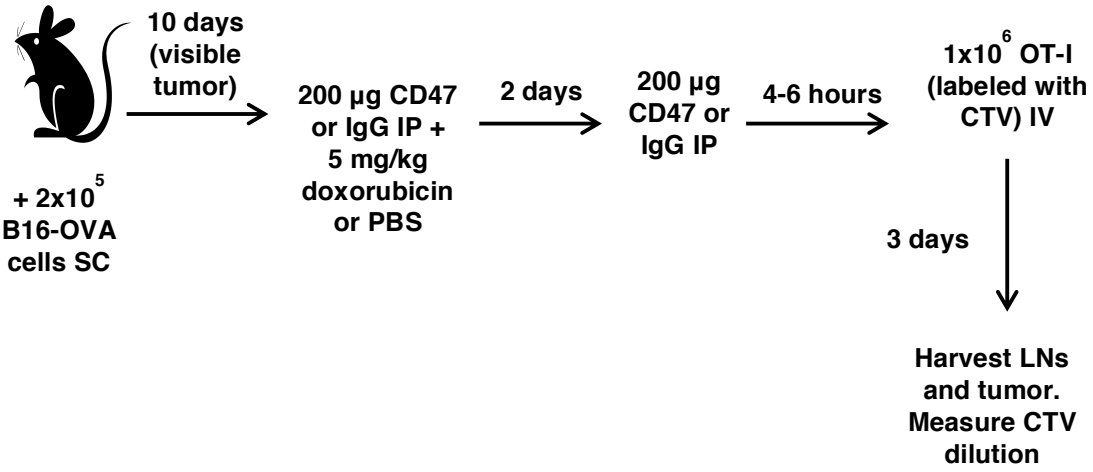

Figure 4-5: Schematic of the experimental design to assess the effects of CD47 blockade and doxorubicin chemotherapy on antigen-specific T cell activation *in vivo*

None of the four treatment groups increased the percent division of OT-I T cells in the DLN, NDLN, or tumor (Figure 4-6). In addition, none of the four treatments increased the division index, which is the average number of cell divisions that a cell in the original population has undergone, in the DLN or NDLN. The division index for OT-I cells within the tumor could not be calculated as we did not recover enough cells for the algorithm to accurately assess the number of cell divisions (Figure 4-6). Percent division and the division index were

decreased in the NDLN (average of 36.5 ± 4.9% division for all groups combined) as compared to the DLN (average of 56.4 ± 6.2% division) or tumor (average of 79.7 ± 3.5% division), which indicates that a tumor-specific response occurred in the system. Treatment with MIAP301 alone lead to a slight increase in CD44 expression in the tumor; however, we observed no change in CD44 expression in the DLN and no change in CD69 expression with MIAP301 treatment (Figure 4-6). No other changes were observed in CD44 or CD69 expression levels. Therefore, combination doxorubicin chemotherapy and CD47 blockade does not lead to an increase in T cell activation in the B16 melanoma model.

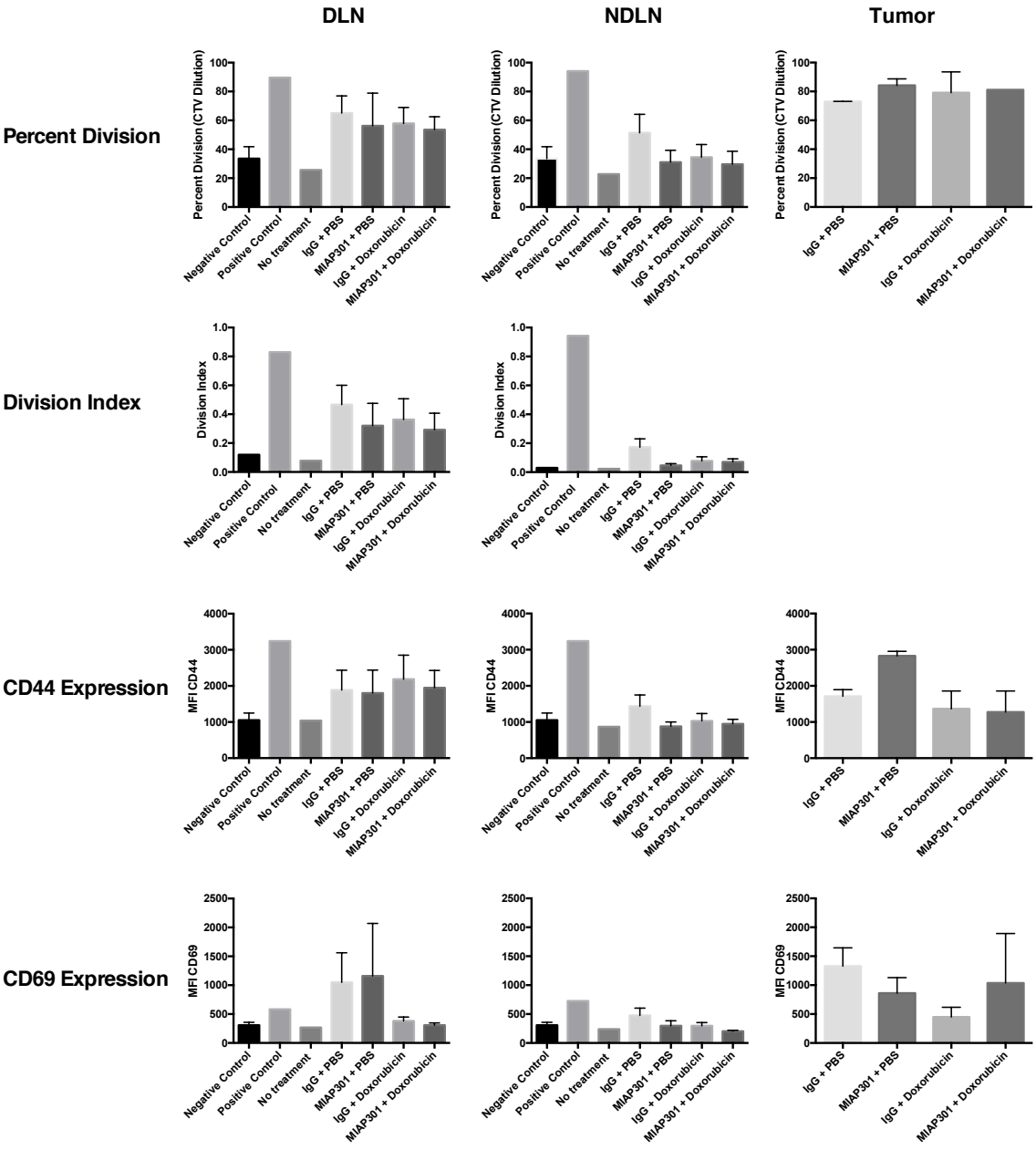

Figure 4-6: Combination doxorubicin chemotherapy and CD47 blockade does not enhance the activation of antigen-specific T cells *in vivo.* B16-OVA tumor bearing mice received an injection of doxorubicin chemotherapy (5mg/kg IP) or an equivalent dose of PBS on day 10 following tumor injection. Groups also received injections of an isotype control antibody or an anti-CD47 antibody (MIAP301 clone) on days 10 and 12 (200μg IP/injection). 1E6 OT-I T cells were purified, labeled with cell trace violet (CTV), and injected IV on day 12. On day 15, the draining lymph node (DLN), non-draining lymph node (NDLN), and tumor of each mouse were harvested and cells were analyzed using flow cytometry. Gating of OT-I cells was performed using congenic cell markers, and division was determined by CTV dilution using proliferation modeling in Flowjo. Activation markers were assessed by labeling the cells with PE anti-mouse CD69 and FITC anti-mouse CD44. Samples containing fewer than 100 OT-I cells were excluded from the final analysis. $p>0.05$ for all treatment groups and parameters, Kruskal-Wallis test.

Previous reports have indicated that endothelial CD47 may be required for T cell transendothelial migration [153,154]. As other reports have demonstrated effective T cell activation and tumor clearance following CD47 blockade [75,83], it is unlikely that CD47 blocking reagents inhibit T cell migration *in vivo*. However, to ensure that treatment with MIAP301 did not alter trafficking of OT-I T cells in our model system, we examined the absolute number of OT-I cells recovered from the DLN, NDLN, and tumor. As the percent division of OT-I cells was unchanged between the groups, any alterations in T cell number should represent a change in T cell trafficking in this system. We observed no change in the number of OT-I T cells in the DLN or NDLN between the groups (Figure 4-7A-B). Treatment with MIAP301 alone lead to a slight increase in the number of intratumoral OT-I T cells (Figure 4-7C), which may indicate that MIAP301 increases trafficking of OT-I cells to the tumor. However, we did not observe an increase in OT-I cell number in the tumors of mice treated with combination doxorubicin chemotherapy and MIAP301 (Figure 4-7C). Overall, we conclude that CD47 blockade with MIAP301 does not inhibit T cell migration in our model system.

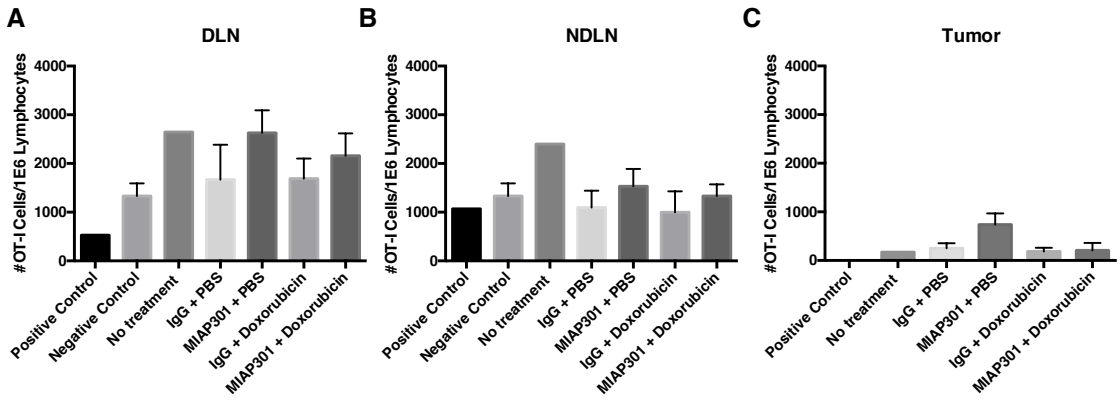

Figure 4-7: Effects of combination doxorubicin chemotherapy and CD47 blockade on antigen-specific T cell numbers. B16-OVA tumor bearing mice received an injection of doxorubicin chemotherapy (5mg/kg IP) or an equivalent dose of PBS on day 10 following tumor injection. Groups also received injections of an isotype control antibody or an anti-CD47 antibody (MIAP301) on days 10 and 12 following tumor cell inoculation (200μg IP/injection). 1E6 OT-I T cells were purified, labeled with cell trace violet (CTV), and injected IV on day 12. On day 15, the draining lymph node (DLN), non-draining lymph node (NDLN), and tumor of each mouse were harvested and cells were analyzed using flow cytometry. Gating of OT-I cells was performed using congenic cell markers, and the number of OT-I T cells was normalized to 1E6 total lymphocytes. $p>0.05$ for all treatment groups in all locations, Kruskal-Wallis test.

Although the antigen-specific T cell response was not affected by combination doxorubicin chemotherapy and CD47 blockade, it was possible that the endogenous T cell response was altered by these treatments. The use of immunoreplete C57BL/6 mice made it possible for us to examine the expression of the T cell activation markers CD44 and CD69 on endogenous $CD8^+$ and $CD4^+$ T cells recovered from the DLN, NDLN, and tumor. Treatment with doxorubicin and/or CD47 blockade did not alter the number of $CD8^+$ or $CD4^+$ T cells in the DLN, NDLN, or tumor (Figure 4-8A). In general, intratumoral $CD8^+$ T cells were more activated than $CD8^+$ T cells in the DLN or NDLN, as measured by expression of the activation markers CD44 and CD69 (Figures 4-8B-C).

However, we did not observe any changes in $CD8^+$ or $CD4^+$ T cell activation status between the treatment groups (Figures 4-8B-C). We also did not observe an increase in CD44 or CD69 expression in $CD8^+$ or $CD4^+$ T cells harvested from the positive control mouse. In this experiment, injection of SIINFEKL peptide, recognized by OT-I cells, served as the positive control for OT-I activation. Exposure to SIINFEKL should not impact endogenous T cell activation, and therefore, this result was expected. We concluded that combination doxorubicin and CD47 blockade did not increase activation of endogenous $CD8^+$ or $CD4^+$ T cells.

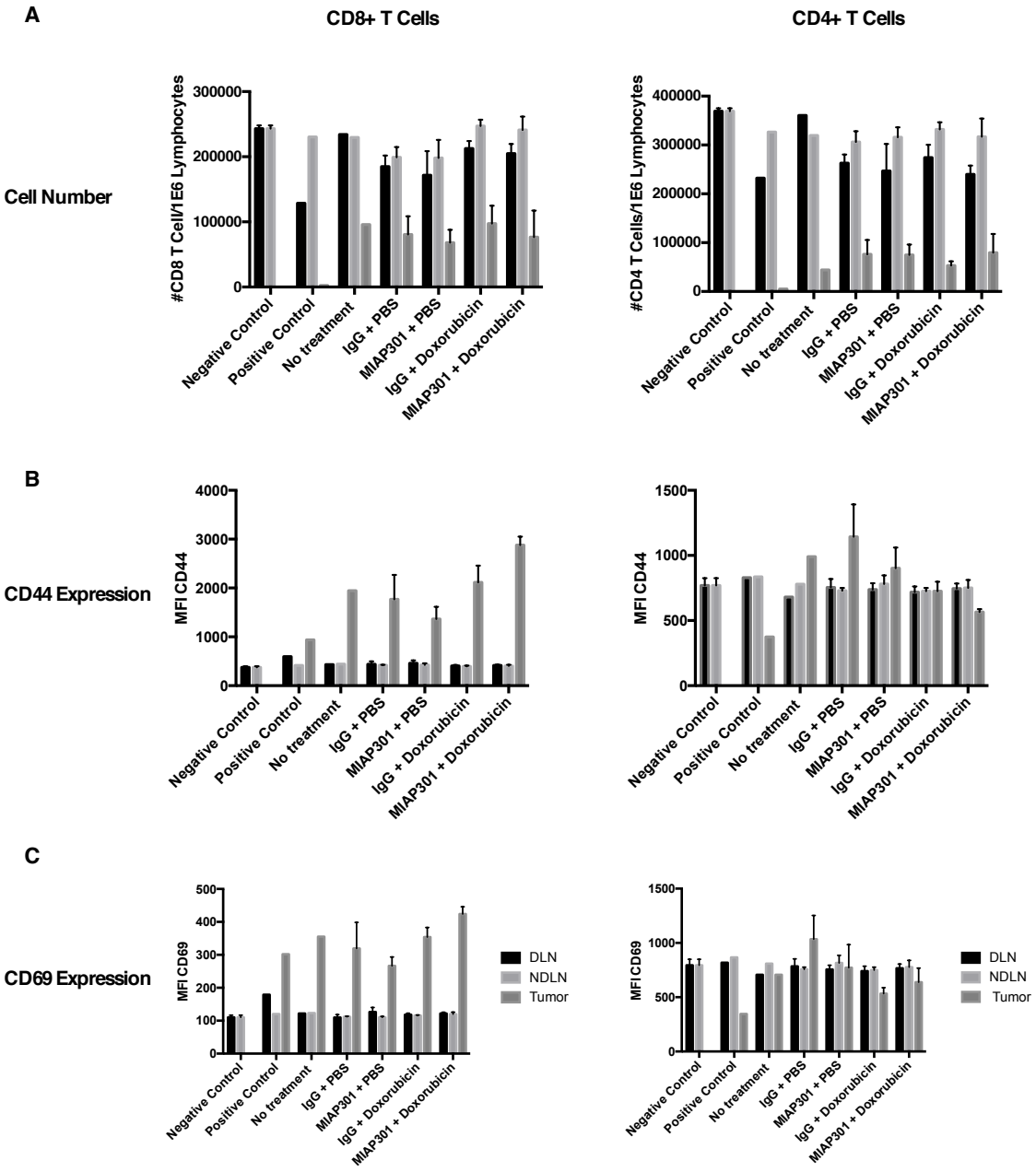

Figure 4-8: Combination doxorubicin and CD47 blockade does not enhance endogenous CD8$^+$ or CD4$^+$ T cell activation. B16-OVA tumor bearing mice received an injection of doxorubicin chemotherapy (5mg/kg IP) or an equivalent dose of PBS on day 10 following tumor injection. Groups also received injections of an isotype control antibody or an anti-CD47 antibody (MIAP301 clone) on days 10 and 12 following tumor cell inoculation (200μg IP/injection). On day 15, the draining lymph node (DLN), non-draining lymph node (NDLN), and tumor of each mouse were harvested and cells were analyzed using flow cytometry. Cell populations were labeled using PerCP-Cy5 anti-mouse CD8 and APC eFluor 780 anti-mouse CD4. Activation markers were assessed by labeling the cells with PE anti-mouse CD69 and FITC anti-mouse CD44. $p>0.05$ for all treatment groups and parameters, Kruskal-Wallis test.

Conclusions: In this chapter, we investigated whether upregulation of pro-phagocytic signals in combination with CD47 blockade could enhance melanoma cell phagocytosis and activation of a tumor-specific T cell response. We demonstrated that low-dose doxorubicin chemotherapy was capable of upregulating expression of the pro-phagocytic signals calreticulin and phosphatidylserine on the surface of mouse melanoma cells without altering membrane integrity. However, combination doxorubicin and CD47 blockade failed to increase melanoma cell phagocytosis *in vitro*. In addition to increasing pro-phagocytic signals through low-dose chemotherapy, we utilized a tumor-specific antibody targeting the melanoma antigen CD271 to provide a pro-phagocytic signal through the Fc receptor. Combination CD271 and CD47 antibody therapy again failed to enhance melanoma cell phagocytosis. In both *in vitro* and *in vivo* T cell activation assays, combination doxorubicin chemotherapy and CD47 blockade failed to enhance antigen-specific T cell activation. Therefore, melanoma cells appear resistant to modulation of known pro-phagocytic and anti-phagocytic signals. In the next chapter, we will explore the possibility that melanoma cells secrete or express additional, uncharacterized anti-phagocytic signals that protect the cells from phagocytosis by the innate immune system.

Chapter 5

Investigation of the mechanisms underlying melanoma cell resistance to phagocytosis

Rationale and Hypothesis: In chapters 1 and 2, we demonstrated that melanoma cells from humans, dogs, and mice are exceptionally resistant to macrophage-mediated phagocytosis, and that this resistance cannot be overcome by modulation of known pro-phagocytic and anti-phagocytic signals. In this chapter, we hypothesize that melanoma cells possess an uncharacterized mechanism of resistance to phagocytosis, such as expression of a soluble or membrane bound “don’t eat me” signal.

Results

Secretion of soluble “don’t eat me” signals is not responsible for melanoma cell resistance to phagocytosis

We first tested the hypothesis that melanoma cell resistance to phagocytosis was mediated by a secreted anti-phagocytic factor. As we previously showed that lymphoma cells are sensitive to macrophage-mediated phagocytosis (Chapter 3, [65,83]), we designed a series of experiments to test if a factor secreted by melanoma cells was capable of inhibiting phagocytosis of lymphoma cells. We incubated human Raji lymphoma cells with varying concentrations of culture supernatants from human M21 melanoma cells and examined the phagocytosis of the lymphoma cells by flow cytometry. We observed no inhibition of lymphoma cell phagocytosis or of the response to CD47 blockade in the presence of melanoma cell supernatants (Figure 5-1A).

We next performed phagocytosis assays in which mouse macrophages were co-incubated with both Raji lymphoma cells (labeled with CFSE) and M21 melanoma cells (labeled with CTV) at varying lymphoma cell to melanoma cell ratios. Macrophages in this assay preferentially phagocytized lymphoma cells as compared to melanoma cells (Figure 5-1B,C). Intriguingly, melanoma cell phagocytosis in this assay appeared to be increased compared to the levels of melanoma cell phagocytosis seen in previous assays (Chapter 3). We needed to exclude the possibility that this result was an artifact of the way data were quantified: in this experiment, we accounted for the variation in the number of tumor cells present between the conditions and therefore quantified phagocytosis as a percent of total tumor cells, rather than as a percent of total macrophages as was done previously. The different quantification methods could alter the absolute measure of phagocytosis. However, it is also possible that the Raji lymphoma cells secrete a pro-phagocytic factor that sensitized melanoma cells to phagocytosis. To distinguish between these two possibilities, we incubated M21 melanoma cells with varying concentrations of culture supernatants from Raji lymphoma cells and analyzed M21 cell phagocytosis. Phagocytosis of M21 cells was extremely low in these experiments, despite the presence of Raji cell supernatant (1.25 $\pm$ 0.35% phagocytosis in the presence of new medium vs. 2.2 $\pm$ 0.12% phagocytosis in the presence of Raji cell supernatant, Figure 5-1D).

Therefore, we concluded that neither M21 cell supernatants or Raji cell supernatants affect macrophage-mediated phagocytosis *in vitro*.

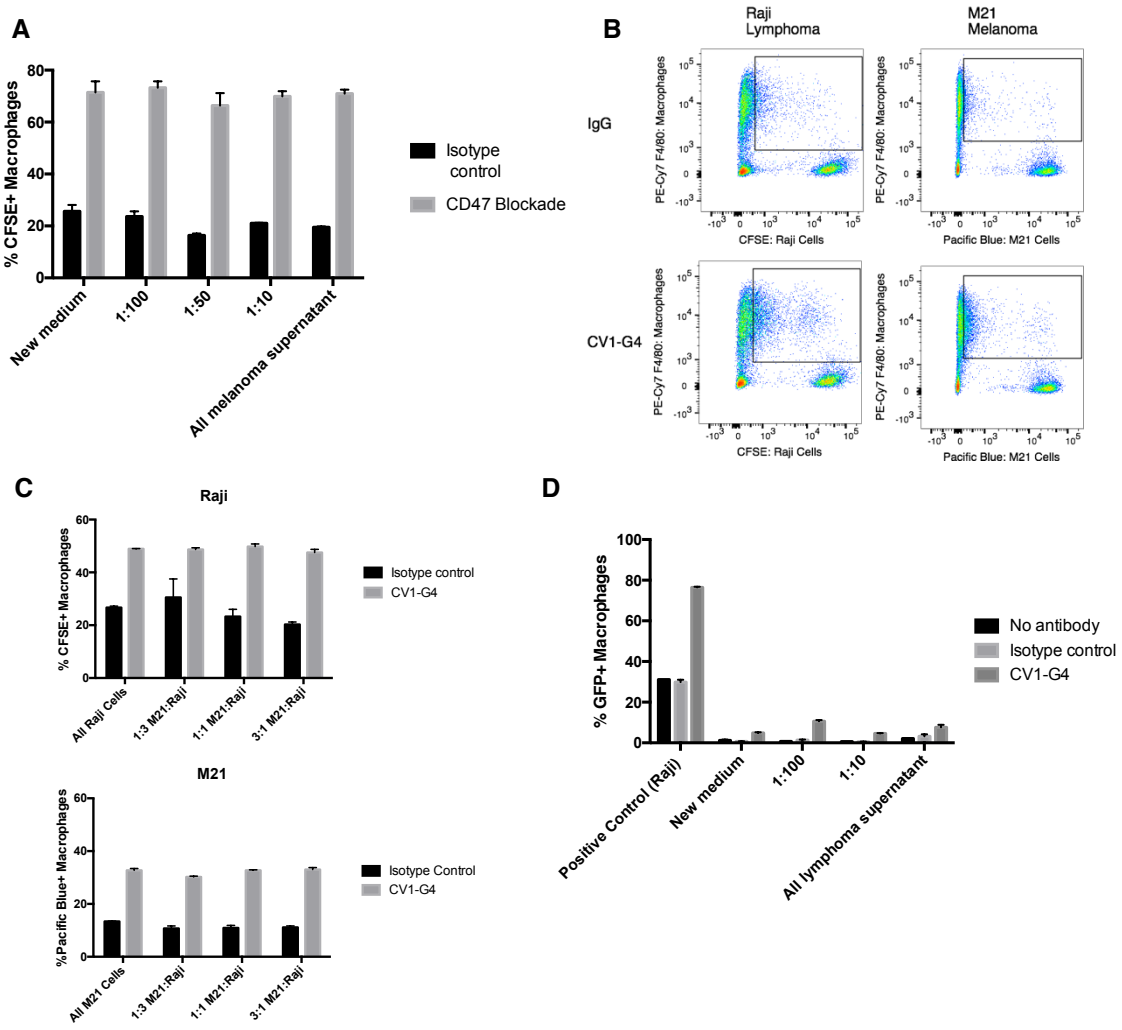

Figure 5-1: Culture supernatants from melanoma or lymphoma cells do not alter tumor cell phagocytosis. A. Effects of melanoma supernatant on lymphoma cell phagocytosis. CFSE-labeled human lymphoma (Raji) cells were incubated with J774 macrophages while suspended in supernatant harvested from cultured M21 melanoma cells and titrated with new IMDM medium. Phagocytosis was quantified as the percent of $F4/80^+$ J774 cells that engulfed $CFSE^+$ tumor cells per total $F4/80^+$ population. Bars show one representative experiment (of three performed) repeated in triplicate (mean± SEM). p= 0.8471 based on two-way ANOVA. B. Effects of co-culturing melanoma cells and lymphoma cells on macrophage phagocytosis of tumor cells. CFSE-labeled Raji lymphoma cells were incubated with CTV-labeled M21 melanoma cells at varying ratios and placed in a phagocytosis assay as described. Phagocytosis was quantified as the percent of $F4/80^+$ J774 cells that engulfed $CFSE^+$ or CTV+ tumor cells per total CFSE+ or CTV+ population. Flow cytometry plots representing the mean percent phagocytosis are shown. C. Quantification of phagocytosis assays. Bars show one representative experiment (of two performed) repeated in duplicate (mean± SEM). p=0.3722 (Raji) or p=0.1506 (M21), Two-way ANOVA. D. Effects of lymphoma supernatant on melanoma cell phagocytosis. The experiment described in panel A was repeated using CFSE-labeled human M21 melanoma cells suspended in supernatant harvested from cultured Raji lymphoma cells. Bars show one representative experiment (of two performed) repeated in triplicate (mean± SEM). $p<0.001$, two-way ANOVA.

To address the possibility that melanoma cells secrete a locally acting or short lived anti-phagocytic factor that is not transferred in cell culture supernatants, we treated M21 melanoma cells with the secretory inhibitor, Brefeldin A (BFA). BFA causes the rapid, reversible dissociation of ADP-ribosylation factor (ARF) from the Golgi complex, which in turn prevents the assembly and budding of secretory vesicles [155]. We first determined that two-hour treatment with 5.0 μg/mL BFA did not significantly increase M21 cell death compared to untreated cells (Figure 5-2A). In control assays, we observed no defect in the phagocytosis of BFA treated Raji cells (Figure 5-2B), which indicates that BFA treatment does not negatively affect macrophage phagocytosis. Similarly, BFA treatment did not enhance phagocytosis of melanoma cells in this system (Figure 5-2B). Together, these results indicate that a secreted factor is not responsible for melanoma cell resistance to phagocytosis.

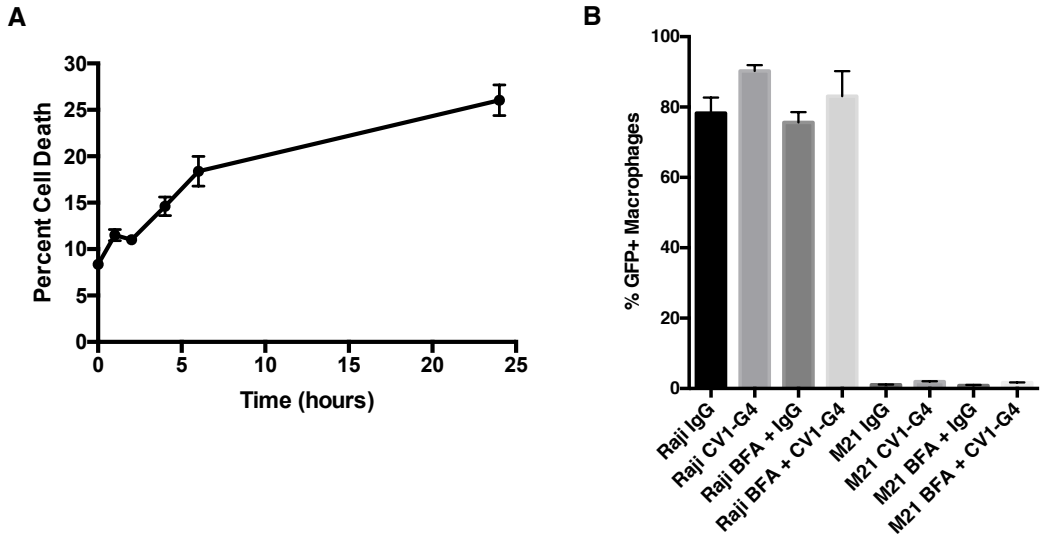

Figure 5-2: Inhibiting secretion does not improve melanoma cell phagocytosis A. Effects of Brefeldin A (BFA) treatment on melanoma cell viability. Human M21 melanoma cells were treated with 5.0 μg/mL BFA. Cell viability was assessed at varying time points by flow cytometry. Cell death was measured as the percent propidium iodide (PI) positive cells. B. Effect of Brefeldin A (BFA) treatment on phagocytosis. M21-GFP or CFSE+ Raji cells were pretreated with 5.0 μg/mL BFA for 2 hours prior to co-culture with J774 macrophages in the presence control IgG4 or CV1-G4. Phagocytosis was analyzed by flow cytometry as in Figure 5-1a. Bars represent two experiments repeated in triplicate (mean± SEM). p=0.2509 (Raji); p<0.001 (M21) by one-way ANOVA.

Melanoma resistance to phagocytosis cannot be overcome by knockdown of 47 membrane-bound proteins with the potential to deliver "don't eat me" signals

To investigate the role of other membrane bound proteins with the potential to deliver "don't eat me" signals as mediators of melanoma cell resistance to phagocytosis, we used gene expression data and published reports in the scientific literature (obtained through PubMed) to identify candidate proteins that were selectively expressed on the surface of melanoma cells as compared to lymphoma, colon cancer, lung cancer, or breast cancer cells. We

utilized data from The Cancer Genome Atlas Research Network (TCGA, http://cancergenome.nih.gov/) to compare gene expression in cutaneous melanoma samples to gene expression in cancers that have demonstrated sensitivity to CD47 blockade, including lymphoma [52], breast cancer [66], colon adenocarcinoma [66,75], lung adenocarcinoma [156], and lung squamous cell carcinoma [157] (See also figure 3-10C). Through this analysis, we identified a unique cluster of genes encoding plasma membrane proteins that were highly expressed in melanoma cells (Figure 5-3).

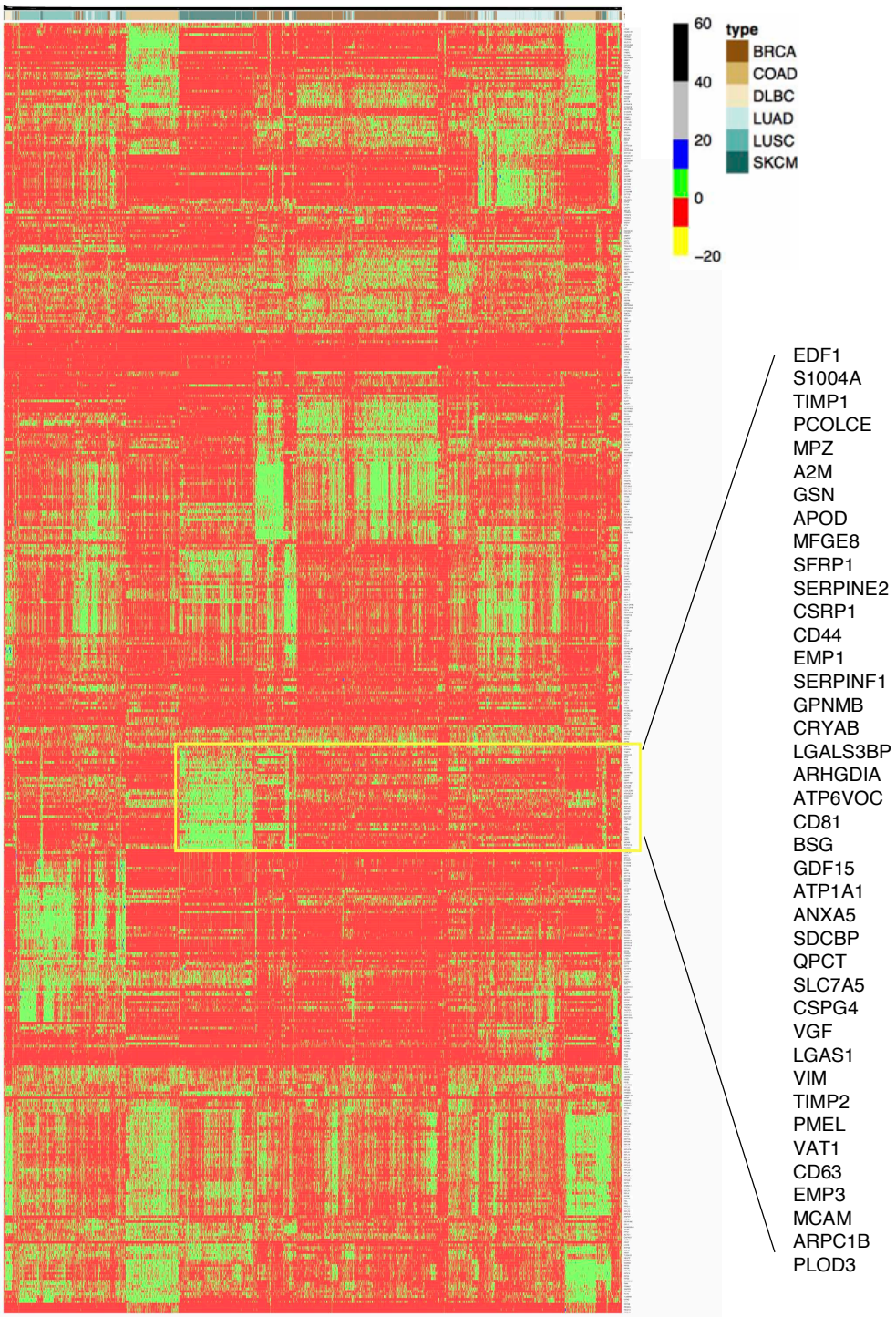

Figure 5-3: Heatmap of the top 500 most variable extracellular genes from a subset of TCGA cancer types. Clustering was performed based on gene expression in transcripts per million (by rows). Gene expression values are centered and scaled.

We also searched the PubMed literature database for proteins expressed on the surface of melanoma cells. Proteins were chosen based on one of four criteria: (1) the gene or protein had been identified as a “don’t eat me” signal in the literature, (2) expression of the gene or protein was restricted to, or expressed almost exclusively by, melanoma cells, increasing the likelihood that it might be responsible for melanoma-specific resistance to phagocytosis, (3) the gene or protein was shown to contribute to melanoma cell growth and metastasis (as evasion of phagocytosis is likely important to cell survival, particularly during metastasis), or (4) the gene or protein was associated with immune suppression in the tumor microenvironment. Based on the gene expression data and literature reports, we developed a siRNA panel targeting 47 genes encoding proteins that are expressed on the plasma membrane (Table 5-1). In addition, we utilized a control siRNA targeting Bcl-2, which we expected to sensitize the melanoma cells to apoptosis. siRNAs allow for rapidly, efficient, target-specific gene knockout without a prolonged cell selection period, which makes siRNAs ideal for large-scale screens [158]. In addition, siRNA function is not dependent on Dicer and other molecules of the microRNA processing pathway, which may be downregulated in cancer [158,159]. Although siRNA mediated knockdown is transient, it should have been sufficient for these assays, in which we only required gene knockdown to persist for the course of phagocytosis assay.

Table 5-1: Targets of the cell surface siRNA panel

Assigned Number	Gene Symbol	Assigned Number	Gene Symbol
1	BCL2	**25**	JAM3
2	CD200	**26**	ITGAV
3	PECAM1	**27**	ITGA2
4	CD151	**28**	ITGA3
5	CD81	**29**	ITGA4
6	SERPINE1	**30**	ITGA5
7	ANXA1	**31**	ITGA6
8	MIF	**32**	ITGA7
9	SELPLG	**33**	ITGB1
10	ECM1	**34**	ITGB3
11	CDH1	**35**	ITGB4
12	CDH2	**36**	ITGB5
13	CDH3	**37**	ICAM1
14	CLDN1	**38**	AGER
15	CLDN12	**39**	LGALS1
16	ALCAM	**40**	LGALS3
17	MCAM	**41**	DSC3
18	NCAM1	**42**	CAV1
19	CEACAM1	**43**	ST8SIA1
20	BCAM	**44**	MLANA
21	L1CAM	**45**	PMEL
22	MADCAM1	**46**	TRPC1
23	EPCAM	**47**	MFGE8
24	F11R	**48**	PXN

Prior to testing the siRNA panel, we optimized transfection of M21-GFP human melanoma cells using a reporter siRNA, siGLO Red Transfection Indicator (Figure 5-4A). We verified that transfection with a CD47-targeting siRNA reduced expression of surface CD47 by 40-60% (Figure 5-4B) and that transfection of an α_v integrin-targeting siRNA reduced expression of surface α_v

integrin by 60-65% (Figure 5-4C). Expression level varied among the cells due to the transient nature of siRNA knockdown, as siRNAs are not replicated during cell division. We utilized a random number generator to select seven genes from the panel and evaluated their expression as well as CD47 expression by quantitative real-time PCR. The results showed a 75-90% reduction in mRNA expression of these proteins following siRNA-mediated knockdown (Figure 5-4D). We concluded that, as predicted, the siRNAs utilized in this experiment efficiently reduced gene expression in human melanoma cells.

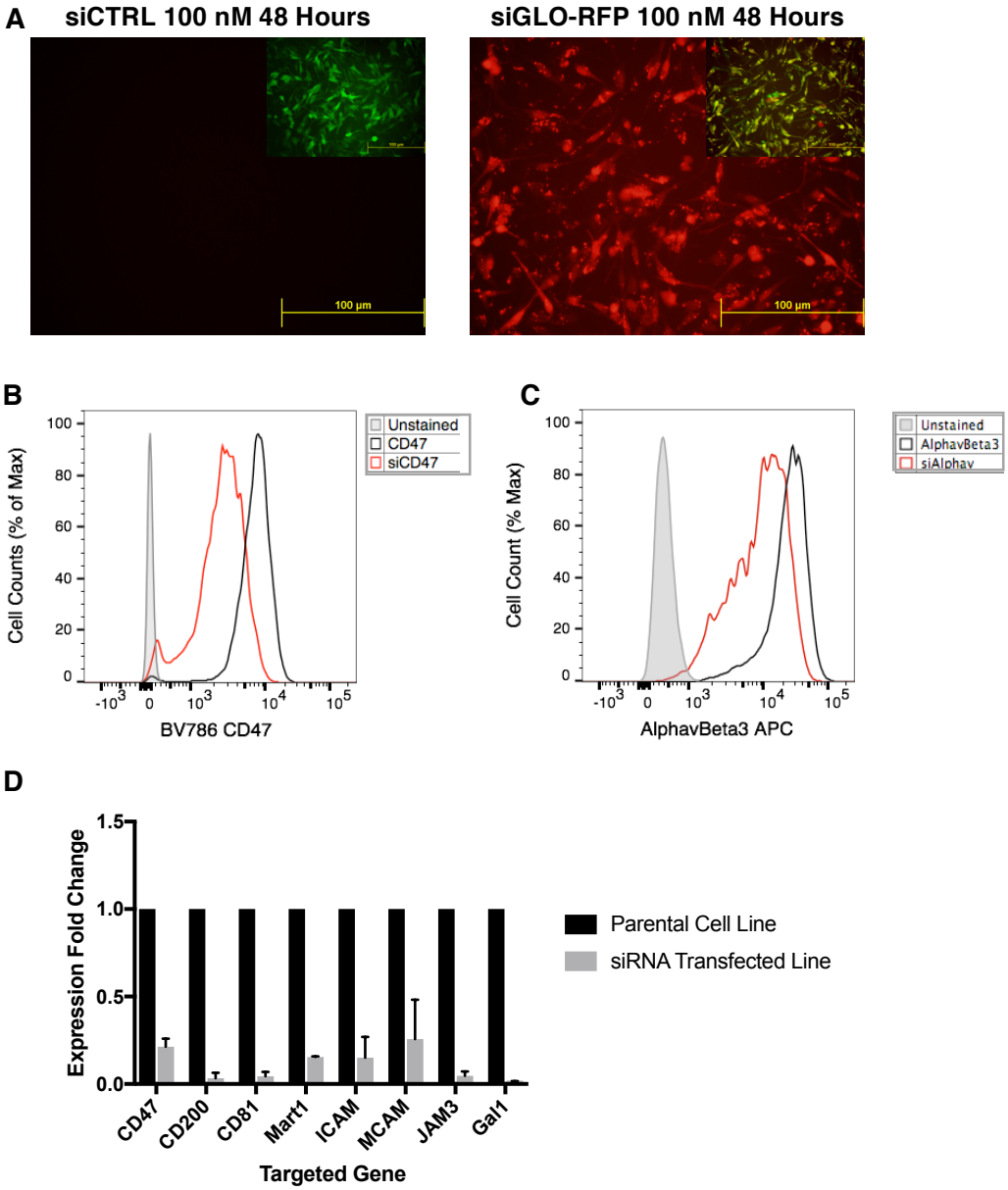

Figure 5-4: Optimization of M21-GFP transfection with siRNA reagents. A. Fluorescent microscopy images of M21-GFP cells 48 hours following transfection with 100 nM non-targeting siRNA (siCTRL) or 100 nM siGLO-RFP. B. CD47 expression of parental M21-GFP cells and cells transfected with siCD47 was evaluated by flow cytometry 48 hours after transfection. C. $\alpha_v\beta_3$ integrin expression of parental M21-GFP cells and cells transfected with siα_v integrin was evaluated by flow cytometry 48 hours after transfection.
D. Expression levels of eight target genes were evaluated by quantitative RT-PCR 48 hours after transfection with siRNA. Gene expression was normalized to GAPDH among samples. Bars represent three transfections (mean± SEM).

To address the possibility that a combination of cell surface proteins, rather than one individual protein, were acting as an anti-phagocytic signal, we utilized a random number generator to combine the 48 siRNAs into pools of three siRNAs plus a siRNA targeting CD47. Each siRNA was used in four different pools to evaluate the effects of different siRNA combinations or to identify any siRNA that consistently affected melanoma cell phagocytosis (Table 5-2).

Table 5-2: siRNA Knockdown Pools

Group 1		Group 2		Group 3		Group 4	
Pool	**siRNA Numbers**	**Pool**	**siRNA Numbers**	**Pool**	**siRNA Numbers**	**Pool**	**siRNA Numbers**
Pool 1	34, 5, 42	Pool 1	12, 37, 44	Pool 1	26, 35, 48	Pool 1	1, 45, 19
Pool 2	21, 38, 20	Pool 2	43, 4, 21	Pool 2	14, 41, 29	Pool 2	34, 30, 46
Pool 3	13, 31, 2	Pool 3	8, 35, 18	Pool 3	20, 28, 44	Pool 3	37, 24, 18
Pool 4	24, 6, 36	Pool 4	23, 11, 41	Pool 4	27, 25, 5	Pool 4	39, 32, 33
Pool 5	30, 22, 33	Pool 5	7, 24, 48	Pool 5	11, 37, 9	Pool 5	36, 31, 2
Pool 6	43, 27, 15	Pool 6	26, 31, 14	Pool 6	3, 31, 24	Pool 6	9, 43, 44
Pool 7	48, 12, 40	Pool 7	28, 29, 6	Pool 7	46, 2, 13	Pool 7	28, 22, 17
Pool 8	23, 45, 4	Pool 8	3, 22, 19	Pool 8	4, 34, 33	Pool 8	23, 16, 6
Pool 9	37, 25, 39	Pool 9	20, 47, 15	Pool 9	10, 47, 45	Pool 9	48, 48, 13
Pool 10	28, 9, 11	Pool 10	25, 30, 13	Pool 10	15, 19, 36	Pool 10	42, 40, 27
Pool 11	19, 3, 1	Pool 11	42, 5, 38	Pool 11	16, 42, 23	Pool 11	3, 11, 29
Pool 12	14, 16, 32	Pool 12	17, 34, 40	Pool 12	7, 21, 12	Pool 12	47, 10, 8
Pool 13	8, 18, 41	Pool 13	36, 46, 32	Pool 13	18, 43, 1	Pool 13	15, 26, 25
Pool 14	39, 47, 35	Pool 14	45, 10, 1	Pool 14	39, 30, 17	Pool 14	12, 7, 4
Pool 15	7, 17, 46	Pool 15	39, 9, 2	Pool 15	22, 40, 8	Pool 15	5, 41, 21
Pool 16	10, 26, 44	Pool 16	33, 16, 27	Pool 16	32, 6, 38	Pool 16	14, 20, 35

To investigate the role of these 47 cell surface proteins and the Bcl-2 control siRNA in melanoma cell phagocytosis, we transfected M21-GFP melanoma cells with the siRNA pools using 100 μM of each siRNA or 400 μM of a non-targeting control siRNA. 48 hours following transfection, we placed the transfected cells into a phagocytosis assay with or without CD47 blockade. We tested the pools of siRNAs in seven experiments, each with its own set of controls. Phagocytosis of Raji lymphoma cells was utilized as a positive control and was consistently within the reference range for the experiments shown in Chapter 3. While testing the second group of siRNAs, poor macrophage viability (98% cell death), severely affected our ability to quantify cell phagocytosis; these data were therefore not included in our final analysis. Knockdown of Bcl-2 failed to decrease melanoma cell viability in these assays as anticipated. However, melanoma cells are notoriously resistant to apoptosis [150], so it is possible that expression of other anti-apoptotic proteins, such as Bcl-xL or Bcl-w, prevented Bcl-2 knockdown from inducing melanoma cell death [160].

Of the 54 pools evaluated, five appeared to slightly increase melanoma cell phagocytosis as compared to the non-targeting control siRNA (Figure 5-5). While other siRNA pools caused a statistically significant increase in phagocytosis, this increase was not clearly apparent on 2-dimensional flow cytometry dot plots, and the overall percent phagocytosis remained very low; so, based on previous data (Chapter 3), we do not believe this increase was therapeutically meaningful.

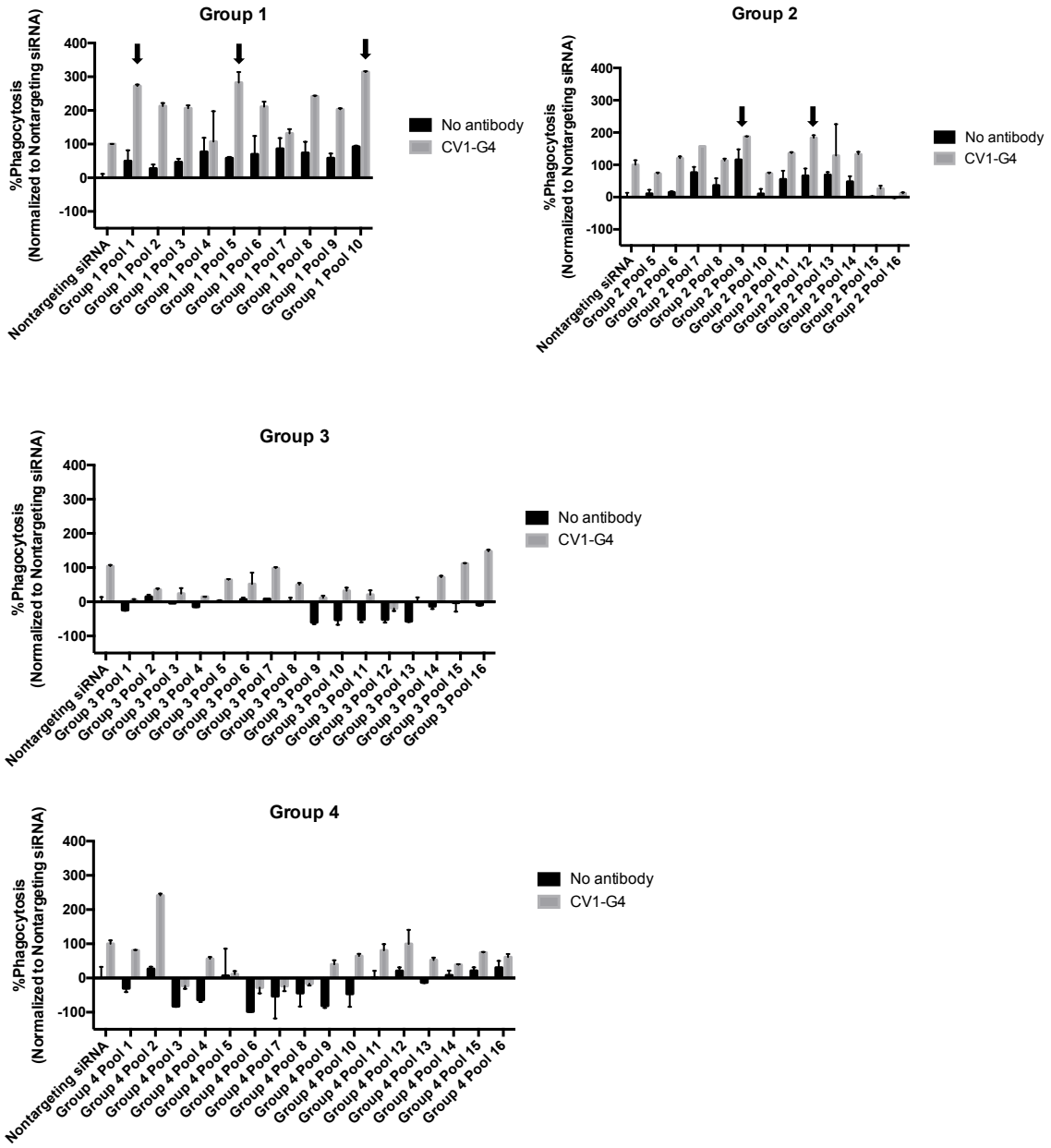

Figure 5-5: Identification of five candidate siRNA pools that increase melanoma cell phagocytosis. M21-GFP melanoma cells were transfected with siRNA pools containing 100 μM of 4 different siRNAs or 400 μM of a non-targeting control siRNA. 48 hours post-transfection, M21-GFP cells were co-cultured with J774 macrophages in the presence of control IgG4 or CV1-G4. Phagocytosis was quantified as the percent of $F4/80^+$ J774 cells that engulfed $CFSE^+$ tumor cells per total $F4/80^+$ population. Data were normalized to the non-targeting control for each experiment. Bars show data from duplicate tests (mean ± SEM) for each pool. p=0.0226 (Group 1), p=0.6783 (Group 2), p<0.0001 (Group 3), p=0.0244 (Group 4), Two-way ANOVA.

To validate whether the siRNAs contained in the five identified pools (Table 5-3) increased melanoma cell phagocytosis, we repeated the transfections using the same experimental conditions. Upon repeat transfection, several of the siRNA pools caused a statistically significant increase in phagocytosis, but again, these increases were not readily apparent on 2-dimensional flow cytometry dot plots and the overall percent phagocytosis remained very low (Figure 5-6). Therefore, we again concluded that the siRNA pools failed to increase melanoma cell phagocytosis compared to the non-targeting control siRNA.

Table 5-3: Repeated siRNA Knockdown Pools

Group Number	Genes Targeted	Assigned Numbers
Group 1 Pool 1	ITGB3, CD81, CAV1	34, 5, 42
Group 1 Pool 5	ITGA5, MADCAM1, ITGB1	30, 22, 33
Group 1 Pool 10	ITGA3, SELPG, CDH1	28, 9, 11
Group 2 Pool 9	BCAM, MFGE8, CLDN12	20, 47, 15
Group 2 Pool 12	MCAM, ITGB3, LGALS1	17, 34, 39

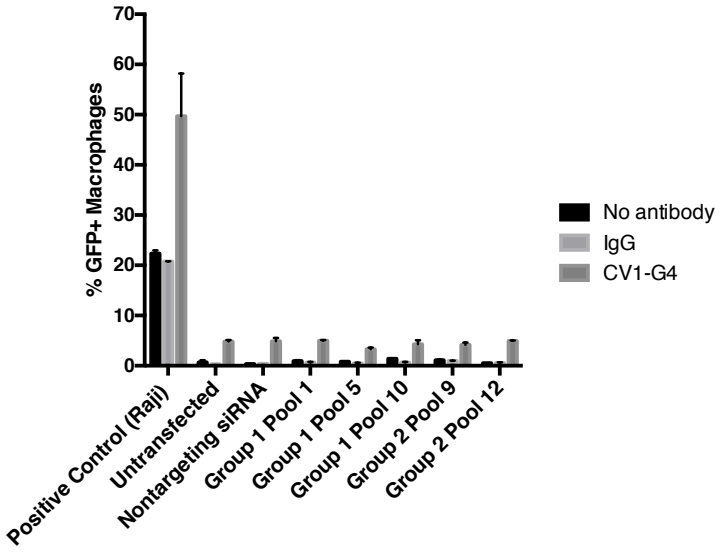

Figure 5-6: siRNA mediated knockdown of candidate proteins does not enhance melanoma cell phagocytosis. M21-GFP melanoma cells were transfected with siRNA pools containing 100 μM of 4 different siRNAs or 400 μM of a non-targeting control siRNA. 48 hours post-transfection, M21-GFP cells were co-cultured with J774 macrophages in the presence of control IgG4 or CV1-G4. Phagocytosis was quantified as the percent of $F4/80^+$ J774 cells that engulfed $CFSE^+$ tumor cells per total $F4/80^+$ population. Bars show data from duplicate tests for each pool (mean ± SEM). p=0.027 by two-way ANOVA

Conclusions: In this chapter, we investigated whether a secreted or membrane-bound anti-phagocytic factor was responsible for melanoma cell resistance to phagocytosis. We demonstrated that supernatant harvested from melanoma cells was not capable of inhibiting Raji cell phagocytosis. In addition, treatment of human melanoma cells with an inhibitor of secretion, Brefeldin A, failed to increase melanoma cell phagocytosis. These results indicate that a secreted factor is not responsible for mediating melanoma cell resistance to phagocytosis. To investigate whether melanoma cells express an uncharacterized, membrane-bound “don’t eat me” signal, we designed an siRNA panel targeting 47 “don’t eat

me” candidate proteins. Despite efficient knockdown of these proteins, none of the siRNAs tested in this panel were capable of enhancing melanoma cell phagocytosis. Therefore, the 47 proteins tested are unlikely to act as anti-phagocytic factors for melanoma cells. Further investigation will be needed to identify the mechanisms that mediate the peculiar resistance of melanoma cells to phagocytosis.

Chapter 6

Conclusion

Classically activated macrophages have the potential to mediate robust anti-tumor immunity through phagocytic clearance of tumor cells and antigen presentation to the adaptive immune system [37]. Phagocytosis relies on a balance of pro-phagocytic ("eat me") and anti-phagocytic ("don't eat me") signals expressed on the surface of target cells [48], which can be therapeutically altered to promote an anti-tumor innate immune response. Induction of "eat me" signals through anthracycline chemotherapy and blockade of the "don't eat me" signal CD47 have been shown to stimulate phagocytosis of both hematopoietic and solid tumor cells *in vitro* and to induce anti-tumor immune responses *in vivo* [64,66,75,83]. Although CD47 blockade has been shown to induce tumor regression in a number of solid tumor models, including ovarian [66], breast [66,73], bladder [66], leiomyosarcoma [74], colon [75], pancreatic [76], and lung [77] cancers, the effect of targeting the CD47-SIRPα axis for the treatment of malignant melanoma was previously unclear. Macrophages containing phagocytosed tumor material have been visualized within mouse melanoma tumors [47], which suggests that macrophage-activating therapies may be efficacious in the treatment of this disease.

Despite recent therapeutic advances, malignant melanoma remains the deadliest form of skin cancer with poor overall survival rates for patients with advanced, metastatic disease [3]. Immunotherapies targeting the adaptive immune system, including antibodies against the checkpoint molecules CTLA-4 and PD-1, have led to complete, durable responses in a subset of malignant

melanoma patients. However, over 40% of patients fail to respond to combination checkpoint blockade, emphasizing the need to develop additional therapeutics for the treatment of this disease. Enhancing tumor cell phagocytosis and antigen presentation may lead to an improved anti-tumor immune response and promote durable remissions in the subset of advanced melanoma patients that display resistance to current treatment modalities.

In addition to the human disease, malignant melanoma occurs in a number of other species, such as dogs and mice. Mouse models of malignant melanoma have been traditionally used to study tumor growth and the interaction of tumor cells with the host immune system. These models are widely used due to the ability to manipulate the mouse genome and the ability to easily harvest tumors and immune organs for further study. However, few spontaneous mouse models of melanoma exist, and these models may fail to recapitulate the heterogeneity and complexity of human tumors [14].

Canine malignant melanoma, which develops spontaneously in the setting of an intact immune system, represents another relevant translational model for human malignant melanoma (see Table 1-2). Unlike human malignant melanoma, canine malignant melanoma typically arises from pigment cells in the oral cavity, although it can also arise from dermal melanocytes. Despite differences in disease distribution and etiology, canine and human malignant melanoma share similar clinical presentations, histopathology, disease progression, and several molecular signaling pathways [22,25,26]. Similar to

human disease, loco-regional control of stage I/II canine melanoma can be achieved using radiation or surgery, but few efficacious treatments exist for advanced, metastatic disease, and the median overall survival for these patients remains poor [22]. The canine model provides the ability to perform preclinical trials in companion dogs that share similar environments to human patients [15]. Although murine and canine models have unique advantages and disadvantages (reviewed in Table 1-1), both models have the potential to significantly inform our understanding of human malignant melanoma. The collective knowledge gained from the use of these models can assist in the development of more efficacious therapies for patients with advanced disease [14].

Our objective in this dissertation was to characterize the anti-tumor immune response following modulation of pro-phagocytic and anti-phagocytic signals in malignant melanoma. Advances in cancer immunotherapy depend on preclinical testing, which provides critical insights into therapeutic efficacy and mechanisms of action. In order to provide a framework for preclinical testing, it is important to understand the similarities and differences in melanoma cell biology between human, mouse, and canine tumors. Identifying similarities in tumors from multiple species could reveal mechanisms of immunoevasion that are likely to be important for tumor cell survival. However, human melanoma may have significant biological differences from mouse or canine melanoma, and awareness of these differences is important to avoid over interpretation of data gained from animal models. Therefore, in this study, we utilized a multi-species

approach to evaluate the response of human, mouse, and canine melanoma cells to modulation of phagocytic signals.

Our first aim was to characterize the anti-tumor immune response to melanoma following CD47 blockade (Chapter 3). We confirmed the expression of CD47 on the surface of human, mouse, and dog melanoma cells and validated the ability of a SIRPα mimotope, CV1-G4, and an anti-CD47 monoclonal antibody, MIAP301, to block the CD47-SIRPα axis on these cells. Surprisingly, we found that melanoma cells from all three species displayed a resistance to phagocytosis that was not seen in lymphoma, breast/mammary gland cancer, or osteosarcoma cells, and the resistance of melanoma cells could not be fully mitigated by CD47 blockade. This defect in phagocytosis did not appear to be macrophage- or reagent-dependent, as similar results were seen with macrophages derived from two different sources and using different CD47 blocking reagents.

Next, we utilized a syngeneic mouse model of melanoma to evaluate the effect of CD47 blockade on anti-tumor T cell responses. CD47 blockade led to a slight increase in antigen-specific $CD8^+$ T cell activation in the tumor draining lymph node. This response appeared to be tumor specific, as no change in T cell activation was observed in the contralateral (non-tumor draining) lymph node. However, the increase in $CD8^+$ T cell activation did not appear to be therapeutically significant as CD47 blockade failed to mediate tumor regression

in this model. These results suggest that CD47 blockade, when used as single-agent therapy, could not overcome melanoma cell resistance to phagocytosis or lead to an anti-tumor T cell response capable of mediating tumor regression.

Although therapies targeting the CD47-SIRPα axis have demonstrated efficacy in a variety of hematopoietic and solid tumor types [64-66], previous studies have produced contradictory results regarding the efficacy of CD47 blockade in the treatment of malignant melanoma. In agreement with our study, Sockolosky et al [85] examined the effects of CD47 blockade in a B16 mouse model of melanoma and demonstrated no increase in tumor cell phagocytosis and no inhibition of tumor growth following treatment with an anti-mouse CD47 nanobody. However, Ngo et al [88] used an anti-CD47 antibody for the treatment of primary human melanoma xenografts and demonstrated an increase in melanoma cell phagocytosis *in vitro* as well as a decrease in tumor growth and metastasis *in vivo* following CD47 blockade. Our work provides a systematic evaluation of melanoma cell phagocytosis by examining the effects of CD47 blockade on melanoma cells derived from human, mouse, and dog cells. Similar to the study by Ngo, we observed a small increase in melanoma cell phagocytosis *in vitro*. However, our work revealed that the overall levels of melanoma cell phagocytosis remained very low compared to lymphoma, breast/mammary gland cancer, and osteosarcoma cell phagocytosis. We

concluded that CD47 blockade alone could not fully mitigate melanoma cell resistance to phagocytosis.

In our model, the small increase in melanoma cell phagocytosis following CD47 blockade did not appear to be therapeutically significant, as CD47 blockade failed to decrease tumor growth *in vivo*, in agreement with Sockolosky et al [85], but contrary to Ngo [88], who demonstrated decreased tumor volume following CD47 blockade. These different sets of results could be explained by the unique features of the model systems used: Ngo used human melanoma tumors xenografted into immunodeficient mice, whereas here, we used a syngeneic model of mouse melanoma. In a xenograft model, only tumor cells express human CD47 and are capable of binding human CD47-targeting reagents. Therefore, xenograft models might achieve higher concentrations of anti-CD47 antibodies in the tumor than syngeneic models, in which both malignant and normal cells are capable of binding CD47, causing much of the antibody to be lost to a large “antigen sink.” Therefore, melanoma cells in an immunodeficient model may be cleared more easily than the syngeneic tumor cells used in our model system. Preclinical studies in cynomolgus macaques have also demonstrated the existence of a large antigen sink from CD47 expressed on circulating red and white blood cells [67], which indicates that our syngeneic model might more accurately reflect a clinical setting.

Treatment with anthracycline chemotherapy has previously been shown to increase the expression of “eat me” signals and enhance tumor cell phagocytosis [53]. However, the effect of combining chemotherapy with CD47 blockade has yet to be examined. Our second goal was to evaluate whether increasing pro-phagocytic signals in combination with CD47 blockade could enhance melanoma cell phagocytosis and activation of a tumor-specific T cell response (Chapter 4). We demonstrated that low-dose doxorubicin chemotherapy was capable of upregulating expression of the pro-phagocytic signals calreticulin and phosphatidylserine on the surface of mouse melanoma cells. Despite this increase, combination doxorubicin and CD47 blockade failed to increase melanoma cell phagocytosis *in vitro*. Combination chemo-immunotherapy also failed to enhance antigen-specific T cell activation *in vitro* and *in vivo*.

In addition to increasing pro-phagocytic signals through low-dose chemotherapy, we utilized a tumor-specific antibody targeting the melanoma antigen CD271 to provide a pro-phagocytic signal through the Fc receptor. Combination CD271 and CD47 antibody therapy, again, failed to enhance melanoma cell phagocytosis. We concluded that melanoma cell resistance to phagocytosis could not be mitigated by modulation of know pro-phagocytic and anti-phagocytic signals.

Having demonstrated that melanoma cells exhibit a unique resistance to phagocytosis, we hypothesized that this resistance was mediated by a soluble or

membrane-bound “don’t eat me” signal expressed by melanoma cells. We demonstrated that phagocytosis of melanoma cells was not enhanced by inhibition of secretory pathways using Brefeldin A, and phagocytosis of sensitive tumor cells (lymphoma) was not impaired in the presence of melanoma culture supernatants. Therefore, we concluded that secreted factors were not responsible for mediating melanoma cell resistance to phagocytosis.

To investigate whether melanoma cells expressed an uncharacterized, membrane-bound “don’t eat me” signal that was responsible for the observed resistance to phagocytosis, we designed a siRNA panel targeting 47 “don’t eat me” candidate proteins. Proteins were selected using gene expression data and published reports in the scientific literature to identify candidate proteins that were selectively expressed on the surface of melanoma cells as compared to lymphoma, colon cancer, lung cancer, or breast cancer cells. None of the 47 siRNAs tested in this panel were capable of enhancing melanoma cell phagocytosis following transfection. It is possible that we did not achieve sufficient protein knockdown using siRNAs to observe a change in cell phagocytosis. However, siRNA treatment achieved a 75-90% reduction in mRNA expression in eight genes selected for testing, and a CD47-targeting siRNA achieving similar levels of knockdown has been shown to increase the phagocytosis of laryngeal squamous cell carcinoma cells *in vitro* [161]. Therefore, we believe the siRNAs used in this study achieved adequate levels of

protein reduction, and we concluded that the 47 proteins tested are unlikely to act as anti-phagocytic factors for melanoma cells.

A number of untested elements may be responsible for melanoma cell resistance to phagocytosis. It is possible that an untested membrane-bound protein is responsible for inhibiting melanoma cell phagocytosis. A genome wide screen could be used to identify this protein; however, if the protein responsible for mediating resistance were stably expressed (and therefore unaffected by a knockout screen), it would not be detected in this assay. It is also possible that a combination of proteins contributes to the resistant phenotype. Such combinations would not be detected by a genome wide screen, and testing the millions of possible protein combinations using genomic screens would be impractical. Although no carbohydrate or lipid-based “don’t eat me” signals have been identified to date, non-protein elements of melanoma cells have the potential to transmit anti-phagocytic signals. Assays to reduce cell glycosylation could be performed to test for the presence of a carbohydrate moiety or a glycosylation pattern that is acting as “don’t eat me” signal. In addition, signaling through ceramide, sphingosine, and other membrane-bound lipids could mediate resistance to phagocytosis. Pharmacologic inhibitors of sphingolipid synthesis have been described and could be used to reduce sphingolipid expression in melanoma cells; however, many of these inhibitors have off-target effects on other molecules, which could make data interpretation challenging [162].

In this study, we observed a unique phagocytosis resistance phenotype in malignant melanoma cells. Evasion of phagocytosis and the innate immune response could be an important component of the primary resistance to immunotherapy seen in many melanoma patients. Thus, advancing our understanding of how melanoma cells avoid elimination by the innate immune system could lead to the development of new therapeutic strategies to improve patient responses and overcome immunotherapy resistance. Further investigation will be needed to identify the mechanisms that mediate the peculiar resistance of melanoma cells to phagocytosis.

REFERENCES

1. Chao MP, Weissman IL, Majeti R. The CD47-SIRPalpha pathway in cancer immune evasion and potential therapeutic implications. Curr Opin Immunol 2012; 24 (2):225-232.
2. Melanoma Treatment (PDQ®)–Health Professional Version. National Cancer Institute 2017.
3. Cancer Facts & Figures 2017. Atlanta: American Cancer Society, 2017.
4. Shah DJ, Dronca RS. Latest advances in chemotherapeutic, targeted, and immune approaches in the treatment of metastatic melanoma. Mayo Clin Proc 2014; 89 (4):504-519.
5. Tentori L, Lacal PM, Graziani G. Challenging resistance mechanisms to therapies for metastatic melanoma. Trends Pharmacol Sci 2013; 34 (12):656-666.
6. Davies H, Bignell GR, Cox C, Stephens P, Edkins S, Clegg S, et al. Mutations of the BRAF gene in human cancer. Nature 2002; 417:949-954.
7. Ehrlich P. The collected papers of Paul Ehrlich: in four volumes including a complete bibliography: Pergamon Press, 1957.
8. Hegde UP, Mukherji B. Current status of chimeric antigen receptor engineered T cell-based and immune checkpoint blockade-based cancer immunotherapies. Cancer Immunol Immunother 2017.
9. Sharma P, Allison JP. Immune checkpoint targeting in cancer therapy: toward combination strategies with curative potential. Cell 2015; 161 (2):205-214.
10. Alexandrov LB, Nik-Zainal S, Wedge DC, Aparicio SA, Behjati S, Biankin AV, et al. Signatures of mutational processes in human cancer. Nature 2013; 500 (7463):415-421.
11. Hodi FS, Chesney J, Pavlick AC, Robert C, Grossmann KF, McDermott DF, et al. Combined nivolumab and ipilimumab versus ipilimumab alone in patients with advanced melanoma: 2-year overall survival outcomes in a multicentre, randomised, controlled, phase 2 trial. The Lancet Oncology 2016; 17 (11):1558-1568.
12. Weber JS, Hodi FS, Wolchok JD, Topalian SL, Schadendorf D, Larkin J, et al. Safety Profile of Nivolumab Monotherapy: A Pooled Analysis of Patients With Advanced Melanoma. J Clin Oncol 2017; 35 (7):785-792.
13. Beaumont KA, Mohana-Kumaran N, Haass NK. Modeling Melanoma In Vitro and In Vivo. Healthcare (Basel) 2013; 2 (1):27-46.
14. Sharma A, Kuzu OF, Nguyen FD, Noory MA. Current State of Animal (Mouse) Modeling in Melanoma Research. Cancer Growth Metastasis 2015; 8 (Suppl 1):81-94.
15. Park JS, Withers SS, Modiano JF, Kent MS, Chen M, Luna JI, et al. Canine cancer immunotherapy studies: linking mouse and human. J Immunother Cancer 2016; 4:97.

16. Anderson KL, Modiano JF. Progress in adaptive immunotherapy for cancer in companion animals: success on the path to a cure. Veterinary Sciences 2015; 2 (4):363-387.
17. Sivan A, Corrales L, Hubert N, Williams JB, Aquino-Michaels K, Earley ZM, et al. Commensal Bifidobacterium promotes antitumor immunity and facilitates anti–PD-L1 efficacy Science 2015; 350 (6264):1084-1089.
18. Vetizou M, Pitt JM, Daillere R, Lepage P, Waldschmitt N, Flament C, et al. Anticancer immunotherapy by CTLA-4 blockade relies on the gut microbiota. Science 2015; 350 (6264):1079-1084.
19. Mirsoian A, Bouchlaka MN, Sckisel GD, Chen M, Pai CC, Maverakis E, et al. Adiposity induces lethal cytokine storm after systemic administration of stimulatory immunotherapy regimens in aged mice. J Exp Med 2014; 211 (12):2373-2383.
20. van der Weyden L, Patton EE, Wood GA, Foote AK, Brenn T, Arends MJ, et al. Cross-species models of human melanoma. J Pathol 2016; 238 (2):152-165.
21. Melnikova VO, Bolshakov SV, Walker C, Ananthaswamy HN. Genomic alterations in spontaneous and carcinogen-induced murine melanoma cell lines. Oncogene 2004; 23 (13):2347-2356.
22. Nishiya A, Massoco C, Felizzola C, Perlmann E, Batschinski K, Tedardi M, et al. Comparative Aspects of Canine Melanoma. Veterinary Sciences 2016; 3 (1):7.
23. Simpson RM, Bastian BC, Michael HT, Webster JD, Prasad ML, Conway CM, et al. Sporadic naturally occurring melanoma in dogs as a preclinical model for human melanoma. Pigment Cell Melanoma Res 2014; 27 (1):37-47.
24. Smith SH, Goldschmidt MH, McManus PM. A Comparative Review of Melanocytic Neoplasms. Vet Pathol 2002; 39:651–678.
25. Paoloni M, Khanna C. Translation of new cancer treatments from pet dogs to humans. Nature Reviews Cancer 2008; 8 (2):147-156.
26. Atherton MJ, Morris JS, McDermott MR, Lichty BD. Cancer immunology and canine malignant melanoma: A comparative review. Vet Immunol Immunopathol 2016; 169:15-26.
27. Wu H, Goel V, Haluska FG. PTEN signaling pathways in melanoma. Oncogene 2003; 22 (20):3113-3122.
28. Piccinin S, Doglioni C, Maestro R, Vukisavljevic T, Gasparotto D, Dorazi C, et al. p16/CDKN2 AND CDK4 gene mutations in sporadic melanoma development and progression. Int J Cancer 1997; 74 (1):26-30.
29. Orlow I, Begg CB, Cotignola J, Roy P, Hummer AJ, Clas BA, et al. CDKN2A germline mutations in individuals with cutaneous malignant melanoma. J Invest Dermatol 2007; 127 (5):1234-1243.
30. Koenig A, Bianco SR, Fosmire SP, Wojcieszyn J, Modiano JF. Expression and Significance of p53, Rb, p21/waf-1, p16/ink-4a, and PTEN Tumor Suppressors in Canine Melanoma. Vet Pathol 2002; 39:458–472.

31. Bergman PJ, Camps-Palau MA, McKnight JA, Leibman NF, Craft DM, Leung C, et al. Development of a xenogeneic DNA vaccine program for canine malignant melanoma at the Animal Medical Center. Vaccine 2006; 24 (21):4582-4585.
32. Poorman K, Borst L, Moroff S, Roy S, Labelle P, Motsinger-Reif A, et al. Comparative cytogenetic characterization of primary canine melanocytic lesions using array CGH and fluorescence in situ hybridization. Chromosome Res 2015; 23 (2):171-186.
33. Bardeesy N, Wong K-K, DePinho RA, Chin L. Animal Models of Melanoma: Recent Advances and Future Prospects. Adv Cancer Res 2000; 79:123-156.
34. Millikan LE, Boylon JL, Hook RR, Manning PJ. Melanoma in Sinclair Swine: A New Animal Model. Journal of Investigative Dermatology 1974; 62 (1):20-30.
35. Gajewski TF, Schreiber H, Fu YX. Innate and adaptive immune cells in the tumor microenvironment. Nat Immunol 2013; 14 (10):1014-1022.
36. Curran E, Corrales L, Kline J. Targeting the innate immune system as immunotherapy for acute myeloid leukemia. Front Oncol 2015; 5:83.
37. Goswami KK, Ghosh T, Ghosh S, Sarkar M, Bose A, Baral R. Tumor promoting role of anti-tumor macrophages in tumor microenvironment. Cell Immunol 2017.
38. Zheng X, Turkowski K, Mora J, Brüne B, Seeger W, Weigert A, et al. Redirecting tumor-associated macrophages to become tumoricidal effectors as a novel strategy for cancer therapy. Oncotarget 2017.
39. Murray PJ, Wynn TA. Protective and pathogenic functions of macrophage subsets. Nat Rev Immunol 2011; 11 (11):723-737.
40. Martinez FO, Gordon S. The M1 and M2 paradigm of macrophage activation: time for reassessment. F1000 Prime Reports 2014; 6:1-13.
41. Asano K, Nabeyama A, Miyake Y, Qiu CH, Kurita A, Tomura M, et al. CD169-positive macrophages dominate antitumor immunity by crosspresenting dead cell-associated antigens. Immunity 2011; 34 (1):85-95.
42. Bernhard CA, Ried C, Kochanek S, Brocker T. CD169+ macrophages are sufficient for priming of CTLs with specificities left out by cross-priming dendritic cells. Proc Natl Acad Sci U S A 2015; 112 (17):5461-5466.
43. Nimmerjahn F, Gordan S, Lux A. FcgammaR dependent mechanisms of cytotoxic, agonistic, and neutralizing antibody activities. Trends Immunol 2015; 36 (6):325-336.
44. Weiskopf K. Cancer immunotherapy targeting the CD47/SIRPalpha axis. Eur J Cancer 2017; 76:100-109.
45. Lee Y, Biswas SK. Rewiring macrophages for anti-tumour immunity. Nat Cell Biol 2016; 18 (7):718-720.
46. Baer C, Squadrito ML, Laoui D, Thompson D, Hansen SK, Kiialainen A, et al. Suppression of microRNA activity amplifies IFN-gamma-induced macrophage activation and promotes anti-tumour immunity. Nat Cell Biol 2016; 18 (7):790-802.

47. Lehmann B, Biburger M, Bruckner C, Ipsen-Escobedo A, Gordan S, Lehmann C, et al. Tumor location determines tissue-specific recruitment of tumor-associated macrophages and antibody-dependent immunotherapy response. Science Immunology 2017; 2:1-11.
48. Chao MP, Majeti R, Weissman IL. Programmed cell removal: a new obstacle in the road to developing cancer. Nat Rev Cancer 2011; 12 (1):58-67.
49. Segawa K, Kurata S, Yanagihashi Y, Brummelkamp TR, Matsuda F, Nagata S. Caspase-mediated cleavage of phospholipid flippase for apoptotic phosphatidylserine exposure. Science 2014; 344 (6188):1160-1164.
50. Ravichandran KS. Beginnings of a good apoptotic meal: the find-me and eat-me signaling pathways. Immunity 2011; 35 (4):445-455.
51. Wiersma VR, Michalak M, Abdullah TM, Bremer E, Eggleton P. Mechanisms of Translocation of ER Chaperones to the Cell Surface and Immunomodulatory Roles in Cancer and Autoimmunity. Front Oncol 2015; 5:7.
52. Chao MP, Jaiswal S, Weissman-Tsukamoto R, Alizadeh AA, Gentles AJ, Volkmer J, et al. Calreticulin is the dominant pro-phagocytic signal on multiple human cancers and is counterbalanced by CD47. Sci Transl Med 2010; 2 (63):63ra94.
53. Obeid M, Tesniere A, Ghiringhelli F, Fimia GM, Apetoh L, Perfettini JL, et al. Calreticulin exposure dictates the immunogenicity of cancer cell death. Nat Med 2007; 13 (1):54-61.
54. Brown E, Hooper L, Ho T, Greshamll H. Integrin-associated Protein: A 50-kD Plasma Membrane Antigen Physically and Functionally Associated with Integrins. The Journal of Cell Biology 1990; 111 (6):2785-2794.
55. Brown EJ, Frazier WA. Integrin-associated protein (CD47) and its ligands. Trends in Cell Biology 2001; 11 (3):130-135.
56. Barclay AN, Brown MH. The SIRP family of receptors and immune regulation. Nat Rev Immunol 2006; 6 (6):457-464.
57. Barclay AN, Van den Berg TK. The interaction between signal regulatory protein alpha (SIRPalpha) and CD47: structure, function, and therapeutic target. Annu Rev Immunol 2014; 32:25-50.
58. Tsai RK, Discher DE. Inhibition of "self" engulfment through deactivation of myosin-II at the phagocytic synapse between human cells. J Cell Biol 2008; 180 (5):989-1003.
59. Oldenborg P-A, Zheleznyak A, Fang Y-F, Lagenaur CF, Gresham HD, Lindberg FP. Role of CD47 as a Marker of Self on Red Blood Cells. Science 2000; 288 (5473):2051-2054.
60. Olsson M, Bruhns P, Frazier W, Ravetch J, Oldenborg PA. Platelet homeostasis is regulated by platelet expression of CD47 under normal conditions and in passive immune thrombocytopenia. Blood 2005; 105:3577-3582.
61. Jaiswal S, Jamieson CH, Pang WW, Park CY, Chao MP, Majeti R, et al. CD47 is upregulated on circulating hematopoietic stem cells and leukemia cells to avoid phagocytosis. Cell 2009; 138 (2):271-285.

62. Reinhold MI, Lindberg FP, Plas D, Reynolds S, Peters MG, Brown E. In vivo expression of alternatively spliced forms of integrin-associated protein (CD47). Journal of Cell Science 1995; 108:3419-3425.
63. Poels L, Peters D, van Megen Y, Vooijs G, Verheyen R, Willemen A, et al. Monoclonal antibody against human ovarian tumor- associated antigens. Journal of the National Cancer Institute 1986; 76:781-791.
64. Majeti R, Chao MP, Alizadeh AA, Pang WW, Jaiswal S, Gibbs KD, Jr., et al. CD47 is an adverse prognostic factor and therapeutic antibody target on human acute myeloid leukemia stem cells. Cell 2009; 138 (2):286-299.
65. Chao MP, Alizadeh AA, Tang C, Myklebust JH, Varghese B, Gill S, et al. Anti-CD47 antibody synergizes with rituximab to promote phagocytosis and eradicate non-Hodgkin lymphoma. Cell 2010; 142 (5):699-713.
66. Willingham SB, Volkmer J-P, Gentles AJ, Sahoo D, Dalerba P, Mitra SS, et al. The CD47-signal regulatory protein alpha (SIRPa) interaction is a therapeutic target for human solid tumors. PNAS 2012; 109 (17):6662-6667.
67. Liu J, Wang L, Zhao F, Tseng S, Narayanan C, Shura L, et al. Pre-Clinical Development of a Humanized Anti-CD47 Antibody with Anti-Cancer Therapeutic Potential. PLoS One 2015; 10 (9):e0137345.
68. Weiskopf K, Ring AM, Ho CC, Volkmer JP, Levin AM, Volkmer AK, et al. Engineered SIRPalpha variants as immunotherapeutic adjuvants to anticancer antibodies. Science 2013; 341 (6141):88-91.
69. Piccione EC, Juarez S, Liu J, Tseng S, Ryan CE, Narayanan C, et al. A bispecific antibody targeting CD47 and CD20 selectively binds and eliminates dual antigen expressing lymphoma cells. MAbs 2015; 7 (5):946-956.
70. Piccione EC, Juarez S, Tseng S, Liu J, Stafford M, Narayanan C, et al. SIRPalpha-Antibody Fusion Proteins Selectively Bind and Eliminate Dual Antigen-Expressing Tumor Cells. Clin Cancer Res 2016; 22 (20):5109-5119.
71. Chao MP, Alizadeh AA, Tang C, Jan M, Weissman-Tsukamoto R, Zhao F, et al. Therapeutic antibody targeting of CD47 eliminates human acute lymphoblastic leukemia. Cancer Res 2011; 71 (4):1374-1384.
72. Kim D, Wang J, Willingham SB, Martin R, Wernig G, Weissman IL. Anti-CD47 antibodies promote phagocytosis and inhibit the growth of human myeloma cells. Leukemia 2012; 26 (12):2538-2545.
73. Kaur S, Elkahloun AG, Singh SP, Chen Q-R, Meerzaman DM, Song T, et al. A function-blocking CD47 antibody suppresses stem cell and EGF signaling in triple-negative breast cancer. Oncotarget 2016; 7 (9):10133-10152.
74. Edris B, Weiskopf K, Volkmer AK, Volkmer J-P, Willingham SB, Contreras-Trujillo H, et al. Antibody therapy targeting the CD47 protein is effective in a model of aggressive metastatic leiomyosarcoma. PNAS 2012; 109 (17):6656-6661.
75. Tseng D, Volkmer J-P, Willingham SB, Contreras-Trujillo H, Fathman JW, Fernhoff NB, et al. Anti-CD47 antibody–mediated phagocytosis of cancer by macrophages primes an effective antitumor

T-cell response. PNAS 2013; 110 (27):11103-11108.
76. Krampitz GW, George BM, Willingham SB, Volkmer JP, Weiskopf K, Jahchan N, et al. Identification of tumorigenic cells and therapeutic targets in pancreatic neuroendocrine tumors. Proc Natl Acad Sci U S A 2016; 113 (16):4464-4469.
77. Weiskopf K, Jahchan NS, Schnorr PJ, Cristea S, Ring AM, Maute RL, et al. CD47-blocking immunotherapies stimulate macrophage-mediated destruction of small-cell lung cancer. J Clin Invest 2016; 126 (7):2610-2620.
78. Weiskopf K, Anderson KL, Ito D, Schnorr PJ, Tomiyasu H, Ring AM, et al. Eradication of Canine Diffuse Large B-Cell Lymphoma in a Murine Xenograft Model with CD47 Blockade and Anti-CD20. Cancer Immunol Res 2016; 4 (12):1072-1087.
79. Zhang M, Hutter G, Kahn SA, Azad TD, Gholamin S, Xu CY, et al. Anti-CD47 Treatment Stimulates Phagocytosis of Glioblastoma by M1 and M2 Polarized Macrophages and Promotes M1 Polarized Macrophages In Vivo. PLoS One 2016; 11 (4):e0153550.
80. Zhao XW, van Beek EM, Schornagel K, Van der Maaden H, Van Houdt M, Otten MA, et al. CD47-signal regulatory protein-alpha (SIRPa) interactions form a barrier for antibody-mediated tumor cell destruction. PNAS 2011; 108 (45):18342-18347.
81. Matozaki T, Murata Y, Okazawa H, Ohnishi H. Functions and molecular mechanisms of the CD47-SIRPalpha signalling pathway. Trends Cell Biol 2009; 19 (2):72-80.
82. Yi T, Li J, Chen H, Wu J, An J, Xu Y, et al. Splenic Dendritic Cells Survey Red Blood Cells for Missing Self-CD47 to Trigger Adaptive Immune Responses. Immunity 2015; 43 (4):764-775.
83. Liu X, Pu Y, Cron K, Deng L, Kline J, Frazier WA, et al. CD47 blockade triggers T cell-mediated destruction of immunogenic tumors. Nat Med 2015; 21 (10):1209-1215.
84. Latour S, Tanaka H, Demeure C, Mateo V, Rubio M, Brown EJ, et al. Bidirectional Negative Regulation of Human T and Dendritic Cells by CD47 and Its Cognate Receptor Signal-Regulator Protein-α : Down-Regulation of IL-12 Responsiveness and Inhibition of Dendritic Cell Activation. The Journal of Immunology 2001; 167:2547-2554.
85. Sockolosky JT, Dougan M, Ingram JR, Ho CC, Kauke MJ, Almo SC, et al. Durable antitumor responses to CD47 blockade require adaptive immune stimulation. Proc Natl Acad Sci U S A 2016; 113 (19):E2646-2654.
86. Aderem A, Underhill DM. Mechanisms of Phagocytosis in Macrophages. Annu Rev Immunol 1999; 17:593–623.
87. Wang Y, Xu Z, Guo S, Zhang L, Sharma A, Robertson GP, et al. Intravenous delivery of siRNA targeting CD47 effectively inhibits melanoma tumor growth and lung metastasis. Mol Ther 2013; 21 (10):1919-1929.

88. Ngo M, Han A, Lakatos A, Sahoo D, Hachey SJ, Weiskopf K, et al. Antibody Therapy Targeting CD47 and CD271 Effectively Suppresses Melanoma Metastasis in Patient-Derived Xenografts. Cell Rep 2016; 16 (6):1701-1716.
89. Rutgen BC, Hammer SE, Gerner W, Christian M, de Arespacochaga AG, Willmann M, et al. Establishment and characterization of a novel canine B-cell line derived from a spontaneously occurring diffuse large cell lymphoma. Leuk Res 2010; 34 (7):932-938.
90. Modiano JF, Ritt MG, Wojcieszyn J, Smith R. Growth Arrest of Melanoma Cells Is Differentially Regulated by Contact Inhibition and Serum Deprivation. DNA and Cell Biology 1999; 18 (5):357-367.
91. Bianco SR, Sun J, Fosmire SP, Hance K, Padilla ML, Ritt MG, et al. Enhancing antimelanoma immune responses through apoptosis. Cancer Gene Ther 2003; 10 (9):726-736.
92. Modiano JF, Kokai Y, Weiner DB, Pykett MJ, Nowell PC, Lyttle CR. Progesterone Augments Proliferation Induced by Epidermal Growth Factor in a Feline Mammary
Adenocarcinoma Cell Line. Journal of Cellular Biochemistry 1991; 45:196-206
93. Thayanithy V, Park C, Sarver AL, Kartha RV, Korpela DM, Graef AJ, et al. Combinatorial treatment of DNA and chromatin-modifying drugs cause cell death in human and canine osteosarcoma cell lines. PLoS One 2012; 7 (9):e43720.
94. Rahman M, Jackson LK, Johnson WE, Li DY, Bild AH, Piccolo SR. Alternative preprocessing of RNA-Sequencing data in The Cancer Genome Atlas leads to improved analysis results. Bioinformatics 2015; 31 (22):3666-3672.
95. Binder JX, Pletscher-Frankild S, Tsafou K, Stolte C, O'Donoghue SI, Schneider R, et al. COMPARTMENTS: unification and visualization of protein subcellular localization evidence. Database (Oxford) 2014; 2014:bau012.
96. Ola MS, Nawaz M, Ahsan H. Role of Bcl-2 family proteins and caspases in the regulation of apoptosis. Mol Cell Biochem 2011; 351 (1-2):41-58.
97. McGary EC, Lev DC, Bar-Eli M. Cellular Adhesion Pathways and Metastatic Potential of Human Melanoma. Cancer Biology & Therapy 2014; 1 (5):459-465.
98. Hong IK, Jin YJ, Byun HJ, Jeoung DI, Kim YM, Lee H. Homophilic interactions of Tetraspanin CD151 up-regulate motility and matrix metalloproteinase-9 expression of human melanoma cells through adhesion-dependent c-Jun activation signaling pathways. J Biol Chem 2006; 281 (34):24279-24292.
99. Sadej R, Grudowska A, Turczyk L, Kordek R, Romanska HM. CD151 in cancer progression and metastasis: a complex scenario. Lab Invest 2014; 94 (1):41-51.
100. Hong IK, Byun HJ, Lee J, Jin YJ, Wang SJ, Jeoung DI, et al. The tetraspanin CD81 protein increases melanoma cell motility by up-regulating metalloproteinase MT1-MMP expression through the pro-oncogenic Akt-dependent Sp1 activation signaling pathways. J Biol Chem 2014; 289 (22):15691-15704.

101. Vences-Catalan F, Rajapaksa R, Srivastava MK, Marabelle A, Kuo CC, Levy R, et al. Tetraspanin CD81 promotes tumor growth and metastasis by modulating the functions of T regulatory and myeloid-derived suppressor cells. Cancer Res 2015; 75 (21):4517-4526.
102. Kamal AM, Flower RJ, Perretti M. An overview of the effects of annexin 1 on cells involved in the inflammatory process. Memórias do Instituto Oswaldo Cruz 2005; 100 (Suppl 1):39-48.
103. Yaddanapudi K, Rendon BE, Lamont G, Kim EJ, Al Rayyan N, Richie J, et al. MIF Is Necessary for Late-Stage Melanoma Patient MDSC Immune Suppression and Differentiation. Cancer Immunol Res 2016; 4 (2):101-112.
104. Oliveira CSd. The role of MIF in melanoma progression. School of Biomedical Sciences and Pharmacy: University of Newcastle, 2012.
105. Tinoco R, Carrette F, Barraza ML, Otero DC, Magana J, Bosenberg MW, et al. PSGL-1 Is an Immune Checkpoint Regulator that Promotes T Cell Exhaustion. Immunity 2016; 44 (5):1190-1203.
106. Yamaoka T, Fujimoto M, Ogawa F, Yoshizaki A, Bae SJ, Muroi E, et al. The roles of P- and E-selectins and P-selectin glycoprotein ligand-1 in primary and metastatic mouse melanomas. J Dermatol Sci 2011; 64 (2):99-107.
107. Lal G, Contreras PG, Kulak M, Woodfield G, Bair T, Domann FE, et al. Human Melanoma cells over-express extracellular matrix 1 (ECM1) which is regulated by TFAP2C. PLoS One 2013; 8 (9):e73953.
108. Harbst K, Lauss M, Cirenajwis H, Winter C, Howlin J, Torngren T, et al. Molecular and genetic diversity in the metastatic process of melanoma. J Pathol 2014; 233 (1):39-50.
109. Lade-Keller J, Riber-Hansen R, Guldberg P, Schmidt H, Hamilton-Dutoit SJ, Steiniche T. E- to N-cadherin switch in melanoma is associated with decreased expression of phosphatase and tensin homolog and cancer progression. Br J Dermatol 2013; 169 (3):618-628.
110. Haqq C, Nosrati M, Sudilovsky D, Crothers J, Khodabakhsh D, Pulliam BL, et al. The gene expression signatures of melanoma progression. PNAS 2005; 102 (17):6092–6097.
111. Vieira AF, Paredes J. P-cadherin and the journey to cancer metastasis. Mol Cancer 2015; 14:178.
112. Leotlela PD, Wade MS, Duray PH, Rhode MJ, Brown HF, Rosenthal DT, et al. Claudin-1 overexpression in melanoma is regulated by PKC and contributes to melanoma cell motility. Oncogene 2007; 26 (26):3846-3856.
113. Morita K, Morita NI, Nemoto K, Nakamura Y, Miyachi Y, Muto M. Expression of claudin in melanoma cells. J Dermatol 2008; 35 (1):36-38.
114. Wai Wong C, Dye DE, Coombe DR. The role of immunoglobulin superfamily cell adhesion molecules in cancer metastasis. Int J Cell Biol 2012; 2012:340296.
115. Jannie KM, Stipp CS, Weiner JA. ALCAM regulates motility, invasiveness, and adherens junction formation in uveal melanoma cells. PLoS One 2012; 7 (6):e39330.

116. Braeuer RR, Zigler M, Villares GJ, Dobroff AS, Bar-Eli M. Transcriptional control of melanoma metastasis: the importance of the tumor microenvironment. Semin Cancer Biol 2011; 21 (2):83-88.
117. Yazawa EM, Geddes-Sweeney JE, Cedeno-Laurent F, Walley KC, Barthel SR, Opperman MJ, et al. Melanoma Cell Galectin-1 Ligands Functionally Correlate with Malignant Potential. J Invest Dermatol 2015; 135 (7):1849-1862.
118. Liu R, Shi Y, Yang HJ, Wang L, Zhang S, Xia YY, et al. Neural cell adhesion molecule potentiates the growth of murine melanoma via beta-catenin signaling by association with fibroblast growth factor receptor and glycogen synthase kinase-3beta. J Biol Chem 2011; 286 (29):26127-26137.
119. Beauchemin N, Arabzadeh A. Carcinoembryonic antigen-related cell adhesion molecules (CEACAMs) in cancer progression and metastasis. Cancer Metastasis Rev 2013; 32 (3-4):643-671.
120. Akiyama H, Iwahana Y, Suda M, Yoshimura A, Kogai H, Nagashima A, et al. The FBI1/Akirin2 target gene, BCAM, acts as a suppressive oncogene. PLoS One 2013; 8 (11):e78716.
121. Kiefel H, Bondong S, Hazin J, Ridinger J, Schirmer U, Riedle S, et al. L1CAM: a major driver for tumor cell invasion and motility. Cell Adh Migr 2012; 6 (4):374-384.
122. Leung E, Kanwar RK, Kanwar JR, Krissansen GW. Mucosal vascular addressin cell adhesion molecule-1 is expressed outside the endothelial lineage on fibroblasts and melanoma cells. Immunology and Cell Biology 2003; 81:320–327.
123. Clawson GA, Matters GL, Xin P, Imamura-Kawasawa Y, Du Z, Thiboutot DM, et al. Macrophage-tumor cell fusions from peripheral blood of melanoma patients. PLoS One 2015; 10 (8):e0134320.
124. Ghislin S, Obino D, Middendorp S, Boggetto N, Alcaide-Loridan C, Deshayes F. Junctional adhesion molecules are required for melanoma cell lines transendothelial migration in vitro. Pigment Cell Melanoma Res 2011; 24 (3):504-511.
125. Arcangeli ML, Frontera V, Bardin F, Thomassin J, Chetaille B, Adams S, et al. The Junctional Adhesion Molecule-B regulates JAM-C-dependent melanoma cell metastasis. FEBS Lett 2012; 586 (22):4046-4051.
126. Duncan L, Bouffard D, Howard C, Mihm M, Byers H. In situ distribution of integrin alpha 2 beta 1 and alpha-actinin in melanocytic proliferations. Mod Pathol 1996; 9 (9):938-943.
127. Aina OH, Maeda Y, Harrison M, Zwingenberger AL, Walker NJ, Lam KS, et al. Canine malignant melanoma alpha-3 integrin binding peptides. Vet Immunol Immunopathol 2011; 143 (1-2):11-19.
128. Kramer RH, Vu M, Cheng I Y-F, Ramos DM. Integrin expression in malignant melanoma. Cancer Metastasis Rev 1991; 10:49-59.

129. Abdel-Ghany M, Cheng HC, Elble RC, Pauli BU. Focal adhesion kinase activated by beta(4) integrin ligation to mCLCA1 mediates early metastatic growth. J Biol Chem 2002; 277 (37):34391-34400.
130. Wayner EA, Orlando RA, Cheresh DA. Integrins alphavbeta3 and alphavbeta5 Contribute to Cell Attachment to Vitronectin but Differentially Distribute on the Cell Surface. The Journal of Cell Biology 1991
; 113 (4):919-929.
131. Quan L, Shi J, Tian Y, Zhang Q, Zhang Y, Zhang Y, et al. Identification of potential therapeutic targets for melanoma using gene expression analysis. Neoplasma 2015; 62 (5):733-739.
132. Nguyen A, Detty S, Agrawal D. Clinical Implications of High-mobility Group Box-1 (HMGB1) and the Receptor for Advanced Glycation End-products (RAGE) in Cutaneous Malignancy: A Systematic Review. Anticancer Res 2017; 37 (1):1-7
.
133. Herwig N, Belter B, Wolf S, Haase-Kohn C, Pietzsch J. Interaction of extracellular S100A4 with RAGE prompts prometastatic activation of A375 melanoma cells. J Cell Mol Med 2016; 20 (5):825-835.
134. Braeuer RR, Shoshan E, Kamiya T, Bar-Eli M. The sweet and bitter sides of galectins in melanoma progression. Pigment Cell Melanoma Res 2012; 25 (5):592-601.
135. Salerno EP, Bedognetti D, Mauldin IS, Deacon DH, Shea SM, Pinczewski J, et al. Human melanomas and ovarian cancers overexpressing mechanical barrier molecule genes lack immune signatures and have increased patient mortality risk. Oncoimmunology 2016; 5 (12):e1240857.
136. Conde-Perez A, Gros G, Longvert C, Pedersen M, Petit V, Aktary Z, et al. A caveolin-dependent and PI3K/AKT-independent role of PTEN in beta-catenin transcriptional activity. Nat Commun 2015; 6:8093.
137. Ohkawa Y, Miyazaki S, Hamamura K, Kambe M, Miyata M, Tajima O, et al. Ganglioside GD3 enhances adhesion signals and augments malignant properties of melanoma cells by recruiting integrins to glycolipid-enriched microdomains. J Biol Chem 2010; 285 (35):27213-27223.
138. Hamamura K, Furukawa K, Hayashi T, Hattori T, Nakano J, Nakashima H, et al. Ganglioside GD3 promotes cell growth and invasion through p130Cas and paxillin in malignant melanoma cells. PNAS 2005; 102 (31):11041-11046.
139. Fetsch PA, Marincola FM, Filie A, Hijazi YM, Kleiner DE, Abati A. Melanoma-Associated Antigen Recognized
by T Cells (MART-1): The Advent of a Preferred Immunocytochemical Antibody for the Diagnosis of Metastatic Malignant Melanoma with Fine-Needle Aspiration. Cancer 1999; 25 (87):37-42.
140. Barrio MM, Abes R, Colombo M, Pizzurro G, Boix C, Roberti MP, et al. Human macrophages and dendritic cells can equally present MART-1 antigen to CD8(+) T cells after phagocytosis of gamma-irradiated melanoma cells. PLoS One 2012; 7 (7):e40311.

141. Shi F, Xu Z, Chen H, Wang X, Cui J, Zhang P, et al. A monoclonal antibody against PMEL. Monoclon Antib Immunodiagn Immunother 2014; 33 (5):354-360.
142. Ghanem G, Fabrice J. Tyrosinase related protein 1 (TYRP1/gp75) in human cutaneous melanoma. Mol Oncol 2011; 5 (2):150-155.
143. Jinushi M, Nakazaki Y, Carrasco DR, Draganov D, Souders N, Johnson M, et al. Milk fat globule EGF-8 promotes melanoma progression through coordinated Akt and twist signaling in the tumor microenvironment. Cancer Res 2008; 68 (21):8889-8898.
144. Akalu YT, Rothlin CV, Ghosh S. TAM receptor tyrosine kinases as emerging targets of innate immune checkpoint blockade for cancer therapy. Immunol Rev 2017; 276 (1):165-177.
145. Curtsinger JM, Lins DC, Mescher MF. Signal 3 determines tolerance versus full activation of naive CD8 T cells: dissociating proliferation and development of effector function. J Exp Med 2003; 197 (9):1141-1151.
146. Fidler IJ. Biological Behavior of Malignant Melanoma Cells Correlated to Their Survival in vivo. Cancer Research 1975; 35:218-224.
147. Gerner M, Casey K, Mescher M. Defective MHC Class II Presentation by DC Limits CD4 T Cell Help for Antitumor CD8 T Cell Responses. The Journal of Immunology 2008; 181:155-164.
148. Gerner MY, Mescher MF. Antigen processing and MHC-II presentation by dermal and tumor-infiltrating dendritic cells. J Immunol 2009; 182 (5):2726-2737.
149. Waclavicek M, Majdic O, Stulnig T, Berger M, Baumruker T, Knapp W, et al. T cell stimulation via CD47: agonistic and antagonistic effects of CD47 monoclonal antibody 1/1A4. The Journal of Immunology 1997; 159:5345-5354.
150. Homet B, Ribas A. New drug targets in metastatic melanoma. J Pathol 2014; 232 (2):134-141.
151. Galluzzi L, Buque A, Kepp O, Zitvogel L, Kroemer G. Immunological Effects of Conventional Chemotherapy and Targeted Anticancer Agents. Cancer Cell 2015; 28 (6):690-714.
152. Belizaire R, Unanue ER. Targeting proteins to distinct subcellular compartments reveals unique requirements
for MHC class I and II presentation. PNAS 2009; 106 (41):17463-17468.
153. Stefanidakis M, Newton G, Lee WY, Parkos CA, Luscinskas FW. Endothelial CD47 interaction with SIRPgamma is required for human T-cell transendothelial migration under shear flow conditions in vitro. Blood 2008; 112 (4):1280-1289.
154. Azcutia V, Routledge M, Williams MR, Newton G, Frazier WA, Manica A, et al. CD47 plays a critical role in T-cell recruitment by regulation of LFA-1 and VLA-4 integrin adhesive functions. Molecular Biology of the Cell 2013; 24 (21):3358-3368.
155. Helms JB, Rothman JE. Inhibition by brefeldin A of a Golgi membrane enzyme that catalyses exchange of guanine nucleotide bound to ARF. Nature 1992; 360:352-354.

156. Zhang X, Fan J, Wang S, Li Y, Wang Y, Li S, et al. Targeting CD47 and Autophagy Elicited Enhanced Antitumor Effects in Non-Small Cell Lung Cancer. Cancer Immunol Res 2017; 5 (5):363-375.
157. Liu L, Zhang L, Yang L, Li H, Li R, Yu J, et al. Anti-CD47 Antibody As a Targeted Therapeutic Agent for Human Lung Cancer and Cancer Stem Cells. Frontiers in Immunology 2017; 8:1-17.
158. Rao DD, Vorhies JS, Senzer N, Nemunaitis J. siRNA vs. shRNA: similarities and differences. Adv Drug Deliv Rev 2009; 61 (9):746-759.
159. Foulkes WD, Priest JR, Duchaine TF. DICER1: mutations, microRNAs and mechanisms. Nat Rev Cancer 2014; 14 (10):662-672.
160. Youle RJ, Strasser A. The BCL-2 protein family: opposing activities that mediate cell death. Nat Rev Mol Cell Biol 2008; 9 (1):47-59.
161. Yang C, Gao S, Zhang H, Xu L, Liu J, Wang M, et al. CD47 is a Potential Target for the Treatment of Laryngeal Squamous Cell Carcinoma. Cell Physiol Biochem 2016; 40 (1-2):126-136.
162. Bieberich E. Ceramide signaling in cancer and stem cells. Future Lipidol 2008; 3 (3):273-300.